

**Role of putative vesicle trafficking proteins
FZL, Synaptotagmin 5.2 and SNARE_AP in
chloroplast development**

**Dissertation
der Fakultät für Biologie
der Ludwig-Maximilians-Universität München**

**vorgelegt von
Manali Kishor Patil**

München, August 2018

Diese Dissertation wurde angefertigt unter der Leitung von Prof. Dr. Jürgen Soll an der Fakultät für Biologie der Ludwig-Maximilians-Universität München.

Erstgutachter: Prof. Dr. Jürgen Soll

Zweitgutachter: Prof. Dr. Marc Bramkamp

Tag der Abgabe: 28th August 2018

Tag der mündlichen Prüfung: 26th October 2018

Abstract:

Differentiation of mature chloroplasts from proplastids is a complex process that involves simultaneous thylakoid membrane biogenesis and assembly of the photosynthetic apparatus. Proplastids contain very little internal membrane structure (pro-thylakoid) that develops into the extensive photosynthetically active thylakoid membrane network in mature chloroplasts. Though early microscopic studies suggest that tubules and vesicles emerging from the chloroplast inner envelope contribute to thylakoid biogenesis, the molecular players involved in this transition remain elusive. Three putative chloroplast vesicle trafficking candidate proteins; Fuzzy Onion-like (FZL), Synaptotagmin 5.2 (SytL5.2) and Soluble N-ethylmaleimide sensitive factor Attachment Receptor (SNARE) associated proteins (SNARE_AP) were investigated as a part of this thesis.

FZL, a membrane-bound dynamin-like GTPase, was found to reside at the inner envelope of chloroplast. Mutant analysis revealed that lack of FZL resulted in instability of the cytochrome *b₆f* complex and thus decreased the photosynthetic efficiency of plants especially in the midvein region of the leaves. Collectively the data show that although FZL is a protein localized to the inner envelope, it affects the maintenance of thylakoid membranes and therefore the function of photosynthetic complexes.

SytL5.2, part of a plant synaptotagmin family protein, characterized as a part of this work was found to be localized to the chloroplast. SytL5.2 mutants displayed an overall crumpled leaf phenotype with a delay in chloroplast maturation at the leaf base as compared to WT. This retardation in chloroplasts recovered as the cells differentiated further near the tip of the leaf along the proximal-distal axis implying that SytL5.2 plays a role in early chloroplast biogenesis in leaves.

Chloroplast localization of SNARE_AP, a predicted plastidial vesicle trafficking SNARE associated protein was verified by *in vivo* GFP localization experiments. The leaves of *snare_ap* plants were pale green with reduced chlorophyll content. The mutants were also found to exhibit reduced accumulation of photosynthetic complexes, but their assembly was unaffected. Transmission electron microscopy analysis to study changes in ultrastructure revealed that chloroplasts in *snare_ap* plants showed disorganized thylakoid architecture and higher number of vesicles. Moreover, delayed greening of etiolated mutant seedlings along with severe phenotype in cotyledons indicate towards a role early during development of chloroplasts.

Zusammenfassung:

Die Differenzierung von Proplastiden in Chloroplasten ist ein komplexer Prozess, der die simultane Bildung und den Aufbau von Thylakoidmembranen und Photosystem Apparaten beinhaltet. Proplastiden enthalten minimale innere Membranstrukturen (Prothylakoide), die sich zu einem ausgedehnten, photosynthetisch aktiven Netzwerk von Thylakoidmembranen im reifen Chloroplasten entwickeln. Mikroskopische Untersuchungen legen nahe, dass das Abschnüren von Tubuli und Vesikeln von der inneren Hüllmembran von Chloroplasten zur Ausbildung der Thylakoidmembran beiträgt; die molekularen Komponenten, die an diesem Vorgang beteiligt sind, sind jedoch noch nicht identifiziert. Drei mögliche Kandidaten, die im Vesikeltransport eine Rolle spielen könnten, Fuzzy Onion-like (FZL), Synaptotagmin 5.2 (SytL5.2) and Soluble N-ethylmaleimide sensitive factor Attachment Receptor (SNARE) associated proteins (SNARE_AP), wurden in dieser Arbeit untersucht.

Die membrangebundene, dynaminähnliche GTPase FZL wurde in der inneren Hüllmembrane von Chloroplasten lokalisiert. Die Analyse der *Arabidopsis fzl* Mutanten ergab, dass das Fehlen von FZL zu einer Instabilität des Cytochrom-*b₆f*-Komplexes führte und somit die photosynthetische Effizienz der Pflanzen vor allem im zentralen Bereich der Blätter verringert war. FZL ist somit maßgeblich an der Aufrechterhaltung der Thylakoidmembranen beteiligt.

Ein neuartiges Pflanzenprotein, das der Synaptotagmin-Familie angehört, SytL5.2, wurde als chloroplastidäres Protein identifiziert. *SytL5.2*-Mutanten zeigten einen zerknitterten (*crumpled*) Phänotyp der Blätter mit Verzögerung der Chloroplastenreifung an der Blattbasis. Diese Verzögerung in der Entwicklung wird kompensiert, wenn sich die Zellen in der Nähe der Blattspitze entlang der proximal-distalen Achse differenzieren. Diese Tatsache impliziert, dass SytL5.2 eine Rolle bei der frühen Entwicklung der Chloroplasten in Blättern spielt.

SNARE_AP ist in chloroplasten lokalisiert. Die Blätter der *snare_ap*-Pflanzen waren blassgrün mit reduziertem Chlorophyllgehalt. Die Mutanten zeigten eine verminderte Akkumulation von photosynthetischen Komplexen, deren Zusammensetzung jedoch nicht verändert war. Die Transmissionselektronenmikroskopie-Analyse zur Untersuchung der Ultrastruktur wies eine unzusammenhängende Thylakoidarchitektur und eine höhere Anzahl von Vesikeln in den Chloroplasten in den *snare_ap*-Pflanzen auf. Eine verzögerte Ergrünung von etiolierten *snare_ap*-Keimlingen zusammen mit stark ausgeprägtem Phänotyp in Keimblättern weisen auf eine Rolle von SNARE_AP während der Entwicklung von Chloroplasten hin.

Abbreviations

aa	amino acid
AP	adaptor protein complex
ATP	adenosine triphosphate
BCA	bicinchoninic acid
BLAST	Basic Local Alignment Search Tool
BN-PAGE	blue native polyacrylamide gel electrophoresis
CCV	clathrin coated vesicles
CHCs	clathrin heavy chains
CLCs	clathrin light chains
Col-0	Arabidopsis thaliana ecotype Columbia
COP	coated protein complex (I and II)
cpSEC	chloroplast Secretory pathway
cpTAT	chloroplast Twin Arginine Translocase
CZ	central zone
DGDG	digalactosyl diacylglycerol
DMF	dimethyl formamide
DRPs	Dynamamin related proteins
DTT	dithiothreitol
ECL	enhanced chemiluminescence
EDTA	Ethylene-diamine-tetra-acetic acid
EGTA	Ethylene glycol bis (aminoethyl ether) -N, N, N', N'-tetraacetic acid
ER	Endoplasmic reticulum
ESCRT	endosomal sorting complex required for transport
E-Syt	extended Synaptotagmins
ETR	electron transfer rates
GAP	GTPase Activation Protein
gDNA	genotmic DNA
GEF	guanine nucleotide exchange factor
GFP	Green fluorescent protein
GO	gene ontology
GTP	guanosine triphosphate
GUS	β -glucuronidase
H	homozygous
hcf	high chlorophyll fluorescence
HEPES	2- (4- (2-hydroxyethyl) -1-piperaziny) ethanesulfonic acid
His tag	Hexa or deca histidine tag
Hpi	hours post imbibition (hpi)
Hsp	heat shock protein
IAA	iodacetamide

IPTG	isopropyl- β -D-thiogalactopyranoside
IRT1	iron regulated transporter 1
kDa	kilodalton
Ler	<i>Arabidopsis thaliana</i> ecotype Landsburg erecta
LHC	light harvesting complex
LMF	light membrane fraction
LMM	lesion mimic mutant
LP	leaf primordia
MBP	Maltose binding protein
MDGD	Mono galactosyl diacylglycerol
MOPS	3- (N-Morpholino) propanesulfonic acid
NADPH	nicotinamide adenine dinucleotide phosphate
Ni-NTA	nickel-nitrilotriacetic acid
NPQ	non-photochemical quenching
NSF	N-ethylmaleimide-sensitive factor
NTMC2	N-terminal-TM-C2 domain genes
PAGE	polyacrylamid gel electrophoresis
PAM	Pulse Amplitude Modulation
PAR	photosynthetically active radiation
PBS	phosphate buffered saline
PCR	Polymerase chain reaction
PEG	polyethylene glycol
PIP2	Phosphatidyl inositol 4,5-bisphosphate
PLBs	prolamellar bodies
PM	plasma membrane
PMSF	phenylmethylsulfonyl fluoride
PS	Photosystem
PVDF	polyvinylidene fluoride
PVP	Polyvinylpyrrolidone
PZ	peripheral zone
RAM	Root apical meristem
Rbcl	ribulose-1,5-bisphosphate
RT	room temperature
RZ	rib zone
SAM	Shoot apical meristem
SDS	sodium dodecyl sulfate
SGDG	sulfoquinovosyl diacylglycerol
SM proteins	Sec1/Munc18-like proteins
SMP	Synaptotagmin-like Mitochondrial and lipid binding protein domain
SPP	stromal processing peptidase
SRP	Signal Recognition Particle

Strep	Strep-tactin tag
SVs	synaptic vesicles
SYT	Synaptotagmin
Tcb	tricalbin
T-DNA	transferred DNA
TEM	transmission electron microscopy
TGN	trans-golgi network
TIC	translocase of the inner membrane of chloroplasts
TM	Transmembrane domain
TOC	translocase of the outer membrane of chloroplasts
TP	transit peptide
TPP	thylakoidal processing peptidase
TPR	tetratricopeptide repeat
vps	vacuolar protein sorting
VSR	vacuolar sorting receptors
WT	wildtype
YFP	yello fluroscent protein
β -DM	β -dodecyl maltoside

Table of contents:

Summary	I
Zusammenfassung	II
Abbreviations	III
Table of contents	VI
1. INTRODUCTION	1
1.1 Origin of mitochondria and chloroplast	1
1.2 The protein targeting and import machineries of chloroplast	2
1.3 Composition and biogenesis of thylakoid membranes	4
1.4 Chloroplast biogenesis from proplastids in meristematic tissue and etioplasts	4
1.5 Vesicle trafficking in chloroplast biogenesis	6
1.6 Vesicle transport system in plants: what is known so far?	8
1.7 Proteins implicated in chloroplast vesicle trafficking so far	10
1.8 Proteins characterized in this study	12
1.8.1 Fuzzy Onion Like (FZL)	13
1.8.2 Synaptotagmin 5.2 (SYTL5.2)	15
1.8.3 SNARE associated protein (SNARE_AP)	19
2. Materials and Methods	20
2.1 Accession numbers	20
2.2 Materials	20
2.2.1 Chemicals	20
2.2.2 Molecular weight and size markers	20
2.2.3 Enzymes	20
2.2.4 Column material	20
2.2.5 Membranes	20
2.2.6 Oligonucleotides	20
2.2.7 Vectors	22
2.2.8 Antibodies	23
2.2.9 software	23
2.3 Microbiological methods	23
2.3.1 Bacterial strains	23
2.3.2 Media and growth	24
2.3.3 Bacterial transformation	24
2.3.4 Transformation of <i>A. tumefaciens</i>	24

2.4	Molecular Biological methods	24
2.4.1	Cloning strategies	24
2.4.2	Polymerase chain reaction (PCR).....	25
2.4.3	Isolation of plasmid DNA from <i>E. coli</i>	26
2.4.4	Sequencing	26
2.4.5	Isolation of plasmid DNA from <i>A.tumefaciens</i> for genotyping PCR	26
2.4.6	Isolation of genomic DNA from <i>A.thaliana</i> for cloning.....	26
2.4.7	Isolation of RNA from <i>A.thaliana</i>	26
2.4.8	cDNA synthesis	27
2.5	Biochemical methods	27
2.5.1	Overexpression of recombinant proteins	27
2.5.2	Purification of proteins from inclusion bodies.....	27
2.5.3	Purification of soluble proteins	28
2.5.4	Nickel affinity purification of proteins.....	28
2.5.5	Isolation of proteins from <i>A.thaliana</i> leaves	28
2.5.6	Determination of protein concentration	28
2.5.7	SDS polyacrylamide gel electrophoresis (SDS-PAGE)	29
2.5.8	Commassie staining of polyacrylamide gels.....	29
2.5.9	Semi-dry electro blot and immunodetection of proteins.....	29
2.5.10	Blue Native PAGE (BN-PAGE) and second dimension SDS-PAGE	30
2.5.11	Silver staining of SDS gels.....	30
2.5.12	<i>In vitro</i> transcription	30
2.5.13	<i>In vitro</i> translation	31
2.5.14	Detection of radio-labelled proteins	31
2.5.15	Mass spectroscopy	31
2.5.16	Chlorophyll isolation.....	31
2.6	Plant biological methods	32
2.6.1	Plant material.....	32
2.6.2	Plant growth conditions.....	32
2.6.3	Cross fertilization of <i>A.thaliana</i>	32
2.6.4	Isolationofintactchloroplastsfrom <i>P. sativum</i>	33
2.6.5	<i>In vitro</i> import into chloroplastsfrom <i>P. sativum</i>	33
2.6.6	Isolation of thylakoid membranes	34
2.6.7	Isolation of inner and outer chloroplast envelope from <i>P. sativum</i>	34
2.6.8	Greening of etiolated seedlings of <i>A.thaliana</i>	34
2.6.9	Stabletransformationof <i>A.thaliana</i> with <i>A. tumefaciens</i>	35

2.6.10	Measurement of chlorophyll fluorescence	35
2.6.11	Transient transformation of <i>N.benthamiana</i>	35
2.6.12	Isolation of protoplast from <i>N.benthamiana</i> for GFP localization	35
2.7	Microscopy.....	36
2.7.1	Laser scanner microscopy for measurement of chloroplast diameter	36
2.7.2	Light and Transmission electron microscopic (TEM) analysis	36
2.8	Transcriptomic profiling using Affymetrix ATH1 microarray	37
2.9	<i>In silico</i> protein structure analysis	38
3.	RESULTS	39
3.1	Fuzzy Onion Like (FZL).....	39
3.1.1	Characterization of <i>fzl</i> mutant lines.....	39
3.1.2	Sub-chloroplast localization of FZL.....	41
3.1.3	Analysis of photosynthetic activity and accumulation of thylakoid membrane complexes	43
3.1.4	Analysis of changes in transcript levels upon onset of the phenotype.....	45
3.1.5	<i>In silico</i> protein structure prediction	49
3.2	Synaptotagmin 5.2 (SYTL5.2).....	50
3.2.1	Characterization of <i>syt/5.2</i> mutant lines	50
3.2.2	Sub cellular localization of SYTL5.2	53
3.2.3	Analysis of chloroplast ultrastructure in <i>syt/5.2</i> plants	56
3.2.4	Accumulation of thylakoid membrane proteins in <i>syt/5.2</i> plants	59
3.2.5	Generation of SYTL5.2 antibody.....	60
3.3	SNARE associated protein (SNARE_AP)	61
3.3.1	Characterization of <i>snare_ap</i> mutant lines	61
3.3.2	GFP localization of SNARE_AP.....	64
3.3.3	Analysis of chloroplast ultrastructure in <i>snare_ap</i> plants.....	65
3.3.4	Lack of SNARE_AP affects the accumulation of photosynthetic complexes and thylakoid membrane protein but not their assembly	66
3.3.5	Generation of SNARE_AP-FL-GFP lines.....	67
3.3.6	Phenotypic analysis of etiolated <i>snare_ap</i> and GFP complementation lines	68
3.3.7	Generation of SNARE_AP antibody	70
4.	DISCUSSION	72
4.1	FZL: The Fuzzy Onion-Like protein.....	72
4.1.1	<i>fzl</i> mutant characterization	72

4.1.2	FZL is primarily localized at the inner envelope membrane of the chloroplast ...	73
4.1.3	Photosynthetic performance of <i>fzl</i> mutants if affected	73
4.1.4	Global transcriptomic analysis of WT vs <i>fzl</i>	74
4.1.5	<i>In silico</i> structural modeling of FZL and its role in vesicle trafficking	75
4.2	Synaptotagmin 5.2	76
4.2.1	<i>Syt15.2</i> mutant characterization	76
4.2.2	SYTL5.2 is chloroplast localized member of plant synaptotagmin family	78
4.2.3	SYTL5.2 affect initial stages of chloroplast differentiation in leaves	79
4.2.4	Lack of SYTL5.2 affects the accumulation of thylakoid membrane proteins but not the overall photosynthetic activity	79
4.3	SNARE_AP	80
4.3.1	Chloroplast localized disrupts the thylakoid network organization.....	80
4.3.2	Deletion of SNARE_AP influences the accumulation of photosynthetic complexes but not their assembly.....	82
4.3.3	SNARE_AP is potentially involved in preliminary stages of chloroplast differentiation	82
5.	Conclusion	84
6.	References	85
	Curriculum vitae	91
	Veröffentlichungen	92
	Eidesstattliche Versicherung	93
	Acknowledgements	94

1. Introduction

1.1 Origin of mitochondria and chloroplast.

Life on earth in its present form is principally due to one key incident; the evolution of photosynthesis approximately about 3 to 3.5 billion years ago (Buick, 2008; Dyall et al., 2004). Approximately 2.4 billion years ago, photosynthesis triggered the so called “great oxidation event” resulting in enrichment of oxygen in earth’s atmosphere. This paved the way for evolution of aerobic respirations in microorganisms and more complex organisms (Buick, 2008). Today approximately 95 % of the earth’s living matter consists of photosynthetic plants and cyanobacteria that are the main source of energy for sustaining life.

The evolution of aerobic respiration and photosynthesis goes hand in hand with the emergence of mitochondria and chloroplasts, the primary site for respiration and photosynthesis respectively. In 1905, the Russian biologist, Mereschkowsky was the first one to put forth a detailed theory about the endosymbiotic origin of mitochondria and chloroplasts (W. Martin et al., 1998; Gray, 2017; W. F. Martin, Garg, & Zimorski, 2015). However, many contemporary scientists at that time preferred to envision that continuous gene duplications, point mutations and micro-mutation processes resulted in origin of eukaryotes. Hence the endosymbiotic theory was neglected until Lynn Sagan (later Margulis) revisited it 60 years later. She describe the first ever unified theory of the origin of eukaryotes from prokaryotes in her 1967 treatise (Gray, 2017). One of the striking features of this article was that it linked eukaryogenesis to the changing atmosphere with increasing free oxygen produced by photosynthetic prokaryotes (Gray, 2017; Martin et al., 2015). According to Lynn Margulis, two separate acquisitions and subsequent changes resulted in mitochondria and plastids. Now this is well established through recent studies based on gene distributions and phylogenetic analysis of protein sequences (Ku et al., 2015). Firstly, a facultatively anaerobic α -proteobacterium (also referred sometimes as the protomitochondrion) was ingested into the cytoplasm of a heterotrophic facultative anaerobe giving rise to a eukaryote with a mitochondrion. Then through another primary endosymbiotic event, this mitochondrion containing eukaryote took up a photosynthetic cyanobacterium as an endosymbiont which led to the evolution of chloroplasts (Dyall et al., 2004; Gray, 2017; Ku et al., 2015; Martin et al., 2015).

1.2 The protein targeting and import machineries of chloroplast

During organellar evolution of plastids into their present complex state, a massive relocation of genetic material took place from the photosynthetic cyanobacterial endosymbiont to the emerging host nucleus (Balsera et al., 2009; Dyall et al., 2004; Kleine et al., 2009; Soll and Schleiff, 2004). After the genetic integration with the host, plastids are semi-autonomous organelles, have their own DNA and duplicate. However, this DNA encodes only about 200 of the 3500-4000 plastidial proteins (Keeling, 2010; Martin and Herrmann, 1998; Soll and Schleiff, 2004). Consequently, the remaining 95 % of the nuclear encoded proteins are synthesized in the cytosol and must be imported into the plastids. This required development of a protein targeting system and import machineries during organellar evolution to maintain bioprocesses inside chloroplast. The contemporary systems include components which bear similarities to the bacterial ancestors as well as newly developed constituents (Balsera et al., 2009).

Specific targeting of precursor proteins to chloroplast is achieved by N-terminal transit peptide (TP) sequences. The TP sequences are highly heterogenous and have a net positive charge owing to lack of acidic residues (Schwenkert et al., 2011; Sjuts et al., 2017). TPs of import competent precursor proteins bind to cytosolic chaperons like Hsp70, Hsp90 and 14-3-3 protein and further interact with the import pathway components (Kovács-bogdán et al., 2010; Schwenkert et al., 2011; Sjuts et al., 2017). The TP is both essential and sufficient for recognition, initial attachment and translocation into the chloroplasts (Sjuts et al., 2017).

The next challenge is translocation of the proteins to their target destination through three membrane systems of chloroplasts: the outer envelope, the inner envelope and the thylakoids, each requiring an independent machinery (Schwenkert et al., 2011). The TOC (Translocase of the Outer Chloroplast envelope) and the TIC (Translocase of the Inner Chloroplast envelope) complexes allow the passage of the preprotein through the outer and inner envelope of chloroplast respectively. The core TOC complex consists of Toc159, Toc34 and Toc75 proteins. Toc34 and Toc159 are receptor proteins with GTP binding domains and Toc75 is a β -barrel translocation channel across the outer envelope (Schwenkert et al., 2011; Sjuts et al., 2017). Toc64 is another auxiliary receptor protein with a tetratricopeptide (TPR) domain that was found to be only transiently associated of the TOC complex (Chang et al., 2012; Sjuts et al., 2017). The next compartment that the preprotein encounters is the intermembrane space with Tic22 as the only protein identified and characterized so far. It is hypothesized to act as a chaperon protein to assist translocation

across the intermembrane space (Kasmati et al., 2013; Rudolf et al., 2013; Sjuts et al., 2017). The TIC complex consists of Tic110, Tic40 and Hsp93 as the minimal functional unit and Tic32, Tic55 and Tic62 form the redox regulon. Tic110 is the main translocation channel protein. Tic40 and Hsp93 are the co-chaperone and chaperone respectively providing the translocation driving force (Balsera et al., 2009; Chang et al., 2012; Schwenkert et al., 2011; Sjuts et al., 2017). Tic55, a Rieske protein, is a potential thioredoxin target while Tic32 and Tic62 are NADP(H) binding dehydrogenases (Kovács-Bogdán et al., 2010; Sjuts et al., 2017; Stengel et al., 2009). Tic32 is involved in regulating the calcium dependent import of preproteins and directly interacts with the N-terminus of Tic110 as well (Hörmann et al., 2004; Kovács-Bogdán et al., 2010). Additionally, Tic20 is an essential protein in *Arabidopsis* that is postulated to form a preprotein translocon channel independent from Tic110 (Reumann et al., 2005; Sjuts et al., 2017). Although Kikuchi et al purified a 1 MDa complex consisting of Tic20, Tic56, Tic100 and Tic214 (Ycf1), the details regarding the function of these proteins are under debate (Bölter and Soll, 2017; Kikuchi et al., 2013; Sjuts et al., 2017). After passing through the TOC and TIC complex the N-terminal transit peptide is cleaved off by the stromal processing peptidase (SPP). The mature protein thus formed is further folded into its native structure with help of Hsp70 chaperone. Additionally, thylakoid luminal proteins are further targeted to thylakoids based on the targeting signal present at the C-terminal of TP (Soll and Schleiff, 2004).

Once inside the stroma, the proteins need to be targeted to either thylakoid membrane or the lumen. This occurs via one of the four pathways which bear similarities to the bacterial systems of membrane protein targeting (Balsera et al., 2009). Two pathways that are specific for membrane proteins are the Signal Recognition Particle (SRP) dependent pathway and “spontaneous” insertion pathway. The luminal proteins follow either the Secretory pathway (cpSec) or the Twin Arginine Translocase (cpTat) pathway. The SecA protein enables translocation of unfolded proteins upon ATP hydrolysis. The cpTat pathway utilizes the proton motive force across the thylakoid membrane for translocation of folded proteins (Albiniak et al., 2012; Balsera et al., 2009; Jarvis and López-Juez, 2013; Schünemann, 2007). The complexities involved in targeting the protein to its destination is vital for the functioning of the chloroplasts thus demanding tight regulation. Not surprisingly any disturbance therein results in lethality or severe defects in chloroplast biogenesis, particularly in structure of thylakoid network.

1.3 Composition and biogenesis of thylakoid membranes

Thylakoids are unique to organisms performing oxygenic photosynthesis and are not observed in bacteria performing anoxygenic photosynthesis. Thus, it is evident that chloroplast inherited this ability to form photosynthetic membranes from their cyanobacterial ancestors and further improvised it (Vothknecht and Soll, 2005). In cyanobacteria and many algae, thylakoids consist mainly of single layers formed by long lamellae. In higher plants, this structure is more complex with tightly appressed layers of thylakoids to form grana stacks connected by longer unstacked stroma lamellae (Adam et al., 2011). This encloses another large sub-compartment of the thylakoid lumen. The most prominent activity occurring during initial stages of chloroplast development is the formation of the thylakoid membrane network. This includes import of nuclear-encoded proteins, boosting the levels of chlorophyll and ultimately assembling the photosynthetic complexes along with lipids to establish the thylakoids (Waters and Langdale, 2009).

The composition of the lipid matrix embedding the photosynthetic protein pigment complexes is unique, since it consists mainly of galactosyl diglycerides but not phospholipids. Mono and digalactosyl diacylglycerol (MGDG and DGDG) represent about 70 to 80% of them while sulfoquinovosyl diacylglycerol (SGDG) and phosphatidylglycerol constitute the rest. MGDG and DGDG are exclusive to plastidial membranes, are synthesized in the chloroplast and are essential for thylakoid formation (Benning, 2009; Kobayashi et al., 2007). A huge gap exists in knowledge regarding membrane formation despite the significant understanding we have acquired about the process of the assembly and repair of the photosystems. Physical properties of the lipids and the proteins involved play a vital role in the process. Although it is presumed that both occur simultaneously, what factors decide the positioning of lipids in respective leaflets in coordination with the agglomeration of the respective complexes, the preservation of same and restoration if disturbed remain unanswered.

1.4 Chloroplast biogenesis from proplastids in meristematic tissue and etioplasts

Plastids cannot be formed de novo and are in general maternally inherited. They multiply via division at later stages of growth. Proplastids are the progenitors of all plastid types and are found in the apical meristem both shoot (SAM) as well as the root (RAM) (Charuvi et al., 2012; Jarvis and López-Juez, 2013). The tissue structure of SAM from angiosperms (flowering plants) has been very well described with organogenesis as a focus (Barton, 2010; Charuvi et al., 2012; Sharma, 2002; Yadav et al., 2009). Classically, SAM is designated into three major zones from which various tissues develop further: the central zone (CZ), the rib

zone (RZ) just below the CZ and the peripheral zone (PZ) around the CZ. The CZ is source of fully undifferentiated stem cells. Further away from the meristem, while the cells of the PZ form the leaf primordia (LP) that mature into true leaves, the internal leaf tissue and stem originate from the RZ (Barton, 2010; Sharma, 2002; Yadav et al., 2009). Also, three distinct layers of stem cells have been observed based on different layers of true leaves that arise from the SAM. These are labelled as L1 that generates epidermis layer, L2 giving rise to outer mesophyll cells and L3 developing the inner mesophyll corpus along with vascular bundle (Barton, 2010; Sharma, 2002). Recently, Charuvi et al used microscopy techniques to characterize the plastidial differentiation, especially the progress in thylakoid network formation in the SAM. The thylakoid network within the plastids of layers L1 and L3 was fairly developed alike the plastids in LP. However, in L2, a gradient was seen in the maturation stage of the proplastids with cells in the center harboring the least differentiated thylakoids as compared to the ones near the LP. This same trend was also true for the presence of photosynthetic proteins (Charuvi et al., 2012). This microscopic analysis and other studies provide a convincing premise for the model for thylakoid network formation (summarized in Fig: 1).

Proplastids are more or less spherical membrane bound organelles. They contain very little internal membranes (pro-thylakoids) along with vesicles. However, they show no differentiated structures. Upon illumination, proplastids develop into mature chloroplast. The pro-thylakoid membrane forms the foundation for building of the photosynthetically active thylakoids. In the course of differentiation, typical ellipsoidal shaped chloroplasts with intertwined network of grana stacks and stroma lamellae develop (Charuvi et al., 2012; Pogson et al., 2015; Vothknecht and Westhoff, 2001). In angiosperms, light is indispensable for differentiation of proplastids into chloroplast and absence of light causes temporary suspension of chloroplast development forming etioplasts (Fig:1). Etioplasts are comprised of paracrystalline structure called prolamellar bodies (PLB) with lamellar pro-thylakoids (PTs) radiating peripherally from them into the stroma (Kowalewska et al., 2016; Solymosi and Schoefs, 2010; von Wettstein, 1995). Etioplastic PLBs majorly consist of lipids, protochlorophyllide: the precursor molecule of chlorophyll a and the enzyme NADPH-dependent protochlorophyllide oxidoreductase (Adam et al., 2011; Kowalewska et al., 2016; Vothknecht and Westhoff, 2001; von Wettstein, 1995). When exposed to light, etioplasts go through a transient etio-chloroplast stage (Grzyb et al., 2013; Solymosi and Schoefs, 2010).

Despite the fact that various stages during establishment of thylakoid network as depicted in Figure 1 have been observed consistently, the molecular players involved are largely unknown.

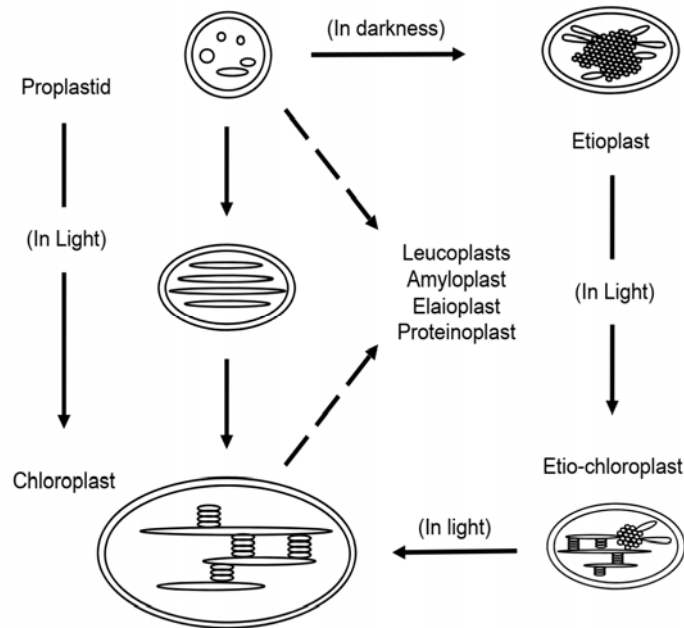


Fig. 1. Overview of chloroplast development. In presence of light, proplastids in SAM differentiate into mature chloroplast with complex internal thylakoid membrane network. Proplastids can also develop into other plastids forms, such as chromoplasts and leucoplasts. In darkness, proplastids form etioplasts which upon illumination develop into chloroplast through an intermediate etio-chloroplast stage. Moreover, fully differentiated plastids retain the ability to interconvert as well. Modified from Vothknecht and Westhoff, 2001.

1.5 Vesicle trafficking in chloroplast biogenesis

There are two hypotheses regarding how the material for formation of thylakoid network is delivered to its destination from the inner envelope of the chloroplast. The first being via direct contacts sites between the inner envelope and thylakoid membrane and the second, more widely accepted hypothesis of vesicles trafficking (Adam et al., 2011; Kowalewska et al., 2016; Morr e et al., 1991a; Shimoni, 2005). Indeed, vesicles pinching off from the inner envelope have been consistently observed in microscopic studies in the proplastids and mature chloroplast. Although tubules emerging from the inner envelope are a common feature of proplastids, they are rarely seen in mature chloroplast (Lindquist et al., 2016; Vothknecht and Westhoff, 2001). This was also seen in transmission electron microscopy (TEM) studies done by our group and is in agreement with the aforementioned electron

tomography (EMT) results of the SAM done by Charuvi *et al* (Charuvi et al., 2012; Westphal et al., 2001). It is suggested that these tubules contribute to thylakoid membrane formation and vesicles carry the building blocks for same. The fact that biosynthesis of carotenoids, fatty acids, polar lipids and prenyl lipids is localized to the inner envelope membrane as well substantiates it's contribution to formation of the thylakoid membrane (Benning, 2009; Dorne et al., 1990).

Despite the well-established knowledge regarding the presence of vesicles in chloroplasts, it wasn't proved until recently that vesicle trafficking as an ongoing process in chloroplast (Morré et al., 1991b; Westphal et al., 2001). Westphal et al treated chloroplast isolated from pea with various inhibitors to demonstrated both fission and fusion of vesicles inside chloroplasts. It was shown that the release of vesicles from the donor membrane involved hydrolysis of GTP and not ATP. In contrast to this, the use of inhibitors of protein phosphatases and calmodulin, as well as a calcium antagonist, resulted in accumulation of vesicles inside chloroplasts (Westphal et al., 2001). Also, low temperature treatment hampered vesicle fusion similar to the observations in yeast (Andersson, 2001; Morré et al., 1991b; Westphal et al., 2001). Moreover, *in organello* galactolipid labelling experiments at low temperatures suggested that galactolipid transport between the inner envelope membrane and thylakoids occurs via vesicles as well (Andersson, 2001). It is interesting that in plastids, these experiments implicated involvement of GTPases, protein phosphatases, calcium and calmodulin; all factors typical to yeast and humans vesicle trafficking pathways (Westphal et al., 2001, 2003). Clathrin coated vesicles (CCVs) and vesicles with coated protein complex I and II (COPI and COPII) have also been known to facilitate the cytosolic transport in plants (Bassham et al., 2008; Hwang and Robinson, 2009). However, evidence for similar plastidial counterparts is largely lacking with an exception of COPII-related proteins: cpSAR1 and CPRabA5e (Garcia et al., 2010; Karim et al., 2014). Consequently, the presence of such a system is assumed to be an acquired trait from the eukaryotic host and is implicated in formation and maintenance of the thylakoid membranes (Vothknecht and Westhoff, 2001; Waters and Langdale, 2009; Westphal et al., 2001).

The evolutionary link of vesicle transport and thylakoid membrane biogenesis is also evident from the fact that vesicles are seen only in embryophytes. Embryophytes include all land plants; bryophytes, pteridophytes and spermatophytes. Both cyanobacteria and algae do not contain the complex thylakoid network with grana stacks and stroma lamellae that is

characteristic of embryophytes. Thus, the establishment of both plastidial vesicle systems and an elaborate thylakoid network seemed to have progressed simultaneously even though the molecular mechanisms linking the two remain largely unexplored (Westphal et al., 2003).

1.6 Vesicle transport system in plants: what is known so far?

Similar to yeast and mammalian systems, plant cytosolic trafficking pathways include the dominant three protein coats: COPI, COPII and Clathrin coated vesicles (CCVs). Additionally, in plants, endosomal trafficking also known to involve ESCRT (endosomal sorting complex required for transport) and retromer coat complexes (Paul and Frigerio, 2007; Reyes et al., 2011). Vesicle trafficking between donor and acceptor membranes classically consists of following steps: assembly, budding and fission, translocation, tethering, docking and fusion. Each step is mediated by specific factors and proteins (Bonifacino and Glick, 2004).

Assembly, budding and fission of vesicles:

At the donor membrane, the cargo molecules are selected for the clustering based on recognition of cargo-sorting signals. These cargo molecules bind to lipids, interact directly or indirectly with adaptor proteins to cluster together. Subsequently, the coat proteins assemble into multimeric complexes which induces membrane curvature during the budding step (Valencia et al., 2016). The assembly and fission of vesicles throughout the plant endomembrane system is regulated by GTPases. These GTPases predominantly belong to the ADP ribosylation factor (ARF) subfamily of small GTPases, which includes the Sar, ARF and ARF-like ARL GTPases (Paul and Frigerio, 2007). After fission of vesicles from donor membrane, the nascent vesicles travel along the cytoskeleton to their destination for fusion at the acceptor organelle membrane. Translocation step also involves uncoating of the coat proteins to allow tethering and finally fusion of vesicles (Bonifacino and Glick, 2004).

Tethering, docking and fusion of vesicles:

The final steps in transporting cargo loaded vesicles to their destination include tethering and docking before finally fusing at the respective acceptor membrane. This is facilitated by small GTPases like RAB GTPases and Soluble N-ethylmaleimide sensitive factor Attachment Receptor (SNAREs). Rab GTPases and their effectors form molecular bridges

to 'tether' the vesicles to their target membrane. *Arabidopsis* genome encodes 57 Rab GTPases which are known to localize at different membranes inside the cell (Rutherford and Moore 2002). These GTPases along with their effector proteins dictate the specificity of the cargo vesicles and their respective target membranes (Paddock et al., 2008; Neilson E. et al., 2008; Uemura and Ueda 2014).

Once the vesicles are docked onto the target membrane, SNAREs mediate vesicle fusion (Illustrated in Fig: 2). SNAREs belong to a large family of membrane-tethered coiled-coil proteins. They are classified into two categories based on their membrane location: vesicle associated v-SNAREs and target-membrane-associated t-SNAREs. However, this terminology is now replaced by R-SNAREs and Q-SNAREs based on conserved arginine and glutamine residues respectively. Further, on the basis of their amino acid composition, Q-SNAREs are classified into Qa-, Qb- and Qc- SNAREs. The *Arabidopsis* genome encodes

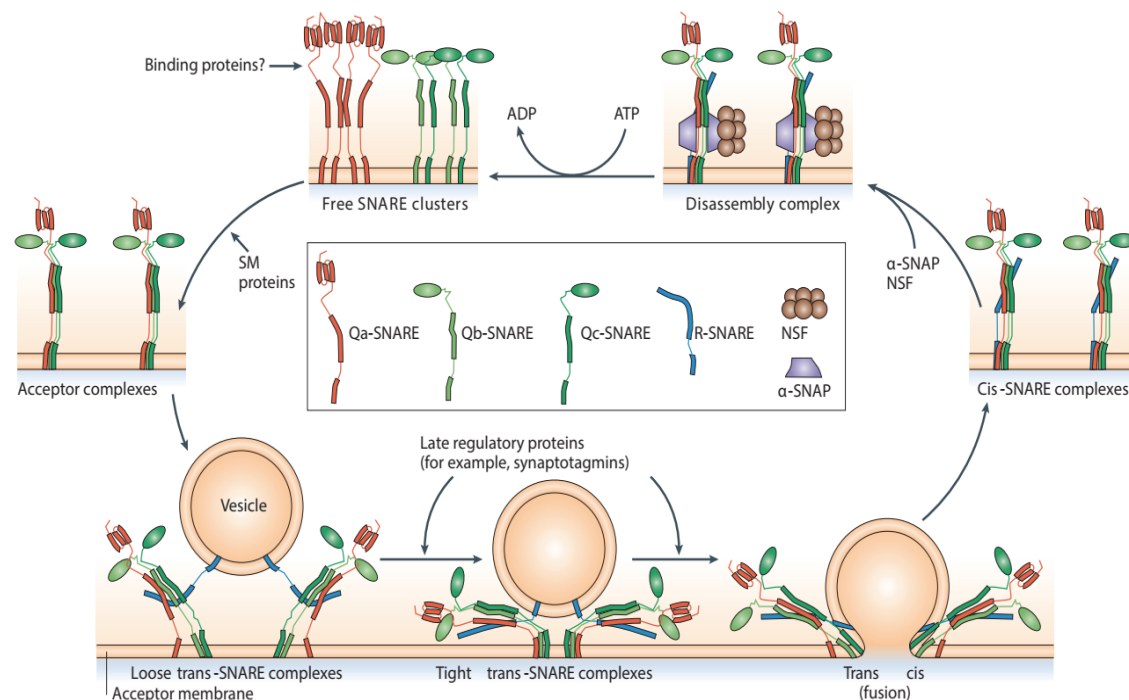


Fig. 2. Overview of SNARE mediated vesicle fusion. 'Open' Q-SNAREs in clusters and assemble to form 'closed' acceptor complexes. This might be aided by SM (Sec1/Munc18-related) proteins (top left). Acceptor complexes interact with the vesicular R-SNAREs forming a four-helical trans complex. Loose trans-complexes are 'zipped up' to a tight state and is followed by membrane fusion. During exocytosis, synaptotagmin (which is activated by an influx of calcium) regulate the intermediate states in some cases (see section 1.8.2). Post fusion, SNARE complexes relax to cis-complexes are disassembled by protein NSF (N-ethylmaleimide-sensitive factor) and SNAPs (soluble NSF attachment proteins) cofactors. Figure reprinted by permission from Springer Nature and is taken from Jahn and Scheller 2006.

more than 60 SNARE proteins (Bassham et al., 2008; Khan et al., 2013). The Qa-, Qb- and the Qc- SNARE assemble into a triple-helix bundle at the target membrane to form an acceptor complex (Fig: 2). This subsequently binds to R-SNARE on the vesicular membrane forming a SNARE complex with a four-helix-bundle. These interactions are mediated via a conserved SNARE motif. This loose four-helix-bundle undergoes parallel twisting or the so called 'zippering' to pull the membranes in close proximity to drive fusion and opening of the fusion pore. After completion of the fusion process, the SNARE-tetra helix complex is disassembled via ATP hydrolysis by the AAA+ (ATPases associated with various cellular activities) protein NSF (N-ethylmaleimide-sensitive factor) along with the co-factor SNAPs (soluble NSF attachment proteins) freeing the SNAREs for the next round of fusion. The SNAREs are then separated and recycled (Fig: 2) (Bassham et al., 2008; Jahn and Scheller, 2006; Saito and Ueda, 2009; Südhof, 2013).

Moreover, recycling of proteins and lipids back to their resident membrane of function is essential. It ensures continuity of the processes and thus making tight regulation of endocytic and endosomal trafficking pathways of utmost importance.

1.7 Proteins implicated in chloroplast vesicle trafficking so far:

Even though the presence of vesicles in chloroplasts is well established knowledge, it is only recently that the proteins that might be involved in vesicle trafficking in chloroplast are being discovered. Vesicle inducing protein in plastids 1 (Vipp1) (Kroll et al., 2001), thylakoid formation protein 1 (THF1) (Wang, 2004), Sar1 (Garcia et al., 2010), CURT1 (Armbruster et al., 2013a) and CPRabA5e (Karim et al., 2014) are among the few proteins implicated in chloroplast vesicle trafficking, however their exact roles still remain to be determined.

Vipp1 is an evolutionarily conserved protein found in both cyanobacteria and *Arabidopsis*. This 33 kDa nuclear-encoded protein is localized to thylakoid as well as to the inner envelope membrane of chloroplast (Kroll et al., 2001; Li et al., 1994). Chloroplasts in deletion mutants of Vipp1 (*hcf155* mutants) showed disorganized thylakoid membrane structure along with abolition of vesicle formation at cold temperatures. This lead to the initial hypothesis that it is involved in thylakoid formation and/or maintenance (Kroll et al., 2001; Vothknecht et al., 2012). Moreover, analysis of mutants expressing only moderate levels of Vipp1 protein revealed that it is essential for thylakoid membrane formation, but not for the assembly of thylakoid protein complexes (Aseeva et al., 2007). Both *Arabidopsis* Vipp1 and its cyanobacterial isoform oligomerize into rings at the highly curved membrane regions and thus postulated to regulate membrane tension and stability during thylakoid formation

(Aseeva et al., 2004; Hennig et al., 2015). It is thought that Vipp1 aids in exchange of lipids, proteins, pigments and electron carriers into the thylakoid membrane by promoting fusion events (Hennig et al., 2015; Kroll et al., 2001; Vothknecht et al., 2012). Additionally, despite lacking the classical GTPase domain, Vipp1 was also shown to have a GTPase activity substantiating the role in membrane remodeling and fusion (Heidrich et al., 2017; Ohnishi et al., 2018).

THF1 was suggested to play a role in thylakoid biogenesis based on its knock-out mutant analysis. Leaves of *thf1* mutants showed variegated pattern with both abnormal and normal chloroplasts. Moreover, the abnormal chloroplasts had large vesicles with little thylakoid structure (Wang, 2004). In another study performed by Huang et al, THF1 was found to interact with light-harvesting LHCII proteins to control PSII–LHCII dynamics during dark induced senescence and light acclimation conditions. In this case THF1 loss-of-function mutations allowed leaves of *thf1* plants to stay-green longer (Huang et al., 2013). Consequently, THF1 might play a more divergent role depending on the developmental stage and environmental conditions (Huang et al., 2013; Rast et al., 2015).

Plastidial Sar1 (cpSAR1, also known as OBGL or OGBC), is homologous to cytosolic SAR1 component of COPII vesicles transport system. It is essential in plants as knockout lines were embryo lethal (Chigri et al., 2009; Bang et al., 2009; Garcia et al., 2010). The embryo development was arrested at globular stage prior to greening of embryos (Chigri et al., 2009; Bang et al., 2009). Moreover, RNA interference lines had pale yellow embryos with only partially developed thylakoid network in chloroplasts. Due to its dual localization in the inner envelope and in vesicles, cpSAR1 is believed to be involved in vesicle formation at the inner envelope analogous to the role of its cytosolic counterpart (Garcia et al., 2010). In contrast to this, another study suggested its role in plastid ribosome biogenesis (Bang et al., 2012). Thus, although cpSAR1 is essential for chloroplast biogenesis, further research is needed to find its exact role. CPRabA5e is a homolog of RAB GTPases, another component of COPII vesicles transport system, localized to stroma and thylakoid. Lack of CPRabA5e resulted in enlarged plastoglobuli, reduced grana stacks, and increased number of vesicles close to the envelopes at low temperatures and under oxidative stress (Karim et al., 2014). Intriguingly, through yeast-two-hybrid experiments, CPRabA5e was also found to interact with Curvature thylakoid 1 (Curt1), a grana margin protein known to induce membrane curvature and maintain thylakoid structure especially during day-night changes (Rast et al., 2015). However, the significance of this interaction in chloroplast needs to be analyzed

further.

Nevertheless, although these proteins are hypothesized to play a role in thylakoid / chloroplast biogenesis either directly or indirectly, the exact molecular mechanisms involved are largely unclear requiring further research in this direction.

1.8 Proteins characterized in this study

Taken together there is ample evidence to indicate the role of tubules and vesicles originating from inner envelope in thylakoid biogenesis. Yet we have very limited knowledge of the factors and the molecular mechanisms involved during the proplastid-chloroplast transition. Proteomic studies and bioinformatic screens serve as a good starting point to identify candidate proteins with a potential role during chloroplast development. **In the present thesis, three such candidate proteins identified from different studies have been characterized: Fuzzy Onion Like (At1g03160), Synaptotagmin 5.2 (At1g19830) and SNARE-associated protein (At1g22850).**

Fuzzy Onion Like (FZL) was identified as a potential candidate from proteomic analysis of light membrane fraction (LMF) isolated from chloroplasts in our group (unpublished data from Vothknecht and Soll). Briefly, chloroplasts were isolated from young *Pisum sativum* (Pea) and membranes were fractionated using density gradient centrifugations. Membrane fraction with lowest buoyant density most probably consisting of vesicular membrane was designated as LMF. FZL was one of the proteins identified from mass spectrometric analysis of this LMF. Moreover, FZL also came up in another proteomic study done by Bischof et al wherein they analyzed a T-DNA insertion line of Toc159 loss-of-function mutant (*ppi2*) in *Arabidopsis* (Bischof et al., 2011). Toc159 was thought to be the main receptor for photosynthetic protein import into the chloroplast and *ppi2* displayed a pale phenotype when grown on medium containing sucrose. Surprisingly, Bischof and co-workers found that although fully mature chloroplasts could not develop, many proteins related to the photosynthetic machinery were nevertheless present in the *ppi2* mutants. Moreover, a set of proteins that were absent in *ppi2* mutants as compared to WT were also identified. The proteins unique to WT chloroplasts might probably play a role in chloroplasts differentiation and thylakoid formation. FZL was one of the 142 proteins shortlisted from these proteins on the basis of their predicted chloroplast localization, early expression, unknown function and non-lethal phenotype of the mutants. Furthermore, loss of function mutants of FZL were also reported to show altered chloroplast ultrastructure by Gao et al

(Gao et al., 2006).

Synaptotagmin 5.2 (SYTL5.2) was identified in a phospho-proteomic analysis of chloroplast envelope membranes. For this purpose, envelope membranes were isolated from pea chloroplasts in the presence of 50 mM NaF to inhibit protein phosphatases. SYTL5.2 belongs to the synaptotagmin protein family of membrane proteins with tandem calcium binding C2 domains (see below in section 1.8.2). Synaptotagmins are primarily known for their role in neurotransmitter release from synaptic vesicles (SVs). They interact with SNAREs forming a complex to bring the membranes closer and enable fusion (Fig: 2; Chapman, 2002; Südhof, 2013). Though no SNARE proteins have been found localized in chloroplasts so far using both bioinformatics and experimental approaches, a few SNARE associated proteins have been predicted using bioinformatics approach (Andersson and Sandelius, 2004; Khan et al., 2013). The identification of the plastidial synaptotagmin led us to investigate one of these SNARE associated proteins (SNARE_AP) further.

1.8.1 Fuzzy Onion Like (FZL)

The fuzzy-onion-like protein (FZL) is a dynamin-like GTPase, which is closely related to the mitochondrial fusion protein, FZO / mitofusin. FZO is conserved across the fungal and animal kingdom. It localizes to the outer membrane of mitochondria and is thought to mediate tethering of mitochondrial outer membranes via its coiled coil domains, which are exposed to the cytosol and can interact with tethering factors on the same and opposing mitochondrial membranes. Its deletion leads to fragmented mitochondria due to defects in fusion (van der Blik et al., 2013; Mozdy and Shaw, 2003).

Interestingly, *FZL* is the only *FZO*-like gene found in the *Arabidopsis* genome. However, *FZL* contains an N-terminal chloroplast targeting sequence (Fig:3a) and is localized to chloroplasts, as shown by the expression of a *FZL*-GFP fusion protein (Gao et al., 2006). The overexpressed *FZL*-GFP fusion protein was detected in thylakoids as well as in the envelopes of chloroplasts in *Arabidopsis*. Moreover, *FZL* protein shows similar domain structure as that of mouse ortholog of *FZO*, consisting a GTPase domain and two coiled-coiled and transmembrane domains. It also has an additional thymine monophosphate domain / TEN1 domain of unknown function (Fig:3a, Hongbo Gao et al., 2006). T-DNA insertion *fzl* mutants in the Columbia-0 (Col-0) background develop pale green leaves and accumulate fewer, but larger, chloroplasts (Fig:3b and c, Hongbo Gao et al., 2006). Similar chloroplast morphology was also observed in *fzl* mutants in the *Landsburg erecta* (Ler) background (Fig:3 d and e, Landoni et al., 2013). Ultrastructural analysis of *fzl*-Col-0

chloroplasts revealed that the morphology of the thylakoids differs from that observed in WT. Intriguingly, larger numbers of vesicles have also been observed in *fzl* chloroplasts (Fig:3 g-j, Hongbo Gao et al., 2006), leading to the initial hypothesis that FZL might be involved in thylakoid biogenesis or maintenance, possibly by promoting vesicle transport from the inner chloroplast envelope (Gao et al., 2006; Waters and Langdale, 2009).

In contrast to the pale green phenotype observed in *fzl* mutants in *Col-0* background, two independent studies have described *fzl* mutants in *Landsburg erecta* (Ler) background, which display a lesion mimic mutant (LMM) phenotype (Landoni et al., 2013; Tremblay et

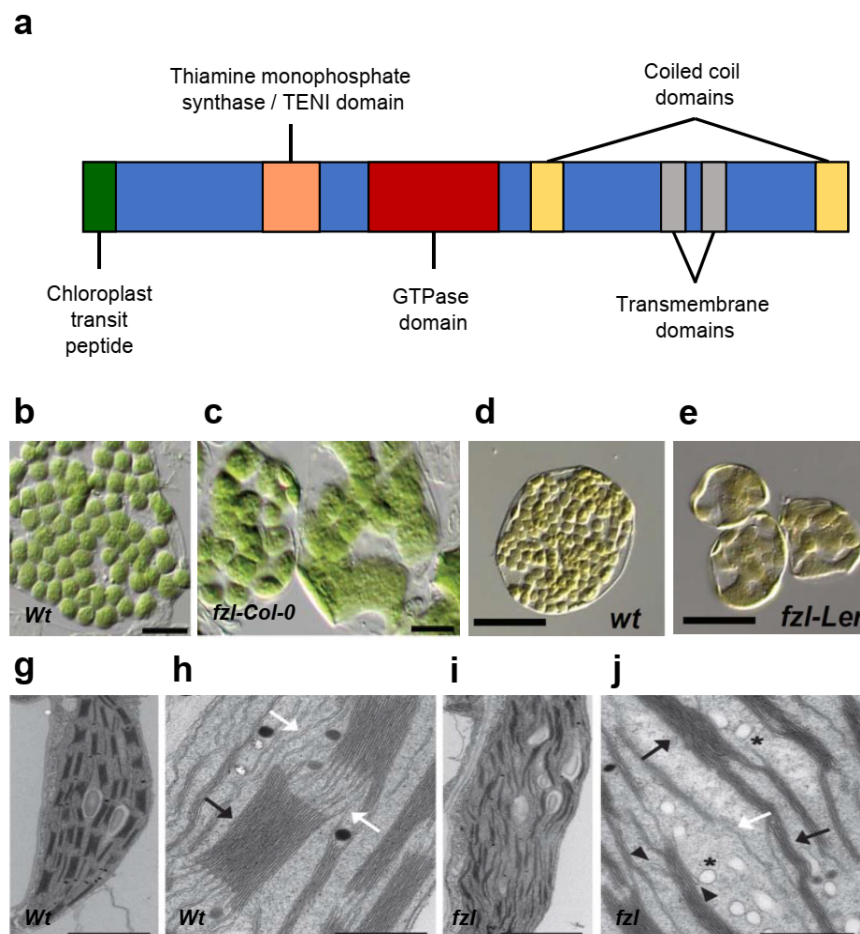


Fig 3: Structure of FZL protein and phenotype of chloroplast in *fzl* mutants

(a) FZL Protein structure with the arrangement of predicted domains structure. (b-e) Chloroplast morphology in *fzl-Col-0* mutants (b and c, Gao et al 2006) and in *fzl-Ler* mutants (d and e, Landoni et al 2013). (g-j) Chloroplast ultrastructure in WT and *fzl* mutant plants (Gao et al 2006). Black and white arrows mark grana and stroma thylakoids, respectively. Arrowheads and asterisk denote inflated lamellae and vesicles in *fzl*.

al., 2016) Typically, the LMM phenotype is associated with constitutively active hypersensitive cell death and defense responses. These responses are activated in WT

not only upon entry into senescence, but also as a reaction to abiotic and biotic stresses, such as pathogen attack (Landoni et al., 2013). FZL mediated cell death was reported to be dependent on salicylic acid and was accompanied with upregulation in the expression levels of several defense and autophagy related genes (Tremblay et al., 2016). The severity of the LMM phenotype is modulated by environmental conditions such as temperature, humidity and light, in addition to variations in the genetic background. In case of *fzl* (Ler) mutants, exposure to elevated temperature (28°C) or low light treatments (50 $\mu\text{mol}/\text{m}^2\text{s}$) was shown to rescue the LMM phenotype. However, the plants nevertheless remained pale green, just like *fzl* (Col-0) mutants (Landoni et al., 2013). As a part of this thesis, the role of FZL in chloroplast has been analyzed further.

1.8.2 Synaptotagmin 5.2 (SYTL5.2)

The synaptotagmin family proteins (SYTs) gained their celebrity status in protein trafficking world for their role in neurotransmitter release from synaptic vesicles (SVs). Synaptotagmin-1 (SYT1) was the first protein identified from this family in 1980s. Thereafter, 17 proteins (numbered 1 – 17) were identified in animals along with several others in invertebrates (Chapman, 2002; Craxton, 2010; Matthew et al., 1981; Südhof, 2013). All proteins of this family have a conserved domain structure. SYTs have an N-terminal transmembrane domain for membrane anchorage followed by one or more tandem Ca^{2+} and phospholipid-binding C2 domains that are linked by a variable linker region (Craxton, 2001; Fukuda, 2007; Schulz and Creutz, 2004; Südhof, 2002). The amino acid sequence of SYTs do not share much homology except in the conserved C2 domains despite their similar general structure (Chapman, 2002; Südhof, 2013; Wang et al., 2015).

Calcium and phospholipid-binding C2 domains:

The C2 domain was originally identified in protein kinase C (PKC) as a conserved sequence that was essential for calcium binding (Chapman, 2002; Sutton et al., 1995). They have a β -sandwich structure of eight anti-parallel strands ($\beta 1$ - $\beta 8$) folded in two different conformations; type 1 and type 2 (Jiménez and Davletov, 2007; Sutton et al., 1995, 1999). There are five conserved aspartic acid residues in the loops 1 and 3 between the β strands that coordinate binding of calcium ions (Sutton et al., 1995, 1999). Interestingly, in synaptotagmins only the top side of the C2A and C2B bind to two and three Ca^{2+} ions respectively (Chapman, 2002; Fernández-Chacón et al., 2002; Fernandez et al., 2001; Fukuda, 2007). Additionally, C2 domains are known to simultaneously interact with

SNAREs, other accessory proteins and lipids during tethering, docking and fusion of vesicles (Chicka et al., 2008; Fuson et al., 2007; Paddock et al., 2008; Zhou et al., 2015, 2017). Consequently, C2 domains are crucial for the functioning of SYTs.

Mechanism of Synaptotagmin-SNARE complex mediated membrane fusion:

The Ca^{2+} sensor SYT1 is the most comprehensively characterized mammalian synaptotagmin isoforms. It facilitates neurotransmitter release via phospholipid binding through its two C2 domains (Chapman, 2008; Martens et al., 2007).

Upon binding to Ca^{2+} ions, the C2 domains undergo a conformational change and partially insert into the lipids of the bilayer. The insertion works as a wedge into the membrane and displaces the polar lipid heads (Fig: 4). This causes the aliphatic chains to tilt resulting in

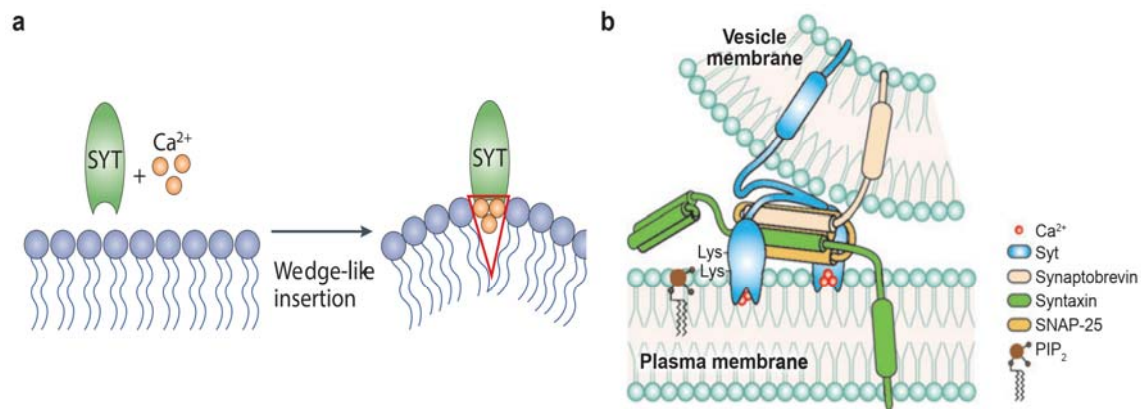


Fig 4: Mechanism of SYT and SNARE induced membrane curvature.

(a) Schematic representation of insertion of Ca^{2+} SYT into the membrane causing it to bend. Image reprinted by the permission from Springer Nature and is taken from **Martens and McMahon, 2008**. (b) C2 domains of SYT1 inserting into the bilayer in presence of Ca^{2+} and binding to Phosphatidylinositol 4,5-bisphosphate (PIP₂). The direct interaction of SNARE and SYT to form a complex connecting the calcium signalling to membrane fusion by bringing the opposing bilayers into close proximity. Abbreviation: SNAP-25, synaptosome-associated protein of 25 kDa. Image rebublished with permission from Annual Reviews, from work of **E. R. Chapman 2008**, permission conveyed through Copyright Clearance Center, Inc.

membrane bending in order to fill up the gap formed in between the head groups. The SYTs and SNARE complexes are thought to coordinate induction of membrane curvature via insertion of multiple molecules in close proximity (Fig: 4). The direct interaction of SNARE and SYT forms a large fusion complex connecting the calcium signaling to membrane fusion (Chapman, 2008; Fukuda, 2007; Martens and McMahon, 2008; Martens et al., 2007; Südhof, 2013).

Functional diversity of Synaptotagmins:

SYTs display a huge diversity in regard to the tissue level expression pattern and their respective functions (Chapman, 2002; Südhof, 2013; Wang et al., 2015). SYT1 and SYT7 are present at the presynaptic neuronal membrane where they trigger rapid and slow synaptic vesicle exocytosis respectively (Südhof, 2013; Zhou et al., 2015, 2017). Moreover, SYT7 is also present in lysosomal membrane where it is involved in plasma membrane repair via Ca^{2+} triggered exocytosis (Andrews, 2005; Andrews and Chakrabarti, 2005; Reddy et al., 2001). In pancreas, SYT7 and SYT9 regulate Ca^{2+} -dependent glucagon exocytosis and insulin secretion in pancreatic β -cells (Grise et al., 2007; Gustavsson et al., 2009). The expression profiles and functions of animal SYTs is summarized in reviews by Südhof (2002) and Fukuda (2013) and references therein.

Synaptotagmins in plants:

In 2001, four genes homologous to human synaptotagmin were first identified in plants through an elaborate genomic BLAST search (Craxton, 2001). This number was later increased to include all classical synaptotagmin and synaptotagmin-like genes in the list (Craxton, 2004, 2007). As of now, there are 13 genes belonging to this family in *Arabidopsis* (Aramemnon database, Schwacke et al., 2003). The nomenclature used for these genes has been inconsistent in literature. Therefore, the overall domain pattern common to all genes (the N-terminal TM region followed by the C2 domain) was used as basis for naming SYTs as **N-terminal-TM-C2** domain genes in plants (Craxton, 2001, 2004, 2010). Moreover, all *NTMC2* genes are currently grouped into 6 sub-groups based on the conserved gene

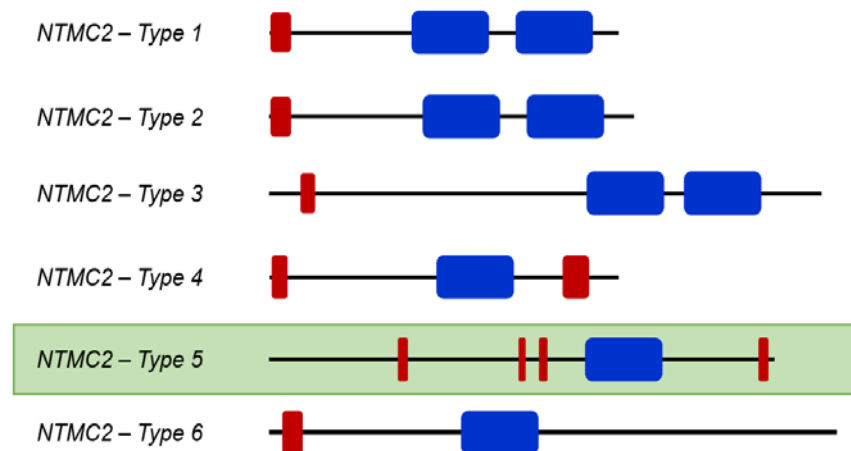


Fig 5: Domain architecture of 6 sub-groups of plant *NTMC2* genes. TM regions are represented by red boxes and C2 domains by blue boxes. The predicted plastidial *NTMC2* - type 5 gene is highlighted in green. Modified from Craxton 2007.

structure namely *NTMC2 Type1*, *NTMC2 Type2* through *NTMC2 Type6* (Fig: 5, Craxton, 2004, 2007; Huang et al., 2017).

Although the presence of *NTMC2* genes in plant genomes was known, it took some time until the experimental evidence regarding their expression and function was obtained. A proteomic study done on cold acclimatized *Arabidopsis* plants provided the first proof that *SYT1* (*NTMC2T1.1*, also known as *SytA*) is expressed (Kawamura and Uemura, 2003). *SYT1* was shown to regulate mechanical stress during high salt conditions, osmotic stress and freezing temperatures. It is proposed that the Ca^{2+} dependent phospholipid binding activities of *SYT1* mediates plasma membrane (PM) resealing via membrane fusion (Schapire et al., 2008; Yamazaki et al., 2008). In other studies, *SYT1* was found at the ER-PM junction and was essential for resistance to mechanical stress, as well as viral cell-to-cell infection (Lewis and Lazarowitz, 2010; Pérez-Sancho et al., 2015; Uchiyama et al., 2014). Recently, *SYT1* was shown to interact with a SNARE complex protein, penetration 1 (*PEN1*) at the PM to negatively regulates the immune secretory pathways upon powdery mildew fungi infection (Kim et al., 2016; Yun et al., 2016). This is of particular significance as it indicates that plant *SYTs* have functions similar to their animal counterparts (Kim et al., 2016; Schapire et al., 2008; Yamazaki et al., 2008; Yun et al., 2016). *SYT2* (*NTMC2T1.2*, also known as *SytB*) is expressed in male and female gametophytes in *Arabidopsis* and participates in pollen germination. During pollen tube tip growth, *SYT2* is delivered to PM from golgi apparatus via conventional secretory pathway (Wang et al., 2015). *SYT2* was also found to regulate unconventional protein transport from golgi to extracellular matrix (Zhang et al., 2011).

SYTL5.2 was identified in a membrane proteomic analysis done in our group and was characterized as a part of this study. *SYTL5.2* is *NTMC2*-type-5 protein in *Arabidopsis* which is annotated as *SYT*-like 5.2 protein (hence referred as *SYTL5.2* here after) in Aramemnon database (Schwacke et al., 2003). *NTMC2*-type-5 proteins are found only in plants, contain single C2 domain along with 4 TM domains rather than one (Fig: 5). Additionally, they all contain an N- terminal transit peptide and are thus putative chloroplastic proteins (Craxton, 2010).

1.8.3 SNARE associated protein (SNARE_AP)

The role of SNAREs and Synaptotagmins in vesicle trafficking is well known, however the part played by the associated proteins is comparatively less explored. One such SNARE-

associated protein (SNARE_AP) was identified in a bioinformatic screen for putative plastidial homologs of cytosolic vesicle trafficking components (Khan et al., 2013). Although homologs for most COPII components such as Sar1, Sec13, Sec23, Sec24, Sec31, SNAREs and the associated proteins were identified through this screen, not much experimental evidence is available as of now for many of them (Khan et al., 2013).

SNARE_AP is a 36.9 kDa protein with an N-terminal chloroplast transit peptide (Target P prediction software, Nielsen et al., 1997; Emanuelsson et al., 2000). SNARE_AP is evolutionarily well conserved protein that is homologous to bacterial Tvp38/DedA family proteins, yeast golgi resident Tvp38 protein (t-SNARE affecting a late Golgi compartment-2 (Tlg2) compartment Vesicle Protein of 38 kDa) as well as slr0305 in *Synechocystis* (Keller and Schneider, 2013). Bacterial DedA family proteins consists of typical DedA domain with TM regions. They are thought to play a role in biogenesis and maintenance of cell membrane (Keller and Schneider, 2013). Yeast Tvp38 was identified through a proteomic screen for golgi proteins. It co-localizes with proteins involved in vesicle transport and was proposed to play a role in membrane trafficking (Inadome et al., 2007; Keller and Schneider, 2013). Taken together this implicates SNARE_AP as a strong candidate protein for similar role in chloroplast and was thus characterized as a part of this thesis.

2. Materials and Methods

2.1 Accession numbers

Table 1 summarises the proteins in this work and the respective gene accession numbers.

Table 1: Gene accession numbers of proteins involved in this work

Name	Accession no
Fuzzy Onion Like (<i>FZL</i>)	At1g03160
Synaptotagmin 5.2 (<i>SYTL5.2</i>)	AT3g19830
SNARE Associated protein (<i>SNARE_AP</i>)	AT1g22850

2.2 Materials

2.2.1 Chemicals

All used chemicals were received from Sigma Aldrich, Roth, Merck, Thermo Fisher Scientific or Serva, unless mentioned otherwise.

2.2.2 Molecular weight and size markers

Lambda phage DNA (Thermo Fisher Scientific) digested using restriction enzymes (either Pst1 or EcoRI and HindIII from New England BioLabs) was used as a marker for agarose gel electrophoresis. peqGOLD[®] protein marker I (VWR, Ismaning, Germany) was used for SDS-PAGE.

2.2.3 Enzymes

Restriction endonucleases, T4 DNA ligase and Phusion DNA polymerase were purchased from New England BioLabs (Frankfurt am Main, Germany), Taq DNA polymerase from BIORON life sciences (Ludwigshafen, Germany) and the enzymes used for gateway cloning (BP and LR Clonase II) were purchased from Invitrogen (Germany).

2.2.4 Column material

Ni-NTA Sepharose beads used for purification of heterologously expressed protein was purchased from Macherey - Nagel.

2.2.5 Membranes

PVDF transfer membrane for western blotting was received from Macherey-Nagel (Germany), blotting paper was obtained from Millipore (Germany).

2.2.6 Oligonucleotides

DNA oligonucleotides were purchased from Metabion (Martinsried, Germany) and are listed in Table 2.

Table 2: Oligonucleotides used for this work

No	Name	Sequence	Purpose
1	FZL AB SalI F	TATAGTCGACTCTGATATCTATCGTGATGCTCGT	Cloning in pET51b+
2	FZL AB NotI R	TATAGCGGCCGCATCTTGTCCAATCGTTTTGATGT	Cloning in pET51b+
3	SYTL5Ab SalI F	ATATGTCGACGGTCTGATTGT	Cloning in pET51b+
4	SYTL5Ab NotI R	ATATGCGGCCGCTTTTAAGTCTT	Cloning in pET51b+
5	SYTL5.2_65 SacI F	ATATGAGCTCATGATTCTACAGTCTT	Cloning in pSP65
6	SYTL5.2_65 HindIII R	ATATAAGCTTTACGGGTTGAAGA	Cloning in pSP65
7	BACKBONE _PST1_ AND_APA1_F	TGCCATCCAGCTGCAGCTCTGGCCCGTG	Gibson cloning
8	BACKBONE _PST1_ AND_APA1_R	AATCATTATTTGGGGCCCGAGATCCATGC	Gibson cloning
9	AttL1_F	CTCGGGCCCCAAATAATGATTTTTATTTGACTGATAGTG	Gibson cloning
10	AttL1_R	GTAGAATCATGGTTCTATCTCCTTGAAG	Gibson cloning
11	SYTL5.2_272aa_ F	AGATAGAACCATGATTCTACAGTCTTCTTCTTC	Gibson cloning
12	SYTL5.2_272aa_ R	CTCCGGATCCATTAAACACGGCGAGATGTC	Gibson cloning
13	AttL2_F	CCGTGTTAATGGATCCGGAGGTGGAGAC	Gibson cloning
14	AttL2_R	AGAGCTGCAGCTGGATGGCAAATAATGATTTTTATTTGAC	Gibson cloning
15	At3g19830 A-F F	ATGGTCTCAGCGGCGGATTCCAGGAGAACGAAGT	Golden gate cloning
16	At3g19830 A-F R	ATGGTCTCAGATTTACCTGACCATTGCCAAAT	Golden gate cloning
17	SYTL5.2 GUS F	GGGGACAAGTTTGTACAAAAAAGCAGGCTTTATTACCGAGAAGACC TTAT	Gateway cloning
18	SYTL5.2 GUS R	GGGGACCACTTTGTACAAGAAAGCTGGGTCACAATCAGACCGTGCT	Gateway cloning
19	SNARE_AP AB SalI F	ATATGTCGACAGATATTTTGCCCGA	Cloning in pMal-c5X
20	SNARE_AP AB EcoR1 R	ATATGAATTCCTAGTGATGATGGTGGTATGAACTTCACAG	Cloning in pMal-c5X
21	SNARE_AP _65 BamHI F	ATATGGATCCATGCGCAGCCTCAC	Cloning in pSP65
22	SNARE_AP _65 HindIII R	CGCGAAGCTTCTTTGCATCTCTC	Cloning in pSP65
23	N618335 LP	TTCTCGGTCCAACCTCATCTG	Genotyping
24	N618335 RP	AATGTGTTTCTCGCCACAATC	Genotyping
25	N533745 LP	CTCTTCCCAAGAAGTGCATTG	Genotyping
26	N533745RP	CTGGTAGCTCGGATTGTGAAG	Genotyping
27	N652584 LP	ACTGCCGAGAAAAAGAATTC	Genotyping
28	N652584 RP	ATCTGCACGTGGAACAAATTC	Genotyping
29	N904515 LP	GAAGACTCACCTGACCATTGC	Genotyping
30	N904515 RP	TGCACAAAAACCTGACAACAC	Genotyping
31	N65685 LP	GCTGACATAAGCCCAAGAGC	Genotyping
32	N65685 RP	TCTGAGAGCGATGATGATGG	Genotyping
33	SALK LB	TCG CTT TCT TCC CTT CCT TTC TCG C	Genotyping
34	WiscDsLox LB	AACGTCCGCAATGTGTTATTAAGTTGTC	Genotyping

2.2.7 Vectors

pUC57 vector was used for sub-cloning gene or gene fragments into expression vectors. Following vectors were used for bacterial expression of proteins: pMAL-c5X vector for N-terminal Maltose binding tag (MBP) and C-terminal His tag fusion protein, pET51b+ vector for N-terminal strep-tag (Promega, Mannheim, Germany) and C-terminal His-tag fusion protein and pET21a vectors for C-terminal His-tag fusion protein (Promega, Mannheim, Germany). pSP65 vector (Promega, Mannheim, Germany) was used for in vitro transcription and translation. For plant transformation the a for mentioned binary vectors were used: pK7FWG2 for GFP tagged protein expression under 35S promoter, pH2GW7 and pB7FWG2 for expression under 35S promoter and pKGWFS7 for GUS expression under endogenous promoter (Plant Systems Biology, Belgium). Cloning into binary vectors was performed using the Gateway system (Thermo Fisher Scientific) via pDONR207 vector or Golden gate cloning. All plasmids used for this work are listed in Table 3.

Table 3: List of plasmids used for this work

No	Gene / Insert	Vector	Description	Purpose	Source
1	FZL-CC1 domain	pET51b+	N-term Strep tag C-term ¹⁰ His tag	Antigen fragment used for antibody generation	This work
2	SYTL5.2	pUC57	-	Sub-cloning	Genscript
3	SYTL5.2 -N term (31-272aa)	pET51b+	N-term Strep tag C-term ¹⁰ His tag	Bacterial Overexpression, N-terminal Antigen fragment used for antibody generation	This work
4	SYTL5.2-C term (516-666aa)	pET21a+	N-term ⁶ His tag	Bacterial Overexpression, C-terminal Antigen fragment used for antibody generation	Genscript
5	SYTL5.2 FL	pSP65	-	In vitro Imports into chloroplasts	This work
6	SYTL5.2::1-272aa	pDONOR-207	-	Entry vector for GFP expression and localization	This work
7	SYTL5.2::1-272aa	pK7FWG2	C-term GFP	GFP expression and localization in Tobacco	This work
8	SYTL5.2 Promoter + intron + exon FL	pCambia	-	Expression in <i>Arabidopsis</i>	This work
9	SYTL5.2	pDONOR-207	-	Entry vector for GUS expression vector (-1000bp to 105bp insert)	This work
10	SYTL5.2	pKGWFS7	C-term GFP and GUS	GUS expression vector (-1000bp to 105bp insert)	This work
11	SNARE_AP FL	pDONOR-207	-	Entry vector	Simon Schrott, bachelor's thesis
12	SNARE_AP FL	pK7FWG2	C-term GFP	GFP expression and localization in Tobacco, Expression in <i>Arabidopsis</i>	Simon Schrott, bachelor's thesis

No	Gene / Insert	Vector	Description	Purpose	Source
13	SNARE_AP - FL	pH2GW7	-	Expression in <i>Arabidopsis</i>	This work
14	SNARE_AP-TP	pMAL-c5X	N-term MBP C-term ⁶ His tag	Bacterial Overexpression, FL-TP Antigen fragment used for antibody generation	This work
15	SNARE_AP FL	pSP65	-	In vitro Imports into chloroplasts	Genscript
16	FNR L1	pSP65	-	In vitro Imports into chloroplasts	Bettina Bölter

2.2.8 Antibodies

Antisera for D1, CoxII, Cytf, PsaF, CP47, CF₁- β and LHCPs were obtained from Agrisera (Lund, Sweden). Antisera against TPI, GAPC-1 and SDH4 were obtained from Phytolab (Vestenbergsgreuth, Germany). Cytb₆ and CF₁- α / β antisera were kind gift from Jörg Meurer, as were G6PDH Antisera from Antje von Schaewen. Toc64, Tic110, FBPase, PORB antibodies were previously raised by our group as described in following articles: Toc64 (Schweiger et al., 2012), Tic110 (Lübeck et al., 1996), FBPase (Benz et al., 2009), and PORB (Duy et al., 2007). Purified atFZL (486-770aa), atSYTL5.2 C-terminal 516-666aa) and atSNARE_AP (94-344aa) protein was injected into rabbits to raise polyclonal antiserum (Pineda antibodies, Berlin, Germany). Antisera against atSYTL5.2N-terminal (31-272aa) fragment was generated using similar method by Biogenes (Berlin, Germany).

2.2.9 Software

Chromas (Technelysium, Australia) was used to align and check DNA sequences. VectorNTI (Thermo Fisher Scientific) was used to analyze and construct plasmid clones. Aramemnon (aramemnon.uni-koeln.de) and Tair (www.arabidopsis.org) databases were used to retrieve DNA / protein sequences and NCBI Blast server (<http://blast.ncbi.nlm.nih.gov>) was used to match sequences. TM Pred, a tool from Expacy proteomics server was used for prediction of transmembrane helices and TargetP server (<http://www.cbs.dtu.dk>) was used for prediction of targeting peptide sequences. Phyre2 (www.sbg.bio.ic.ac.uk/~phyre) was used for protein structure prediction. Image analysis was done using Fiji ImageJ software.

2.3 Microbiological methods

2.3.1 Bacterial strains

E. coli TOP10 or NEB super competent cells were used for cloning and propagation of plasmid DNA. *E. coli* BL21(DE3) cells, BL21 pLys cells, Rosetta 2 cells or RIPL (BL21-CodonPlus (DE3)-RIPL strain) cells were used for heterologous expression of fusion proteins.

A. tumefaciens AGL1 cells were used for transient transformation of *Nicotiana tabacum* with GFP tagged protein. For stable transformation of *A. thaliana* plants, *A. tumefaciens* GV3101 (pMP90RK) cells were used.

2.3.2 Media and growth

E. coli was cultivated in either liquid LB culture or on LB agar plates supplemented with the appropriate antibiotics (1% tryptone, 0.5% yeast extract, 1% NaCl ± 1.5% agar) at 37°C. Antibiotic concentrations used were as follows: ampicillin 100 µg/ml, kanamycin 50 µg/ml, gentamycin 50 µg/ml and spectinomycin 100 µg/ml.

Agrobacterium was cultivated in either liquid LB culture or on LB agar plates supplemented with the appropriate antibiotics at 28°C. Antibiotic concentrations used were as follows:

- For GV3101 cells: 50 µg/ml kanamycin
- For AG1 cells: 100 µg/ml carbenicillin
- For Ti-plasmid: 100 µg/ml rifampicin
- For transformed vector: spectinomycin 100 µg/ml or kanamycin 50 µg/ml

2.3.3 Bacterial transformation

The transformation of the bacteria was done using heat shock method as described in Sambrook *et al.*, 1989.

2.3.4 Transformation of *A. tumefaciens*

0.5 – 1 µg plasmid was added to chemically competent *Agrobacteria* for stable transformation of *A. thaliana*. Cells were incubated for 5 min on ice, 5 min in liquid nitrogen followed by heat shock for 5 min at 37°C. Then 800 µl LB media was added to the cells and incubated at 28°C. After shaking for 4 hr, cells were plated on LB plates with appropriate antibiotics and grown for 3 days at 28 °C.

2.4 Molecular Biological methods

2.4.1 Cloning strategies

All the plasmids used in this study were made using either of the following methods: classical cloning method using restriction enzymes, GIBSON cloning, Gateway cloning or golden gate cloning strategy. Table 4 summarizes the detailed strategy used for each clone. Briefly, classical cloning method was used for fusion protein overexpression clones. PCR products were amplified with phusion Taq polymerase (Thermo Fisher Scientific) using primers containing appropriate restriction sites. The purified PCR product and the vector was digested with respective enzymes and ligation was carried out overnight at

4°C using T4 ligase. For transient or stable plant transformation clones, GIBSON cloning (New England BioLabs), gateway cloning system (Thermo Fisher Scientific) or golden gate cloning strategy (Binder et al. 2014) was used to clone constructs via homologous recombination from pDONR207 into binary vectors pK7FWG2, pKGWFS7, pH2GW7 or pB7FWG2. Cloning was performed according to the manufacturer's instructions.

Table 4: list of plasmids and the respective cloning strategy used.

	Gene / Insert	Vector	Purpose	Cloning Strategy
1	FZL-CC1 domain	pET51b+	Antigen fragment used for antibody generation	Classical cloning (Sall / NotI)
2	SYTL5.2 -N term (31-272aa)	pET51b+	Bacterial Overexpression, N- terminal Antigen fragment used for antibody generation	Classical cloning (Sall / NotI)
3	SYTL5.2-C term (516-666aa)	pET21a+	Bacterial Overexpression, C- terminal Antigen fragment used for antibody generation	Classical cloning (NdeI / XhoI)
4	SYTL5.2 FL	pSP65	In vitro Imports into chloroplasts	Classical cloning (SacI / HindIII)
5	SYTL5.2_1-272aa	pDONOR-207	Entry vector for GFP expression and localization	GIBSON cloning
6	SYTL5.2_1-272aa	pK7FWG2	GFP expression and localization in Tobacco	Gateway cloning
7	SYTL5.2 Promoter + intron + exon FL	pCambia	Expression in <i>Arabidopsis</i>	Golden gate
8	SYTL5.2	pDONOR-207	Entry vector for GUS expression vector (-1000bp to 105bp insert)	Gateway cloning
9	SYTL5.2	pKGWFS7	GUS expression vector (-1000bp to 105bp insert)	Gateway cloning
10	SNARE_AP FL	pDONOR-207	Entry vector	Gateway cloning
11	SNARE_AP FL	pK7FWG2	GFP expression and localization in Tobacco, Expression in <i>Arabidopsis</i>	Gateway cloning
12	SNARE_AP -FL	pH2GW7	Expression in <i>Arabidopsis</i>	Gateway cloning
13	SNARE_AP-TP	pMAL-c5X	Bacterial Overexpression, FL-TP Antigen fragment used for antibody generation	Classical cloning (Sall / EcoRI)
14	SNARE_AP FL	pSP65	In vitro Imports into chloroplasts	Classical cloning (BamHI – HindIII)

2.4.2 Polymerase chain reaction (PCR)

Genomic DNA, cDNA or plasmid DNA was used as templates for PCRs. PCR for cloning was performed with Phusion polymerase which has a proof-reading activity. PCRs for

genotyping of mutant lines or for screening positive colonies during cloning were done using DFS Taq polymerase. For cloning PCRs, 10-20 ng of plasmid DNA or 1:10 diluted cDNA was used as template and for genotyping PCRs 1 µl genomic DNA (isolated as mentioned in section 2.4.5) was used as template. Annealing temperature and elongation time were adapted depending on the oligonucleotides, polymerase used and the length of the PCR fragment. PCR products were run on a 1 % agarose gel run in TAE buffer (40 mM Tris, 2.5 mM EDTA, 1 % acetic acid). For cloning or sequencing purposes, the PCR bands were excised from the gel and purified using NucleoSpin Gel and PCR Clean-up kit (Macherey-Nagel).

2.4.3 Isolation of plasmid DNA from *E. coli*

Plasmid DNA was isolated from 4 ml overnight *E. coli* culture using the NucleoSpin Plasmid EasyPure kit (Macherey-Nagel) according to the manufacturer's instructions.

2.4.4 Sequencing

The T-DNA insertions in the mutant lines and the sequence of all the plasmids used in this work was confirmed by sequencing. The sequencing service of the Faculty of Biology (Ludwig-Maximilian's-Universität München, Germany) performed the sequencing using 150 - 200 ng of vector / DNA with appropriate primer.

2.4.5 Isolation of plasmid DNA from *A. tumefaciens* for genotyping PCR

One leaf was homogenized in 500 µl high purity extraction buffer (100m M Tris pH 7.5, 50 mM NaCl, 50 mM EDTA, 1% (w/v) PVP) using tissue lyser. 66 µl of 10% SDS and 166µl of potassium acetate buffer (5 M potassium acetate, 11.5 % glacial acetic acid) was added to the sample, mixed and centrifuged at 16000 g at room temperature for 15 min. Supernatant was transferred to new tube and 0.7 volume of isopropanol was added to the sample, mixed and incubated for 20 min at 4°C. The sample was then centrifuged at 16000 g at room temperature for 15 min to pellet the gDNA and washed once with 70 % ethanol before drying at 37 °C. DNA was resuspended in 40 µl H₂O.

2.4.6 Isolation of genomic DNA from *A. thaliana* for cloning

gDNA from 7-14 days old *A. thaliana* leaves was isolated using the DNeasy Plant Mini kit (Qiagen) according to the manufacturer's instructions.

2.4.7 Isolation of RNA from *A. thaliana*

RNA from *A. thaliana* leaves was isolated using the RNeasy Plant Mini kit (Qiagen) according to the manufacturer's instructions.

2.4.8 cDNA synthesis

cDNA was synthesized using M-MLV reverse transcriptase (Promega) kit using 1 µg RNA according to the manufacturer's instructions.

NOTE: General methods not listed above were performed according to Sambrook *et al.* (1989).

2.5 Biochemical methods

2.5.1 Overexpression of recombinant proteins

E. coli transformed with appropriate plasmid for overexpression were grown in LB medium (1 % peptone from casein, 0.5 % yeast extract, 1 % NaCl) at 37 °C. After the cell density of OD600 of 0.4 - 0.5 was reached, expression was induced by addition of 0.5 mM isopropyl β-D-1-thiogalactopyranoside. *E. coli* strains and conditions for overproduction were depending on the construct and are listed in Table 5.

Table 5: Conditions for overproduction and way of purification of recombinant proteins

No	Construct	<i>E. Coli</i> strain	Temperature	Time	Solubility of expression
1	pET51b+_FZL-CC1 domain	BL21 (DE3)	37°C	3hr	Inclusion bodies
2	pET51b+_SYTL5.2 -N term (31-272aa)	Rosetta 2	18°C	overnight	Inclusion bodies
3	pET21a+_SYTL5.2-C term (516-666aa)	RIPL	18°C	overnight	Soluble and Inclusion bodies
4	pMal-c5X_SNARE_AP-TP	BL21 pLys	18°C	overnight	Soluble and Inclusion bodies

2.5.2 Purification of proteins from inclusion bodies

Cell pellet of 1 l culture expressing the respective recombinant protein in inclusion bodies was resuspended in 30 ml resuspension buffer (50 mM Tris-HCl pH 8.0, 200 mM NaCl, 5 mM β-Mercaptoethanol). Cells were disrupted using microfluidizer (Microfluidics, Westwood, USA) or French press, sonified and pelleted at 48298 g for 5 min at 4 °C. The pellet was sequentially washed 3-5 times with detergent buffer (20 mM Tris-HCl pH 7.5, 200 mM NaCl, 1 % Deoxycholic acid, 1 % Nonidet P-40, 10 mM β-Mercaptoethanol) followed by 2 washes with triton X-100 buffer (20 mM Tris-HCl pH 7.5, 0.5 % Triton X-100, 5 mM β-Mercaptoethanol) and 2 washes with tris buffer (20 mM Tris-HCl pH 8.0, 10 mM DTT). For each wash the pellet was resuspended in buffer, vortexed for 5 min and then centrifuged at 7728 g, 5 min at room temperature. Finally, the pellet of inclusion bodies was resuspended in 5 ml of tris buffer and stored at -20 °C or solubilized.

Solubilization of inclusion bodies was done in either SDS buffer (50 mM Tris pH 8.0, 100 mM NaCl, 1 % SDS) or urea buffer (50 mM Tris pH 8.0, 100 mM NaCl, 7 M urea) by overnight rotation at room temperature. The desaturated protein was then obtained by centrifugation at 20,000 g, room temperature for 15 min in the supernatant and purified using affinity chromatography.

2.5.3 Purification of soluble proteins

1 l culture of bacterial cells expressing the respective recombinant protein in inclusion bodies was centrifuged at 12075 g for 10 mins at 4 °C and the cell pellet was resuspended in 30 ml of lysis buffer (50 mM Tris pH 8, 100 mM NaCl, 20 mM imidazole). Cell disruption was performed by a microfluidizer (Microfluidics, Westwood, USA) and the solution was centrifuged at 20000 g, 4 °C for 30 min to obtain the supernatant that was further used for Nickel affinity purification.

2.5.4 Nickel affinity purification of proteins

The supernatant containing the recombinant protein was incubated with 250 µl Ni NTA Sepharose at 4 °C overnight for binding of His tagged proteins to the beads. The beads were washed three times with 5 ml wash buffer (50 mM Tris pH 8, 100 mM NaCl, 40 mM imidazole). Recombinant proteins were eluted in 200 – 500 µl fractions with elution buffer (50 mM Tris pH 8, 100 mM NaCl, 500 mM imidazole).

2.5.5 Isolation of proteins from *A. thaliana* leaves

A. thaliana leaves were either homogenized in 300 µl homogenization medium (50 mM Tris pH 8.0, 10 mM EDTA, 2 mM EGTA, 10 mM DTT) using an electronic micro pestle or crushed in liquid nitrogen using mortar and pestle. The crushed powder was then resuspended in equal volume of homogenization medium. The suspension was incubated for 10 min in the dark on ice for protein extraction, filtered through gauze and centrifuged at 9300 g, 4 °C for 10 min. Soluble proteins were separated in the supernatant and pellet resuspended in homogenization medium contained membrane proteins.

2.5.6 Determination of protein concentration

Concentration of soluble proteins was determined using Bradford reagent (0.1 % Coomassie brilliant blue G-250, 5 % ethanol, 10 % phosphoric acid). 1 µl protein was mixed with 1:5 diluted Bradford reagent and absorption was measured against buffer at 595 nm. Concentration of membrane proteins was determined using BCA (bicinchoninic acid) method using Pierce BCA Protein Assay Kit (Thermo Scientific, Rockford, USA) as per manufacturer's instructions.

2.5.7 SDS polyacrylamide gel electrophoresis (SDS-PAGE)

The separation of proteins was performed according to (Laemmli, 1970). Purified proteins were resolved on discontinuous SDS-PAGE gels (ratio of acrylamide to N, N'- ethylene bisacrylamide 30:0.8). Depending on the size of the proteins being separated and analysed, resolving gel with 10 -15 % polyacrylamide was used, with a stacking gel of 5 % polyacrylamide. Samples prepared in SDS loading buffer (62.5 mM Tris pH 6.8, 2 % SDS, 10 % glycerol, 5 % β -mercapto ethanol, 0.004 % bromphenol blue) were loaded onto the gels, run at 25 mA in SDS running buffer (25 mM Tris, 192 mM glycine, 0.1 % SDS).

2.5.8 Commassie staining of polyacrylamide gels

SDS-PAGE gels were stained with either Coomassie (45 % methanol, 9 % acetic acid, 0.2 % Coomassie brilliant blue R-250). The gels were destained by incubating the gels in destaining solution (40 % methanol, 7 % acetic acid) and later water before drying under vacuum.

2.5.9 Semi-dry electro blot and immunodetection of proteins

Proteins separated on SDS gels were electro transferred onto a PVDF membrane (Zefa Transfermembran Immobilon-P, 0.45 μ m, Zefa-Laborservice GmbH, Harthausen, Germany) using semi-dry-blot apparatus (Amersham Biosciences) for immunodecoration. The PVDF membrane was activated by incubation in methanol for 2 min at room temperature. Blot was assembled in following order: three blotting papers soaked in transfer buffer (25 mM Tris, 192 mM glycine, 20 % methanol), activated membrane, gel, three blotting papers soaked in transfer buffer. Transfer was done for 2 h at 0.8 mA / cm² of surface area of the blot and protein transfer onto the membrane was tested by staining with ponceau solution (5 % acetic acid, 0.3 % ponceau S). For immunodetection of proteins, membrane was blocked for 1 h with 5 % skimmed milk in TBST (20 mM Tris pH 7.6, 137 mM NaCl, 0.075 % Tween), washed with TBST and incubated overnight in appropriate primary antibody at 4 °C. The membrane was washed thrice in TBST for 10 min each before incubating in appropriate horse radish peroxidase conjugated secondary antibody for 1 h at room temperature. This was followed by three washes of 10 min each in TBST. The signal was detected using Enhanced Chemiluminescence (ECL) method. ECL solution I (100 mM Tris pH 8.5, 1 % luminol, 0.44 % coumaric acid) and ECL solution II (100 mM Tris pH 8.5, 0.018 % H₂O₂) were mixed in ratio 1:1, added onto the immune decorated blots and signal was detected with Image Quant LAS 400 (GE Healthcare).

2.5.10 Blue Native PAGE (BN-PAGE) and second dimension SDS-PAGE

BN-PAGE was performed as described previously in Nickel et al (Nickel et al., 2016). Thylakoid membranes were isolated from the leaves of WT and mutants and total protein and chlorophyll concentration was measured. Sample preparation was done as follows: WT thylakoid membranes equivalent to 30 µg chlorophyll were pelleted at 3300 g, 3 min, 4 °C. For mutant samples, thylakoid membranes corresponding to equal amount of protein compared to WT were used. Pellets were solubilized in 70 µl ACA buffer with 1 % n-dodecyl β-D-maltoside (β-DM) for 10 min on ice and centrifuged for 10 min at 16000 g, 4 °C. 6 µl BN loading buffer (750 mM aminocaproic acid, 5 % Serva-G 250) was added to the supernatant prior to loading on BN-PAGE. The gel was run at 30 mA overnight (approximately 14 h) with cathode buffer (50 mM tricine, 15 mM Bis-Tris pH 7.0, 0.2 % comassie Serva-G 250) and anode buffer (50 mM Bis-Tris pH 7.0). When the samples had run till half the total length of the gel, further run was done using the cathode buffer without comassie (50 mM tricine, 15 mM Bis-Tris pH 7.0). The protein complex from the first dimension were further resolved on SDS gel containing 4 M urea. For this one lane of the BN gel was placed on top of an SDS gel and run overnight at 4 mA. The SDS gel was stained by silver staining method to visualise the spots.

2.5.11 Silver staining of SDS gels

Silver staining was done according to Ansorge et al (Ansorge, 1985). Briefly, proteins in gel were fixed by overnight incubation in fixative solution (50 % ethanol, 12 % acetic acid, 0.05 % formaldehyde), washed three times for 30 min in 50 % ethanol followed by pre-impregnation in 0.02 % sodium thiosulfate for 90 s. The gels were washed thrice in water (30 s each) prior to 30 min impregnation in darkness using 0.2 % silver nitrate and 0.075 % formaldehyde. Gels were washed again in water for 3 s each, three times and stained in developing solution (6 % Na₂CO₃, 0.05 % formaldehyde, 0.0004 % sodium thiosulfate) till the protein spots were visible. The reaction was ceased with stop / destain solution (50 % ethanol, 12 % acetic acid).

2.5.12 *In vitro* transcription

pSP65 vector containing SP6 promoter was used for *in vitro* transcription of full length proteins (See table 3). For transcription reaction, 1 µg plasmid, 0.05 % BSA, 2 mM DTT, 0.25 mM m⁷G(5')ppp(5')G Cap analog (Ambion), 0.4 mM ACU (Roche), 50 U RibolockRI (Thermo Fisher Scientific), 30 U SP6 RNA polymerase (Thermo Fisher Scientific), 1x transcription buffer (Thermo Fisher Scientific) was added in total volume of 50 µl, incubated at 37 °C for 15 min for RNA capping. To this capped RNA, 1.2 mM GTP was added and reaction was incubated at 37 °C for 120 min for final mRNA.

2.5.13 *In vitro* translation

In vitro translation of radiolabelled proteins was done using reticulocyte lysate (Promega). 1 µl *in vitro* transcription product was used for 10 µl translation reaction with 30µCi ³⁵S methionine (Perkin Elmer, Walluf, Germany), 80 µM amino acid mixture without methionine, 66 % reticulocyte lysate and 70 mM KCl. Translation was carried out at 30 °C for 50 min.

2.5.14 Detection of radio-labelled proteins

Radio-labelled proteins imported into chloroplast were separated on a SDS gel, stained with Commassie staining method and dried. The SDS gels were exposed to BAS-MS phosphor imaging plates (FUJIFILM) overnight before being analysed on a Typhoon scanner (GE healthcare).

2.5.15 Mass spectroscopy

Mass spectrometry was done at MSBioLMU core facility (Department Biology I, Ludwig-Maximilians-Universität München) to confirm the peptide sequence of proteins sent for antibody generation.

2.5.16 Chlorophyll isolation

Isolation of chlorophyll from leaf material was performed as previously described by Lichtenthaler *et al* (LICHTENTHALER and WELLBURN, 1983). Under green light, leaf material was homogenised in 1 ml of 100 % acetone and CaCO₃ using mortar and pestle. The homogenate was centrifuged for 5 min at 16000 g at 4 °C and then 500 µl of hexane and 50 µl of 5 M NaCl was added to the supernatant. Samples were then centrifuged again for 5 min at 16000 g at 4 °C to remove contaminations by phase separation of chlorophylls. Absorbance was measured at 645 nm, 663 nm and 750 nm and chlorophyll concentrations were determined as described by Arnon *et al* (Younis *et al.*, 2012). Using the following formula:

$$\text{mg chlorophyll / ml} = 8.02 \times (\text{E663} - \text{E750}) + 20.2 \times (\text{E645} - \text{E750})$$

Isolation of chlorophyll from cotyledon samples from greening experiment was done using dimethyl formamide (DMF) as described by (Porra *et al.*, 1989). Cotyledon tissue samples were harvested, weighed and then incubated in 1 ml DMF for 2 h in the dark. Absorbance was measured at 663, 750 and 645 nm and chlorophyll concentration were calculated using the above formula.

2.6 Plant biological methods

2.6.1 Plant material

For all experiments performed with *Arabidopsis thaliana* plants, ecotype Columbia-0 (Col-0, Lehle Seeds; Round Rock, USA) were used. The T-DNA lines used in this study are summarized in table 6 below and were purchased from NASC (University of Nottingham, GB). Peas (*Pisum sativum*) var. “Arvica” were ordered from Bayerische Futtersaatbau (Ismaning, Germany).

Table 6: T-DNA insertion lines used in this study

No	Name	Line	NASC Id	T-DNA insertion
1	Fuzzy Onion Like (<i>fzl-1</i>)	SALK_118335C	N618335	1st Exon
2	Fuzzy Onion Like (<i>fzl-1</i>)	SALK_033745C	N533745	2nd Exon
3	Fuzzy Onion Like (<i>fzl-1</i>)	SALK_152584C	N652584	4th Exon
4	Synaptotagmin 5.2 (<i>syt5.2</i>)	WiscDsLoxHs048_01C	N904515	7th Exon
5	SNARE associated protein (<i>snare_ap</i>)	SALK_095443	N65685	3rd Exon

2.6.2 Plant growth conditions

Arabidopsis thaliana WT Columbia ecotype (Col-0) and the mutant plants were grown either on soil or on half-strength MS (Murashige and Skoog) medium supplied with 1 % sucrose and 1.2 % Phyto-agar under controlled conditions in a growth chamber. For plants grown on soil; Seeds were sown and vernalized at 4 °C in the dark for 2 days to synchronize germination. For sowing seed on sterile plates, seeds were surface-sterilized by washing once with 70 % ethanol with 0.1 % Tween-20 for 15 min and then thrice with 100 % ethanol, dried before sowing. The plates were sealed and vernalized at 4 °C for 2 days. For phenotyping analysis plants were grown on soil in long day condition (16 h/8h light/dark, 22 °C, 100 $\mu\text{mol}/\text{m}^2\text{s}$ in fluorescent light conditions) or in case of *fzl* plants under LED light (22 °C, 200 $\mu\text{mol}/\text{m}^2\text{s}$ light, 16 /8 h light/dark).

Peas (*Pisum sativum*) plants were grown on sand and vermiculite in fluorescent light conditions (12/12 h dark/light, 22 °C, 100 $\mu\text{mol}/\text{m}^2\text{s}$) in growth chambers and *Nicotiana benthamiana* plants were grown under controlled conditions in green house.

2.6.3 Cross fertilization of *A. thaliana*

FZL mutant lines (*fzl-1*: SALK_118335, *fzl-2*: SALK_033745C and *fzl-3*: SALK_152584C) were back crossed with WT *Arabidopsis thaliana* plants, ecotype Columbia-0. Briefly, mature flowers with visibly dehiscent anthers were used as male parent and the unopened flower buds that had no dehiscent anthers were used as female parents. For each female

parent flower, using thin sharp forceps, the carpels were carefully isolated by removing the sepals, petals and anthers. Pollen from the male parent flowers were then brushed on to this isolated carpel. After 2-4 weeks, the elongated siliques resulting from the cross were carefully harvested. The F1 and F2 generations of the mutant plants obtained after crossing were screened for heterozygous and homozygous T-DNA insertion lines respectively by genotyping PCR and sequencing.

2.6.4 Isolation of intact chloroplasts from *P. sativum*

Leaf material from 8-10 days old peas (plants used were taken from dark to avoid starch accumulation that results in breaking of chloroplasts) was mixed in isolation buffer (330 mM sorbitol, 20 mM MOPS, 13 mM Tris pH 7.6, 3 mM MgCl₂, 0.1 % BSA) using a kitchen blender. The solution was filtered through 1 layer of gauze and centrifuged for 1 min at 1900 g, 4 °C. The pellet was resuspended in 10-20 ml isolation buffer, loaded on a discontinuous percoll gradient to separate intact and broken chloroplasts by centrifugation for 5 min at 8000 g, 4 °C. Percoll gradients were made by overlaying 12 ml 40 % percoll solution on top of 8 ml 80 % percoll solution, both made in 330 mM sorbitol, 1 M HEPES pH 7.6. The intact chloroplast thus obtained were washed twice with washing buffer (330 mM sorbitol, 1 mM HEPES pH 7.6, 1 mM MgCl₂), 1 min at 8000 g, 4 °C. To quantify the amount of chlorophyll, 1 µl chloroplast solution was mixed in 1 ml 80 % acetone, filtered through a gauze and absorbance was measured at A645, A663 and A750. The amount of chlorophyll was calculated using the formula described in section 2.3.13.

2.6.5 *In vitro* import into chloroplasts from *P. sativum*

In vitro import of radio-labelled protein was done using freshly isolated chloroplasts equivalent to 10 µg chlorophyll in final reaction volume of 100 µl. Each 100 µl reaction contained 1 x import buffer (330 mM sorbitol, 50 mM HEPES pH 7.6, 3 mM MgCl₂, 10 mM methionine, 10 mM cysteine, 0.2 % BSA, 20 mM kalium gluconate, 10 mM NaHCO₃, 3 mM ATP) and 5 µl ³⁵S labeled reticulocyte lysate translated preprotein. The reaction was incubated at 15 min at 25 °C to allow linear import of preproteins into the chloroplasts. Then the sample was overlaid on 300 µl of 40 % percoll and centrifuged at 4500 g, 5 min, 4 °C to re-isolated intact chloroplasts. Pellet was washed twice in 100 µl washing buffer (330 mM sorbitol, 50 mM HEPES/KOH, pH 7.6 and 3 mM MgCl₂, 1100 g, 1 min, 4 °C) and further treated with thermolysin (10 µg/ml, 2 min on ice) to digest residual protein that was not imported. The proteolysis reaction was arrested using 1 µl 500 mM EDTA and the pellet was washed in 100 µl washing buffer. The final pellet was

resuspended in SDS loading buffer, heated for 2 min at 95 °C and loaded on SDS gel. Radioactive signals were detected by phosphor plate imaging.

2.6.6 Isolation of thylakoid membranes

Leaf material from 21 days old *A. thaliana* plants grown on either soil (in case of *fzi* plants) or on MS-sugar plates (in case of *snare_ap* plants) was used to isolate thylakoid membranes. The material was homogenized in 25 ml isolation medium (330 mM sorbitol, 50 mM HEPES pH 7.5, 2 mM EDTA, 1 mM MgCl₂, 5 mM ascorbic acid) using polytron homogenizer. The suspension was filtered twice through a gauze and centrifuged at 760 g at 4 min, 4 °C. Pellet was washed in washing buffer (5 mM sorbitol, 50 mM HEPES pH 7.5) and resuspended in TMK buffer (100 mM sorbitol, 50 mM HEPES pH 7.5, 5 mM MgCl₂). The sample was incubated in dark for 10 min on ice, centrifuged and resuspended in approximately 1 ml of TMK buffer. Total protein and chlorophyll content was determined and samples preparation for BN-PAGE was done as described in section 2.3.10.

2.6.7 Isolation of inner and outer chloroplast envelope from *P. sativum*

Plant material from 20 trays of 9-11 days old pea seedlings was harvested in dark and homogenized in 5-7 l of isolation medium (330 mM sorbitol, 20 mM MOPS, 13 mM Tris, 0.1 mM MgCl₂, 0.02 % (w/v) BSA). The suspension was filtered through four layers of mull and one layer of gauze (30 µm pore size) and centrifuged for 5 min at 1500 g. Using a soft brush, the pellet was gently resuspended in small volume of isolation medium and overlaid onto discontinuous Percoll gradient (as described in section 2.4.4). Intact chloroplasts separated at the interface were transferred to 250 ml beakers and washed twice with wash media (330 mM sorbitol, Tris-base pH 7.6). The chloroplasts were burst by incubation in a hypotonic 0.7 M sucrose buffer and then pottering in down's homogenizer. The suspension was further treated according to the modification (Waegemann et al., 1992) of the previously described method (Keegstra and Yousif, 1986).

2.6.8 Greening of etiolated seedlings of *A. thaliana*

Sterile seeds were densely put out on half strength MS (Murashige and Skoog) plates with sugar and vernalized at 4 °C for 2 days. The plates were exposed to light (100 µmol / m²s, 22 °C, fluorescent light conditions) for 2 h and kept in the dark for etiolation. After 6 days, the plates were illuminated, and samples were collected after 4, 6, 8 and 24 hrs for chlorophyll isolation and PAM measures.

2.6.9 Stable transformation of *A. thaliana* with *A. tumefaciens*

25 ml preculture inoculated with *A. tumefaciens* (strain GV3101) transformed with appropriate plasmid was used to inoculate 400 ml culture and grown overnight at 28 °C. The cell pellet harvested after centrifugation for 20 min at 1900 g was resuspended in infiltration medium (5 % sucrose, 0.05 % silwet L-77) such that cell density of OD₆₀₀ 0.8 - 1 was reached. Flowers of 6 - 7 weeks old *A. thaliana* plants were dipped in this medium with agrobacteria for 5 - 10 sec to allow transformation. The seeds harvested from these plants were selected for transformed lines either on soil in case of BASTA resistance or on plates in case of Kanamycin and Hygromycin resistance.

2.6.10 Measurement of chlorophyll fluorescence

The photosynthetic performance of plants was evaluated by measuring chlorophyll fluorescence of dark-adapted plants. The measurements were done at room temperature using the MINI version of the Imaging PAM (Walz). The area of interest of leaves in the mid-vein region was selected from the digital images using the ImagingWin (Walz) software and F_v / F_m ratios were determined to quantify photosynthetic performance. The electron transfer rates through PSII [ETR] was calculated from the light curves obtained by successively illuminating the plants with increasing light intensities with interval of 20 s each.

2.6.11 Transient transformation of *N. benthamiana*

Subcellular localization of proteins was analysed by transient expression of GFP-fusion proteins in 3 - 4 weeks old *Nicotiana benthamiana* plants. *Agrobacterium tumefaciens* (AGL1) transformed with plasmid of interest was grown in LB medium with appropriate antibiotics. When cell density of 0.5 OD₆₀₀ was reached, cells were pelleted (centrifugation: 15 min at 4000 rpm) and resuspended in infiltration medium (10 mM MgCl₂, 10 mM MES/KOH pH 5.6, 150 µM Acetosyringone) such that OD₆₀₀ is 1. This cell suspension was incubated in dark for 2 h (rotating) and then used to infiltrate the abaxial surface of *Nicotiana benthamiana* leaves. Infiltrated plants were grown for two-three days before isolation of protoplast for observing the expression of GFP-fusion protein.

2.6.12 Isolation of protoplast from *N. benthamiana* for GFP localization

Nicotiana benthamiana leaves transiently expressing GFP-fusion proteins were used for isolation of protoplasts. The leaves cut approximately 0.2 - 0.4 cm wide and 1 cm long stripes were incubated in 10 ml enzyme solution (1 % Cellulase R10 and 0.3 % Macerozyme R10) made in F-PIN medium (MS medium PC-vitamins (200 mg/l Myoinositol, 1 mg/l thiamin-HCl, 2 mg/l Ca-panthotenate, 2 mg/l nicotinic acid, 2 mg/l pyridoxin-HCl, 0.02 mg/l biotin, 1 mg/l 6-benzylaminopurin (BAP), 0.1 mg/l α-

naphtaleneacetic acid (NAA), 20 mM MES, pH 5.8 (KOH), 80 g/l glucose, Osm 550) for 2 h rotating in dark at 40 rpm on bench top shacker. After a short 1 min rotation at 80 rpm, the suspension was filtered through 100 μ M Nylon-membrane and overlaid with 2 ml F-PCN medium (F-PIN, except instead of glucose, sucrose was added as the osmoticum). The gradient was centrifuged for 10 min at 70 g (slow deceleration) to separate intact protoplasts at the interface between the F-PIN and F-PCN media. The protoplasts were transferred to new tubes and washed with 10 ml W5 buffer (centrifugation: 10 min at 50 g). GFP fluorescence was observed with a TCS-SP5 confocal laser scanning microscope (Leica, Wetzlar, Germany).

2.7 Microscopy

2.7.1 Laser scanner microscopy for measurement of chloroplast diameter

The diameter of chloroplasts was measured by detecting the chlorophyll auto-fluorescence using confocal laser scanning microscope from Leica, Type: TCS SP5. Leaves from 21-day old *fz*/mutant and the respective outcrossed WT lines were used for imaging as described in Schweiger and Schwenkert, 2014 (Schweiger and Schwenkert, 2014). Diameters of at least 50 chloroplasts were measured using Fiji ImageJ software.

2.7.2 Light and Transmission electron microscopic (TEM) analysis

For preparation and microscopic analysis of *syt15.2* and WT plants:

Sample preparation and imaging was performed by Dr. Irene Gügel. 14-day-old plants harvested in the morning before onset of light. Five plants were prefixed immediately with 2.5 % (w/v) glutaraldehyde (4 °C) in 75 mM cacodylate buffer (2 mM MgCl₂, pH 7.0). The dissection of vegetative leaf 4 was done systematically in ice-cold fixative. Two positions of the leaf were chosen. The tip sample was dissected at about 90 % of the total leaf length and the base at 5 to 15 % (Gügel and Soll, 2017). The samples were further fixed with 2.5% (w/v) glutaraldehyde (4°C, at least 24 h) in 75 mM cacodylate buffer (2 mM MgCl₂, pH 7.0) and processed as described previously (Li et al., 2015). For light microscopy, semithin-sections (1-2 μ m) were prepared oriented from the margin to the midrib and as perpendicular cross cuts of the leaf sample with a glass knife (Pyramitome 11800, LKB). Overviews were taken at 400x magnification. Ultrathin-sections (45-60 nm) for transmission electron microscopy were prepared with an ultramicrotome (EM UC6, Leica) and post-stained with aqueous lead citrate (pH 13.0). Micrographs were taken at 80 kV with a 268-electron microscope (Fei Morgagni) at 1800x (overview of leaf tissue), 7100 x (overview of cells) and 22000x (plastids and chloroplasts). Serial lateral micrographs at the base leaf position from cells one to 18 (edge to midrib) for palisade parenchyma plastids and cells one to 15 respectively were taken to further localize plastids and to analyze grana and stroma thylakoid layers and development. The

appearance of vesicles and vesicular and tubular invaginations of the inner envelope membrane were further investigated. At least three representative samples of each plant leaf position were systematically analyzed.

For preparation and microscopic analysis of *snare_ap* and WT plants:

Sample preparation and imaging was performed by Prof. Dr. med. Andreas Klingl (Department of Biology I, Ludwig-Maximillan's-University Munich). Plants were harvested after 7 and 14 days in the morning before onset of light to avoid starch accumulation. The fixation and embedding of the samples was performed as follows. Samples were fixed in fixation buffer containing 75mM cacodylate buffer, 2mM MgCl₂, 2.5% glutaraldehyde pH 7 and then cut to appropriately (length of the specimens was less than 1 mm). After fixation, the samples were washed four times with fixation buffer without glutaraldehyde (15 min, 30 min, 1 h and 80 min) and then stained with 1% osmium tetroxide in water. This was followed by two washes with fixation buffer for 10 min and four washes with distilled water for 15 min, 30 min, 1 h and 2 h each. Thereafter, the samples were dehydrated using series of increasing concentrations of acetone and infiltrated with Einbettharz (Spurr's Resin). For infiltration, the samples were incubated in serially increasing concentrations of resin / acetone mixtures; initially in a 1: 1 resin / acetone mixture followed by 3 h in 2: 1 resin / acetone and finally 3 h in 100% resin. Prior to sectioning, samples were placed in fresh resin and incubated at 63 ° C for polymerization. Ultrathin sections were cut using microtome. The slides were further stained with lead citrate for 2 min to enhance the contrast. The electron microscopic imaging was done using Zeiss EM 912 with OMEGA filter at 80 kV in zero-loss mode. The images were taken with a Tröndle 2k x 2k slow-scan CCD camera.

2.8 Transcriptomic profiling using Affymetrix ATH1 microarray

Transcriptomic profile was done using samples from the mid vein region of leaves from 10 and 13-day-old *fzl-1* plants grown on soil under LED light using Affymetrix ATH1 chips. Three samples were harvested from 10 individual plants and Plant RNeasy Extraction kit (Qiagen) was used for total RNA extraction. 200 ng of purified RNA was used to generate biotinylated cRNA probes by using Affymetrix 3'-IVT Express kit (Affymetrix, High Wycombe, UK) according to the manufacturer's instructions. A total of 15 µg biotinylated cRNA was fragmented and hybridized to GeneChip *Arabidopsis* ATH1 arrays containing 22810 probe sets. Washing and staining were done on an Affymetrix GeneChip Fluidics Station 450. The array chips were scanned using an Affymetrix GeneArray Scanner 3000. Raw signal intensity values (CEL files) were computed from the scanned array images using the Affymetrix GeneChip Command Console 3.0. The raw intensity values were processed with Robin software using default settings (Lohse et al., 2010) to check for

quality and perform normalization. Background intensity correction was done across all arrays using the robust multiarray average normalization method (Irizarry et al., 2018). Statistical analysis of differential gene expression was carried out using the linear model-based approach (Smyth, 2004) and the P values thus obtained were corrected for multiple testing as described previously by Benjamini and Hochberg (Benjamini and Hochberg, 1995). Genes were only considered to be differentially expressed in WT as compared to *fz1-1* if the P value was > 0.05 and \log_2 fold-change value of at least 1. Functional annotation of all the differentially expressed genes was done using Mapman BINs (Usadel et al., 2009).

2.9 *In silico* protein structure analysis

To determine the protein structure, *in silico* structural modeling was performed using Phyre2 program. The FZL (288-912 aa) sequence was used as the query. Structural prediction analysis was run in intensive mode against the PDB database. BDLP (PDB Id: 2J68, Low and Löwe, 2006) was used as a templet for one on one treading. PyMOL software was used to visualize the PDB output files obtained.

3. Results

3.1 Fuzzy Onion Like (FZL)

3.1.1 Characterization of *fzl* mutant lines

Three independent T-DNA insertion lines in the background of Col-0 (henceforth referred to as *fzl-1*, *fzl-2* and *fzl-3*) were isolated (Fig: 6a). The homozygous plants from each line were backcrossed with Col-0 WT to obtain respective homozygous and WT lines with same background. The F2 generation obtained after backcrossing was screened for homozygous and WT plants through genotyping (for oligonucleotide sequences refer Material and methods, section 2.2.6) (Fig: 6b). The position of the insertion was confirmed by sequencing (Fig: 6a).

The phenotype was analyzed in long day conditions under LED light (22°C, 200 $\mu\text{mol}/\text{m}^2\text{s}$ light intensity). The leaves of *fzl* plants grown under LED light turned pale green 11-13 days after germination (Fig: 6b and d). The phenotype was most pronounced in the mid vein region (Fig: 6b, d and e). An anti atFZL (486-770aa) specific polyclonal antibody was raised and used to confirm the knockout of FZL function at the protein level. A band of approximately 95 kDa, corresponding to the mature FZL protein in both Col-0 and the backcrossed WT line was observed, which was absent in the loss of function mutants (Fig. 6c). Moreover, the phenotype was also observed under fluorescent light (22°C, 100 $\mu\text{mol}/\text{m}^2\text{s}$ light intensity) to compare with the earlier report by Gao *et al* (Gao et al., 2006). The leaves of *fzl* plants grown in fluorescent light conditions displayed a pale green phenotype although the phenotype was weaker as compared to LED lights. The phenotype first became manifest only in 14-day-old plants and not earlier (Fig: 7a).

Previously, it was observed that *fzl* leaves display smaller and fewer chloroplasts as compared to WT (Gao et al., 2006; Landoni et al., 2013). Thus, to test if the mutants used in this study displayed the same phenotype, the average diameter of chloroplasts was measured. Indeed, the average diameter of chloroplasts was higher in leaves of all mutant lines compared to WT (Fig: 7b). Moreover, leaves from 25-day-old plants were used to quantify the amount of chlorophyll. The chlorophyll content was significantly reduced to 70 % as compared to WT when grown under 100 $\mu\text{mol}/\text{m}^2\text{s}$ fluorescent light (Fig: 7c).

Since the phenotype was identical in all three mutant lines (Fig:6b and d, Fig: 7a) further experiments were performed with *fzl-1* grown in LED light focusing on the midvein area of the leaves (Fig. 6d).

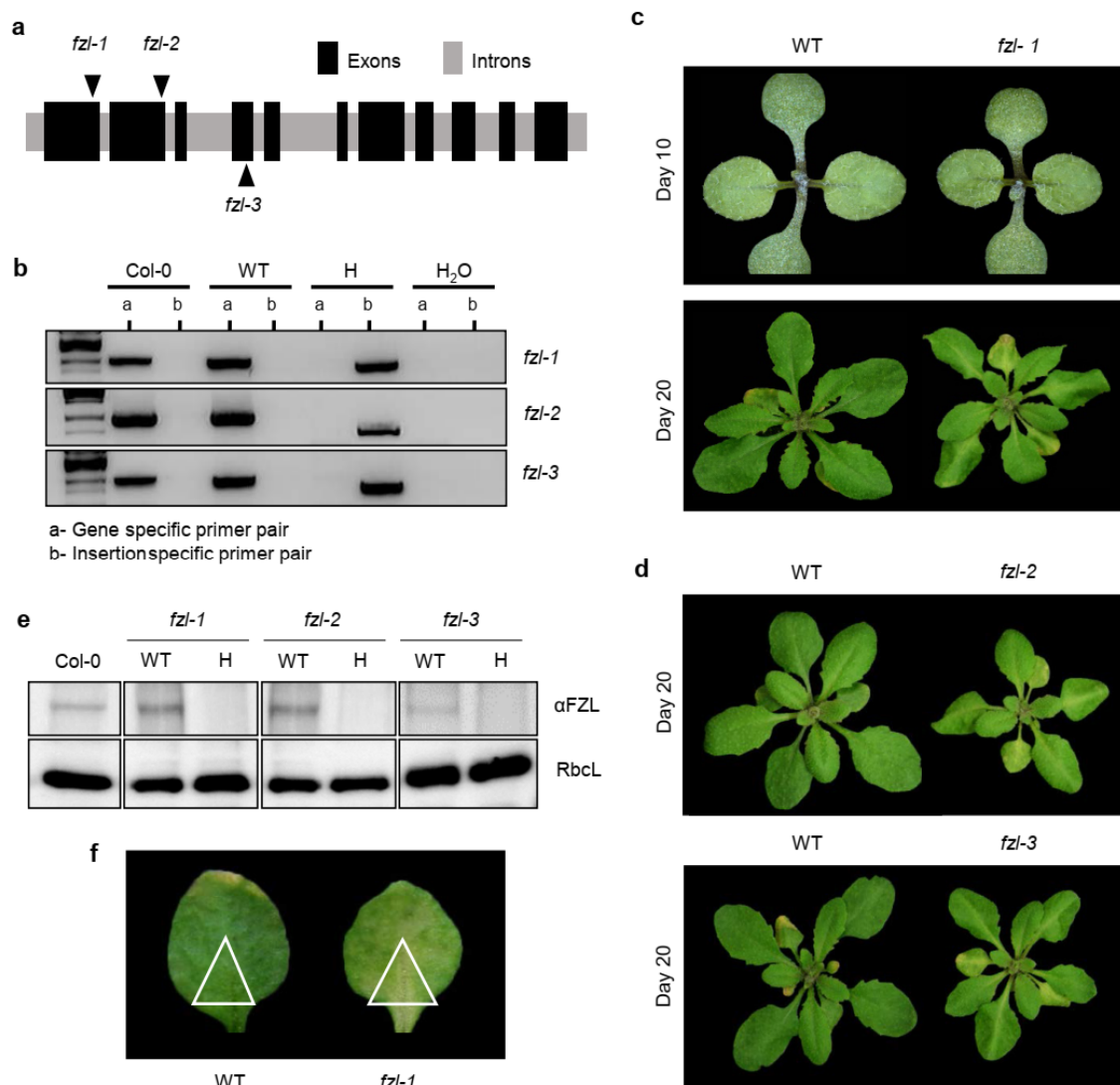


Fig 6: Phenotype of *fzl* mutant plants grown under LED light

(a) The T-DNA insertion sites mapped to the *FZL* gene in the three Salk *fzl* lines are indicated by the black arrowheads (black, exons; grey, introns). (b) Genotyping of *fzl* mutant and WT lines. (c) Phenotype of *fzl-1* mutants grown under long day conditions at 200 $\mu\text{M}/\text{m}^2\text{s}$ LED light. Top panel, 10-day-old *fzl-1* mutants with phenotype similar to WT. Bottom panel, 20-day-old *fzl-1* mutants when grown in high light show a stronger pale green phenotype especially at the mid rib region compared to WT. (d) Pale green phenotypes of *fzl-2* and *fzl-3* mutants grown in long-day conditions under LED light (200 $\mu\text{M}/\text{m}^2\text{s}$). (e) Immunoblot analysis of *fzl-1*, *fzl-2* and *fzl-3* lines using anti FZL antisera (upper panel). 15 μg of total protein loaded on a 10 % SDS gel. Lower panel, equal loading is shown by the antisera's cross reactivity with Ribulose-1,5-bisphosphate carboxylase (RbcL). H, homozygous mutant; WT, backcrossed WT. (f) The leaf material near the mid-vein region that was used for analysis of the levels of photosynthetic efficiency, levels of proteins by immunoblotting, BN-PAGE and microarray experiment is shown enclosed into a triangle. Published in Patil et al. 2018.

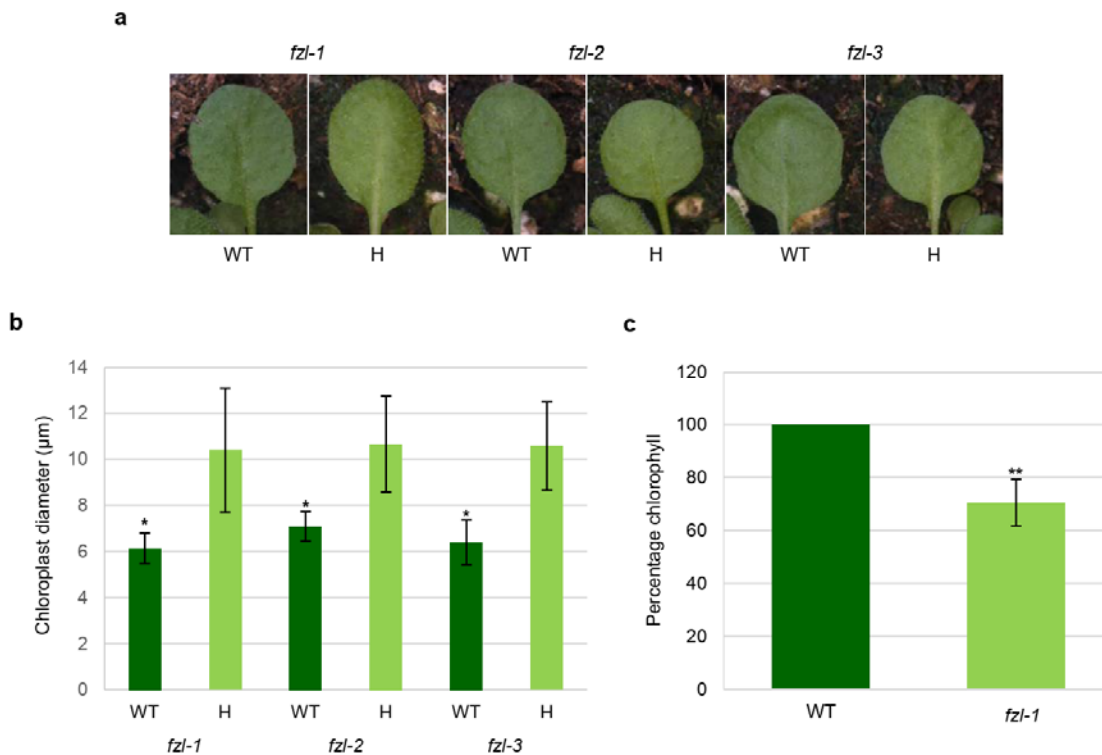


Fig 7: Characterization of *fzl* mutant plants grown under standard light conditions.

(a) Phenotype of *fzl* mutants grown in long-day conditions under 100 $\mu\text{M}/\text{m}^2\text{s}$ light intensity. On day 20, *fzl* plants show a pale green phenotype. (b) Chloroplast size measurement in *fzl* plants. The diameters of 50 individual chloroplasts were measured using ImageJ software based on confocal micrographs of the chlorophyll autofluorescence of 21-day-old leaves. Student's t-test was performed, and P-values were calculated for the 95 % confidence interval. P-value <0.00001. (c) Chlorophyll concentration was measured using leaves from 25-day-old plants grown in normal light. In the *fzl* plants, chlorophyll concentrations were reduced to 70 % of WT levels. P-value: 0.004, n=3. Published in Patil et al. 2018.

3.1.2 Sub-chloroplast localization of FZL

Gao *et al.* generated an *Arabidopsis* line overexpressing a FZL-GFP fusion protein and showed that FZL-GFP is localized to chloroplasts using fluorescence microscopy (Gao et al., 2006). They also performed immunoblotting with anti-GFP antibodies to detect FZL-GFP in both the chloroplast envelope and the thylakoid membrane (Gao et al., 2006). The sub-chloroplast localization of the endogenously expressed FZL was investigated here using an atFZL specific antibody. Outer and inner envelope, stroma and thylakoids fractions were isolated from *Pisum sativum* chloroplasts and subjected to immunoblot analysis. Unexpectedly, FZL could be detected primarily in the inner envelope fraction but was beyond

the limit of detection in thylakoids (Fig: 8a, upper panel). The purity of the fractions was confirmed using antibodies against the marker proteins Toc64 (outer envelopes), Tic110 (inner envelope), FBPase (stroma) and D1 (thylakoids) that served as controls (Fig. 8a, lower panels).

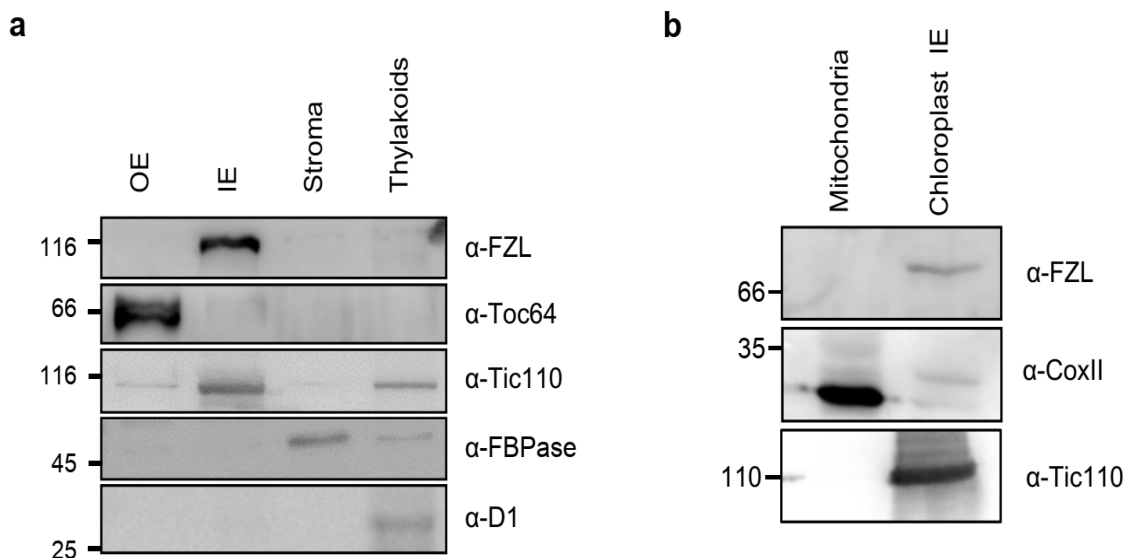


Fig 8: FZL is localized in inner envelope of chloroplast and not mitochondria

(a) Isolated pea chloroplasts were fractionated into inner envelopes, outer envelopes, thylakoid membranes and a stroma and samples (equivalent to 15 μ g protein) were loaded on a 12 % SDS gel. After electrophoresis and membrane transfer, blots were probed with the anti-FZL antiserum. Antibodies against the outer envelope protein TOC64, inner-envelope protein Tic110, the soluble stromal protein FBPase and the thylakoid membrane protein D1 were used as controls. (b) FZL is not present in mitochondria. Purified *Arabidopsis* mitochondria (50 μ g protein) and chloroplast inner envelope fraction (15 μ g protein) was loaded on a 10 % SDS gel and were electrophoresed, blotted and probed with anti-FZL as described as described above. The mitochondrial protein, CoxII and chloroplast inner envelope protein, Tic110 were used as control. Published in Patil et al. 2018.

In silico analysis using TargetP predicted FZL to be dually localized in chloroplasts and/or mitochondria. *Arabidopsis* mitochondria and pea chloroplast inner envelopes samples were immune-decorated with the FZL antibody. FZL could be detected only in the inner envelope of chloroplasts and not in the mitochondria (Fig: 8b). The mitochondrial protein CoxII and inner-envelope protein Tic110 served as control. This is consistent with the experiments using FZL-GFP/YFP protein expression in *Arabidopsis* which showed localization only in chloroplasts (Gao et al., 2006; Tremblay et al., 2016).

3.1.3 Analysis of photosynthetic activity and accumulation of thylakoid membrane complexes

Lack of FZL is known to result in alterations in the structure of the thylakoid membrane (Gao et al., 2006). Since this could influence the photosynthetic ability of plants, the efficiency of the photosynthetic performance and the levels of thylakoid membrane proteins were investigated using the midvein region of the leaves which were most predominantly pale green (Fig. 6e). The maximum quantum efficiency F_v/F_m , was measured in the dark-adapted

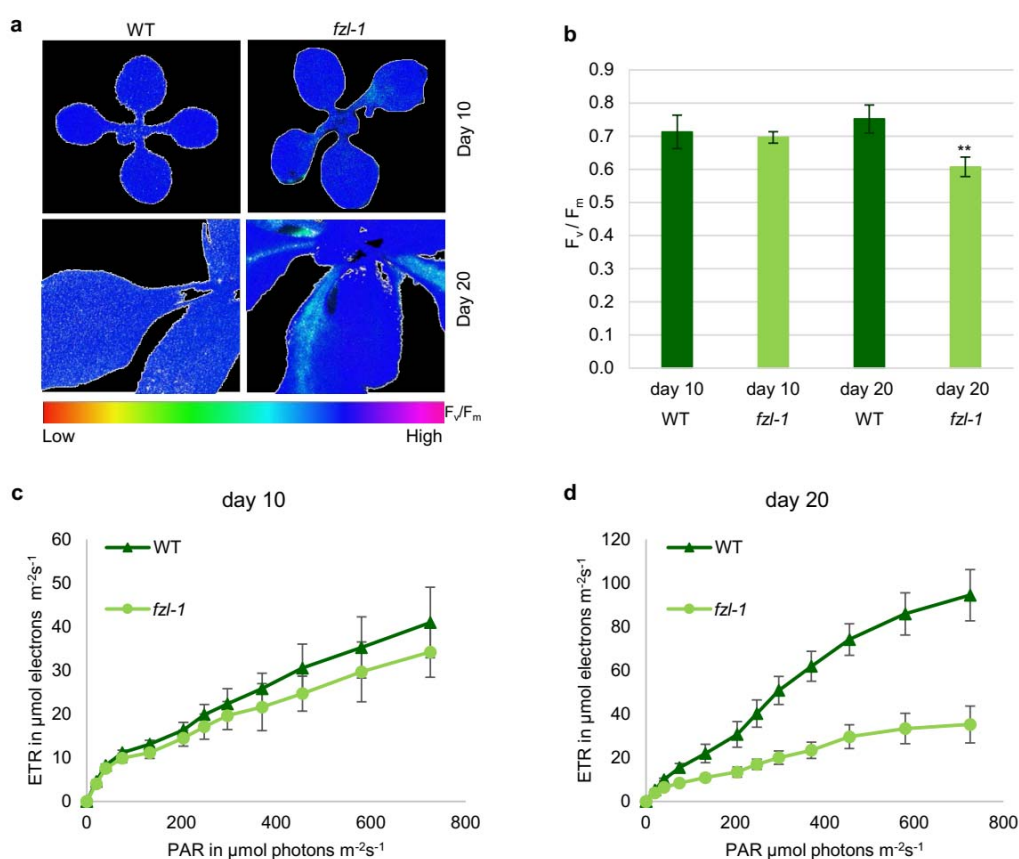


Fig 9: Photosynthetic performance of *fzl* mutants

(a) Photosynthetic performance of *fzl* mutants is reduced in comparison to WT. The PSII yield of *fzl* and WT plants monitored using an Imaging PAM system at day 10 (top panel) and day 20 (bottom panel) after germination. The colour scale indicates the relative photosynthetic activity with red being the lowest and magenta being highest F_v/F_m values. (b) Quantification of PSII yield measurements as shown in (a), P -value: 2,86336E-07, $n \leq 9$. (c and d) Quantification of electron transfer rate (ETR) measured at increasing light intensities on day 10 (c) and day 20 (d), $n \leq 9$. Published in Patil et al. 2018.

10-day-old and 20-day-old plants based on chlorophyll *a* fluorescence to analyze the photosynthetic performance (Fig. 9a).

To analyze the electron transfer rate (ETR) from PSII to downstream components of the photosynthetic electron transport chain, light curves were measured at various levels of illumination with photosynthetically active radiation (PAR). Similar to PSII yields, no significant difference was observed in the ETRs in 10-day-old *fzI* mutant and WT leaves (Fig. 9c). Nevertheless, the ETR in 20-day-old *fzI* plants was significantly reduced with increasing light (PAR) intensities relative to WT, indicating that the photosynthetic apparatus downstream of PSII could be impaired in its function (Fig. 9d).

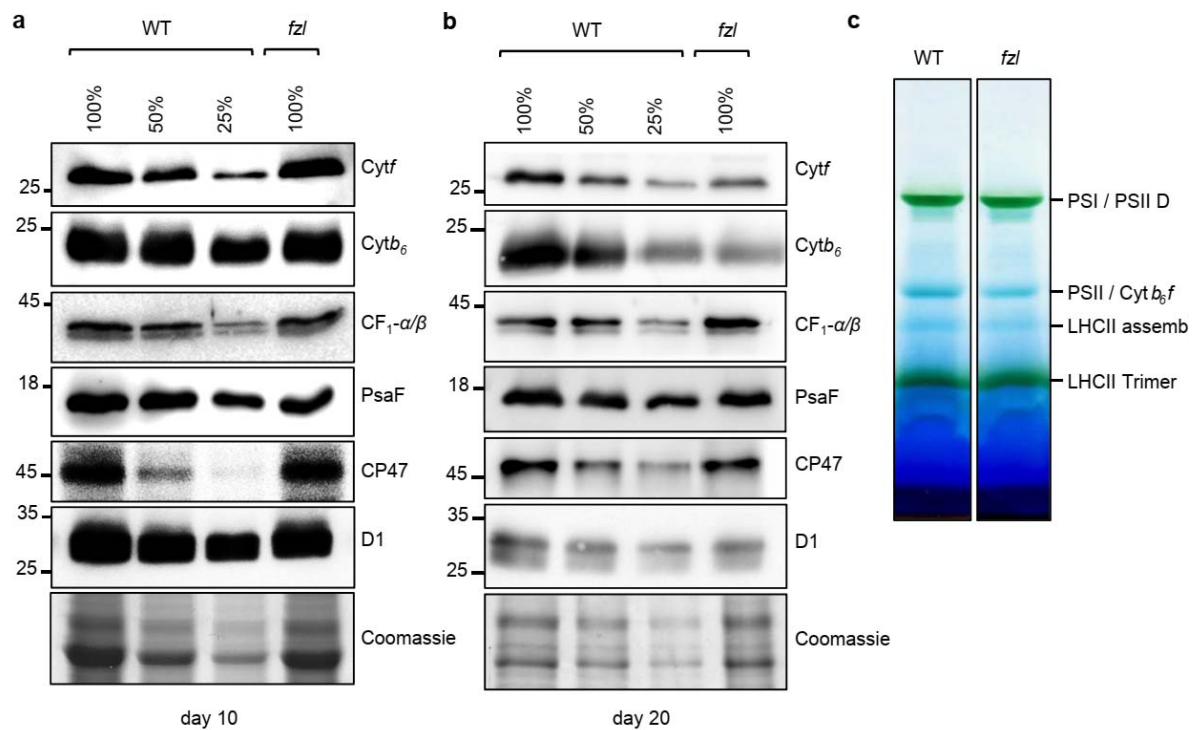


Fig 10: Accumulation of thylakoid membrane proteins in *fzI* mutants

(a and b) Total membrane protein isolated from the midrib region of leaves from 10-day-old **(a)** and 20-day-old **(b)** plants grown under LED light. Samples were loaded on a 12 % SDS gel, fractionated, blotted and probed with antibodies against proteins of the Cytochrome *b₆f* complex, ATP synthase complex, PSI and PSII. 100% protein equals 10 µg of protein **(c)** Thylakoids of WT and *fzI* plants were isolated from the midrib region of leaves from 20-day-old plants grown under LED light, solubilized in 1 % β-dodecyl-maltoside and photosynthetic complexes were separated by BN-PAGE. Published in Patil et al. 2018.

As a next step, the levels of thylakoid membrane proteins in 10-day-old and 20-day-old, WT and *fzI* mutants were analyzed by immunoblotting. The subunits of PSII (CP47, D1), PSI

(PsaF), the cytochrome *b₆f* complex (Cyt*f* and Cyt*b₆*) and the ATP synthase (CF₁- α/β) were tested. Interestingly, hardly any difference was visible in the levels of thylakoid proteins between *fzI* and WT in 10-day-old plants (Fig. 10a). However, in 20-day-old plants more obvious changes were observed. Although the levels of CP47 and PsaF were only slightly reduced, Cyt*f* and D1 were reduced to approximately 50% in *fzI* plants and Cyt*b₆* was found to be as low as 75% when compared to WT levels. The amount of the ATP synthase was marginally higher in *fzI* plants (Fig. 10b). Further, the assembly of the photosynthetic complexes was investigated by BN-PAGE analysis. Thylakoid membranes were isolated from the midvein sections of WT and *fzI* mutants. The photosynthetic protein complexes were separated on a 5-15 % BN gel after solubilizing the membrane complexes in 1 % dodecyl- β -D-maltoside. Equal amount of protein was loaded for each sample. Not surprisingly, the band corresponding to the PSII monomer / Cyt *b₆f* complex was slightly reduced in the *fzI* mutant as compared to WT (Fig. 10c). Taken together, these results indicate that the reduced levels of cytochrome *b₆f* complex proteins, due to lack of FZL possibly impairs the efficiency of photosynthetic electron transport in the mid-vein region.

3.1.4 Analysis of changes in transcript levels upon the onset of the phenotype

To understand the probable role of FZL, a global transcriptomic study was performed to identify differentially regulated genes (DEGs) in the *fzI* mutant relative to WT. For this the leaf samples from the mid vein area were used as the phenotype was most prominent in this region (Fig. 6f). Also, since the phenotype was apparent only after 11-13 days, leaf samples before (10-day-old) and after (13-day-old) the onset of phenotype were analyzed as described in Materials and Methods. The Affymetrix experiment was performed by Franka Seiler.

There was a considerable increase in the total number of DEGs after the onset of phenotype (Fig:11). At day 10, 1107 genes were up regulated whereas 955 genes were found to be down regulated in *fzI* compared to WT (Fig. 11a). Remarkably, 3397 genes were upregulated and 3570 down regulated in the mutant by day 13 (Fig. 11b). Moreover, it is striking that at day 13 in contrast to day 10, the number of genes down-regulated was significantly higher than the up-regulated genes in the mutant as compared to WT (Fig: 12). The DEGs were annotated to various gene ontology (GO) molecular function categories based on Mapman BINs (Usadel et al., 2009) (Fig: 12).

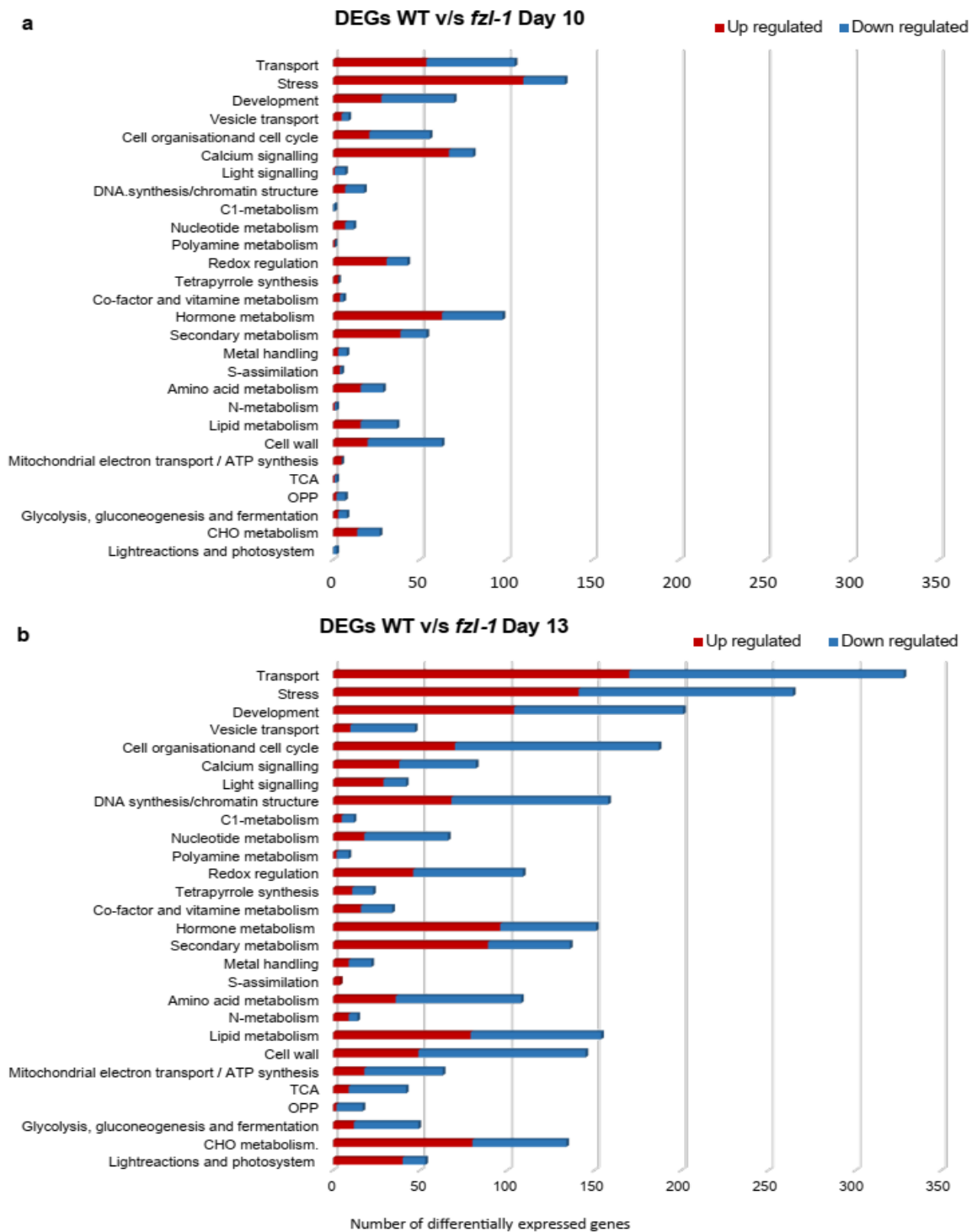


Fig 11: Number of differentially expressed genes of various GO molecular function categories
 The graphs show the numbers of genes differentially regulated in *fzl* relative to WT on day 10 (a) and day 13 (b) that were assigned to the indicated GO molecular function categories. Published in Patil et al. 2018.

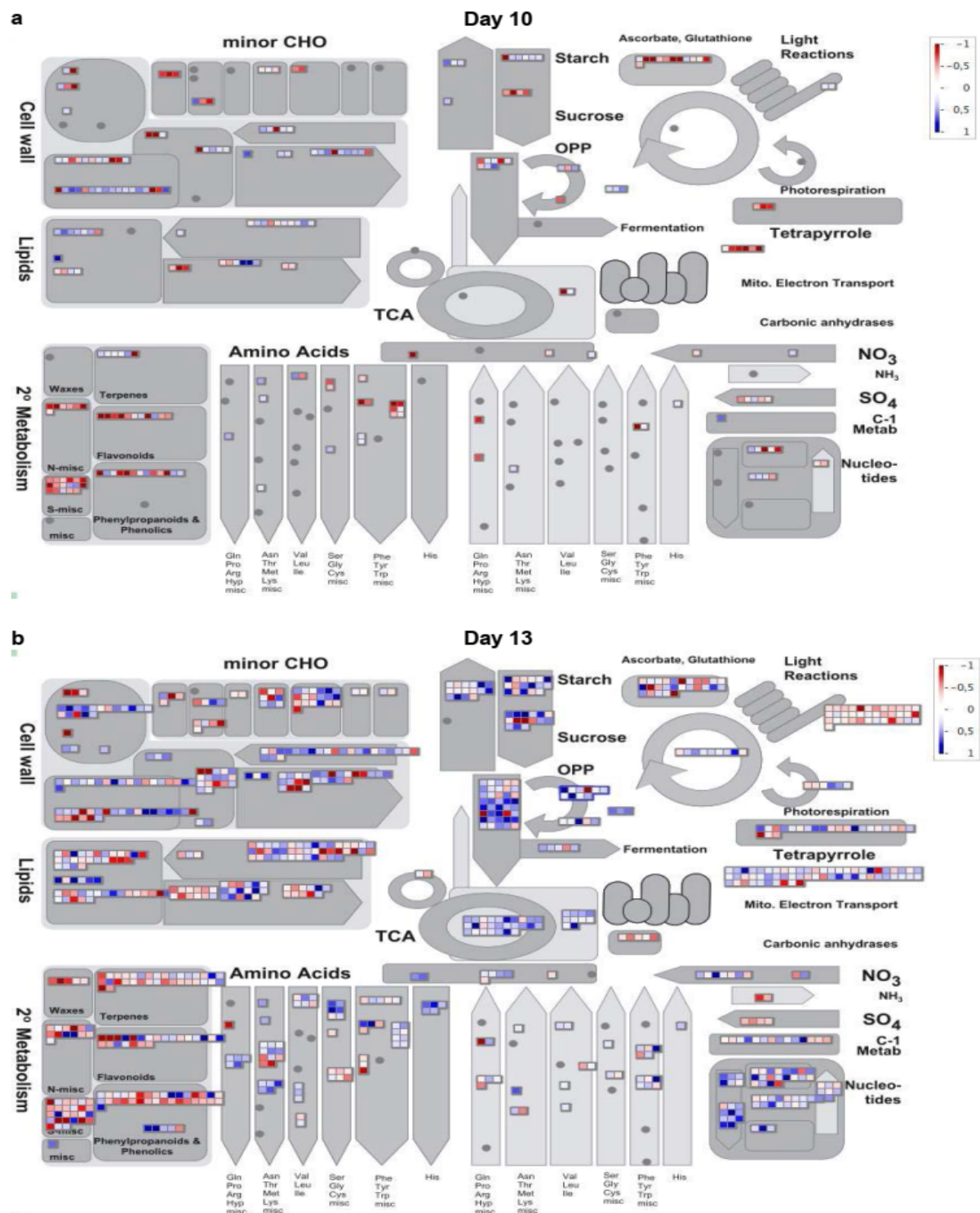


Fig 12: Differentially regulated genes as annotated based on Mapman BINs

Differentially regulated genes in *fzI* as compared to WT annotated to various GO molecular function categories as on day 10 (**a**) and day 13 (**b**). Published in Patil et al. 2018.

The leaves of *fz1* plants have reduced chlorophyll content as compared to WT (Fig: 7c). Correspondingly, the genes related to tetrapyrrole synthesis were deregulated in *fz1* plants but unexpectedly genes related to photosystem and light reaction (light harvesting complex (LHCs) proteins) were up-regulated. Hence, the protein levels of LHCa (LHCa1, LHCa2 and Lhca4) and LHCb (Lhcb1, Lhcb2 and Lhcb4) proteins and PORB (protochlorophyllide oxidoreductase B, chlorophyll metabolism) were tested by immunoblot analysis by Stephanie Seifert. With an exception of LHCa1 protein which showed slight increase, no striking differences were found at the protein levels of LHCs and PORB (Fig. 13a and b, upper panel).

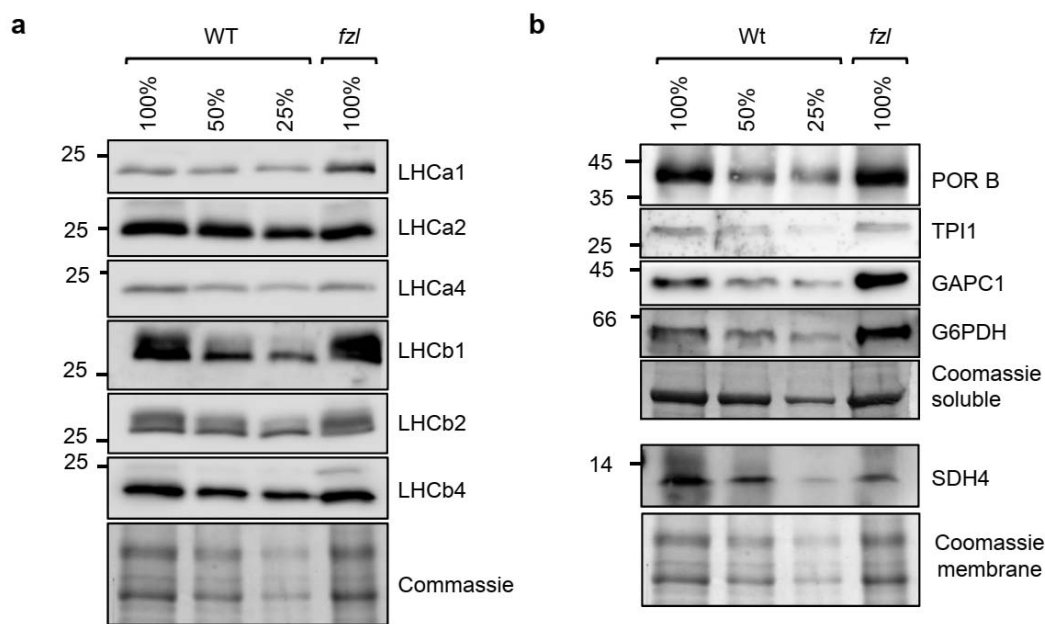


Fig 13: Quantification of protein products of selected differentially expressed genes in *fz1* mutants

Levels of light-harvesting-complex proteins (LHCs) (a) and products of chlorophyll- and carbohydrate metabolism related genes (b) that are differentially regulated in *fz1* relative to WT were determined by immunoblot analysis with cognate antibodies. Total membrane or soluble protein fractions electrophoresed on a 12% SDS gel and immunodecorated. 100% protein equals 10 μ g. PORB, protochlorophyllide oxidoreductase B; TIP, triose-phosphate isomerase; GAPC1, glyceraldehyde -3-phosphate dehydrogenase; SDH4, succinate dehydrogenase; G6PDH, glucose-6-phosphate dehydrogenase. Published in Patil et al. 2018.

Carbohydrate metabolism was another gene ontology (GO) molecular function category that consisted of 19 genes with at least 2-fold variation. Consequently, the levels of the following enzymes were analyzed by immunoblotting: triose-phosphate isomerase (TIP), glyceraldehyde-3-phosphate dehydrogenase (GAPC1), succinate dehydrogenase (SDH4)

and glucose-6-phosphate dehydrogenase (G6PDH). Corresponding to the reduced transcript levels, SDH4 protein levels were also reduced in the *fzI* mutant as compared to WT. However, in contrast to the reduced transcript levels, the amount of GAPC1 and G6PDH protein was increased and that of TIP remained unchanged (Fig. 13b). These differences could be accounted by the different mechanisms of regulation of transcript and protein levels and their lifetimes.

3.1.5 In silico protein structure prediction

Recently, Löwe *et al.* crystalized BDLP, the closest homolog of FZL and proposed the mechanism for BDLP induced membrane fission or fusion (Low and Löwe, 2006; Low et al., 2009). Since the mode of action might be similar for entire dynamin-like family, we did *in silico* structural prediction for FZL using Phyre2 program. FZL (288-912 aa) sequence was modelled on the structure of GDP bound BDLP by one on one threading. The FZL predicted structure is highly similar to that of BDLP (100 % confidence) (Fig: 14). This suggests that FZL could act in analogous way mediating membrane fission.

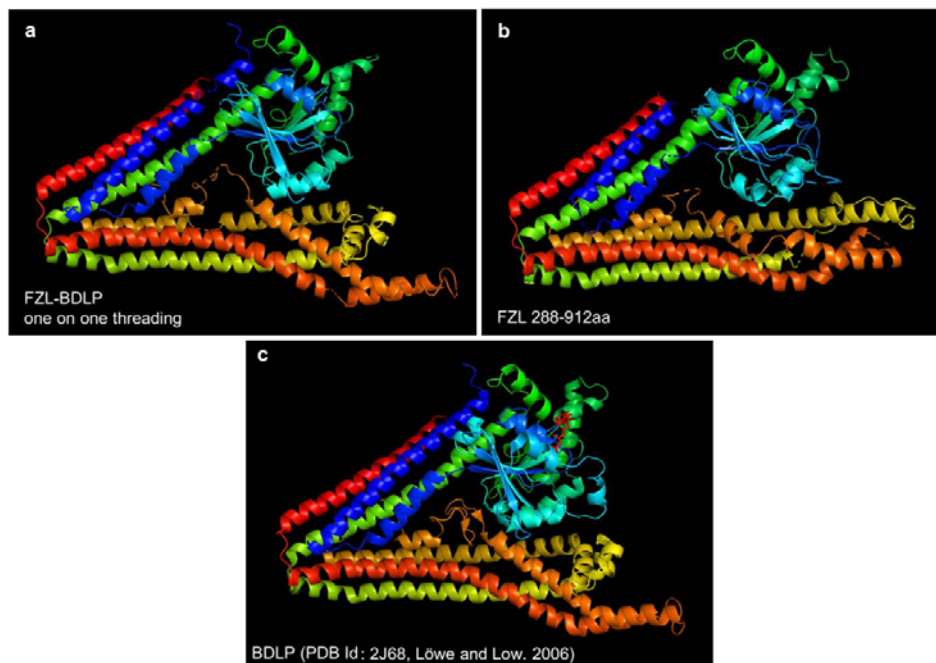


Fig 14: In silico modeling of FZL with BDLP

In silico structural prediction analysis was performed using Phyre2 web portal. (a) FZL (288-912 aa) structure predicted with 100% confidence interval based on the structure of GDP bound BDLP (PDB Id: 2J68). (b) One on one threading of FZL (288-912 aa) to the GDP bound BDLP protein structure (PDB Id: 2J68). (c) Structure of GDP bound BDLP (PDB Id: 2J68). Published in Patil et al. 2018.

3.2 Synaptotagmin (SYTL5.2)

3.2.1 Characterization of *syt15.2* mutant lines

To study the effect of loss of SYTL5.2 in plants, the T-DNA insertion *syt15.2* line (NASC ID: N904515, WiscDsLoxHs048_01C) in the background of Col-0 was analyzed. Homozygous and out-crossed WT plants were identified by performing genotyping PCR (for oligonucleotide sequences refer Material and Methods, section 2.2.6). Sequencing confirmed the position of the T-DNA insertion in 7th exon (Fig:15 a and b). The phenotype of *syt15.2* plants grown in fluorescent light (22 °C, 100 µmol/m²s light, 16 / 8 h light / dark) was analyzed. Homozygous *syt15.2* plants were significantly smaller with retarded growth and displayed a crumpled leaf phenotype in comparison to WT (Fig:15 c and f). The *syt15.2* leaves, were extremely compressed with curled edges bending downwards. The leaf petioles were broad, paler and strongly vascularized (Fig:15 f). The cauline leaves also displayed a curly phenotype (Fig:15 d and e). Both the WT and *syt15.2* plants started bolting at around day 30, however the elongation of inflorescence was significantly delayed in *syt15.2* plants (Fig:15 i) and the flowers were severely deformed. The sepals and the petals of *syt15.2* flowers were wrinkled and reduced in size (Fig:15 j and k). In contrast to WT, the *syt15.2* flower buds exhibited premature elongation of the gynoecium that protruded out of partially closed buds. The papillae of the stigma were never-the-less small and underdeveloped. The androecium of *syt15.2* flowers had shorter filaments with delayed anther maturation and pollen release (Fig:15 j and k). This defect in the androecium and gynoecium was also reflected in seed formation. Consistent with the siliques of *syt15.2* plants being shorter and slightly twisted (Fig:15 h) with fewer number of seeds. The total yield of seeds was significantly reduced in *syt15.2* plants as compared to WT (Fig:15 i).

Further, to confirm that the phenotype observed in *syt15.2* plants was caused due to lack of SYTL5.2 and not a result of unknown background insertion/s, complementation of the mutant line was done. The entire genomic region of SYTL5.2 (promoter region consisting of 1000bp upstream of start codon, introns and exons with the stop codon) was cloned and the plasmid was transformed into homozygous *syt15.2* plants. The seeds were selected against kanamycin and BASTA resistance to obtain F1 generation plants which were screened for presence of the insert using genotyping PCR. The complementation lines gave a PCR product for both gene specific and T-DNA insertion specific primer pairs (for oligonucleotide sequences refer Material and Methods, section 2.2.6) (fig:16 a).

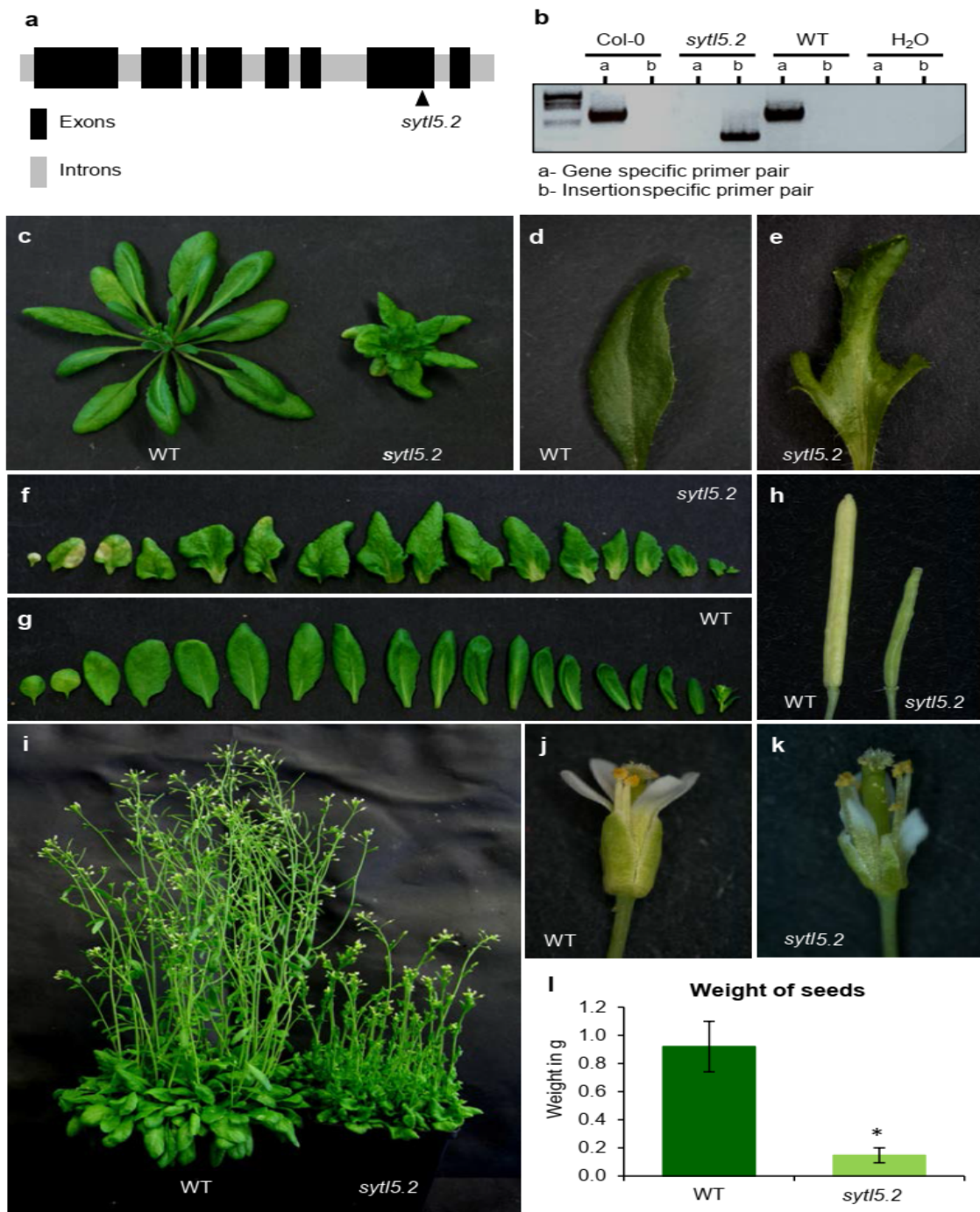


Fig 15: Phenotype of *sytl5.2* mutant plants

(a) The T-DNA insertion site mapped to the *SYTL5.2* gene in the SALK N904515 line as indicated by the black arrowheads (black, exons; grey, introns). (b) Genotyping of *sytl5.2* mutant and WT lines. (c) Phenotype of *sytl5.2* mutants grown under standard long day, normal light conditions at 100 $\mu\text{M}/\text{s}/\text{m}^2$ intensity. (d and e) Cauline leaf phenotype of WT (d) and *sytl5.2* mutant (e). (f and g) Leaves of *sytl5.2* mutant (f) and WT (g) separated from the rosette. (h) Siliques of WT (left) and *sytl5.2* mutant (right) (i) The inflorescence of WT (left) and *sytl5.2* mutant

(right) **(j and k)** The flowers of WT **(j)** and *sytl5.2* mutant **(k)**. **(l)** Weight of seeds from WT and *sytl5.2* mutant plants, n=5, p<0.00001.

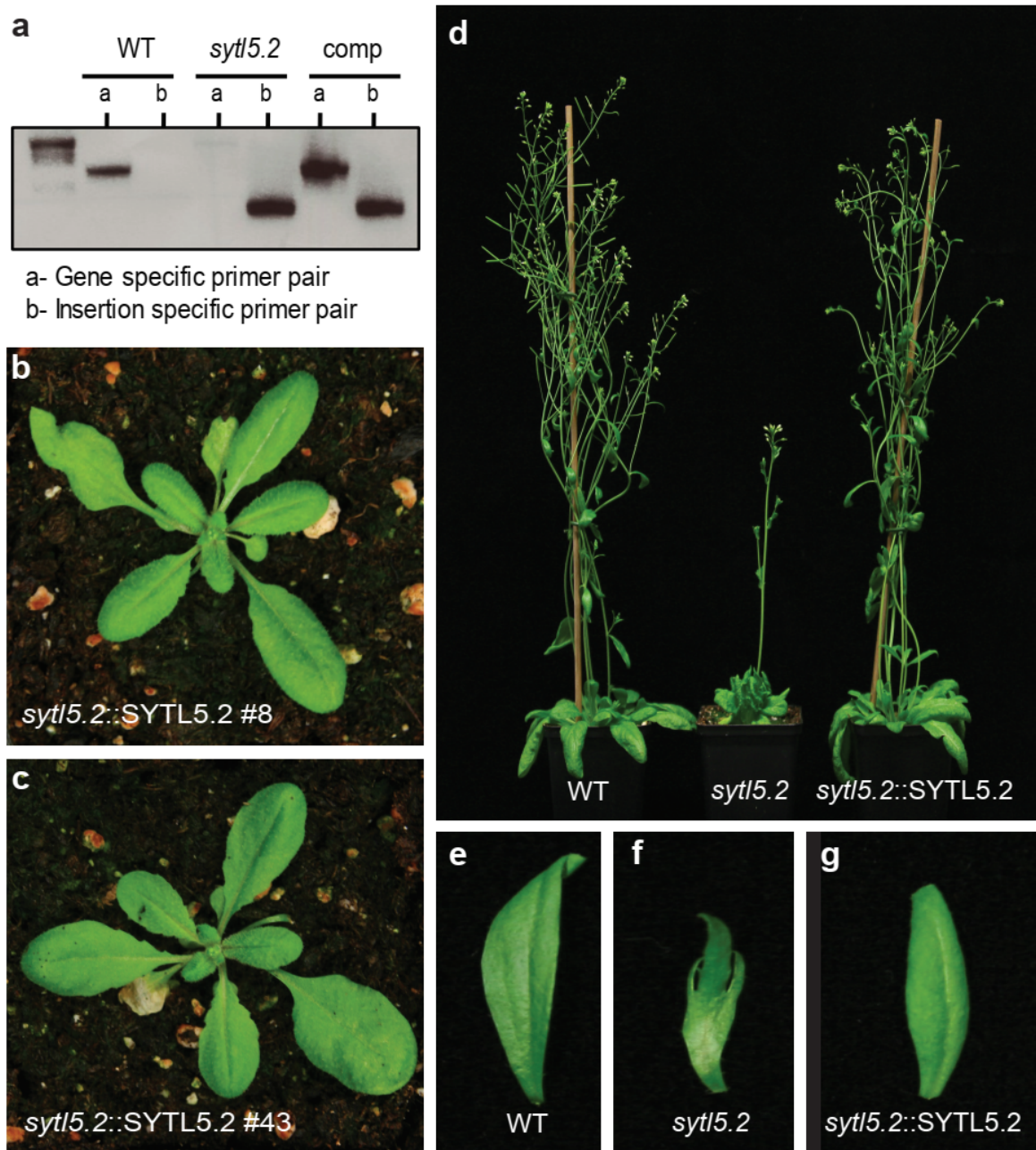


Fig 16: Complementation of *sytl5.2* mutant plants

(a) Genotyping of WT, *sytl5.2* mutant and *sytl5.2::SYTL5.2* complementation lines. **(b and c)** Phenotype of *sytl5.2::SYTL5.2* complementation lines #8 and #43 grown under standard long day, normal light conditions at 100 $\mu\text{M}/\text{s}/\text{m}^2$ intensity. **(d)** The inflorescence of WT, *sytl5.2* mutant and *sytl5.2::SYTL5.2* complementation lines. **(e, f and g)** Cauline leaf phenotype of WT **(e)**, *sytl5.2* mutant **(f)** and *sytl5.2::SYTL5.2* complementation lines **(g)**.

The phenotype of *sytl5.2* plants was completely rescued and no retarded growth, curly leaves and defects in flower as well as seed development were observed in complementation lines (Fig:16 b-g).

3.2.2 Sub cellular localization of SYTL5.2

In silico protein sequence analysis of SYTL5.2 predicted it to be a plastid protein with 25 amino acids long cleavable TP (Target P). Consequently, the subcellular localization was analyzed by *in vivo* expression of a construct with the first 272 aa of SYTL5.2 including the TP fused to GFP (as indicated in Fig:17 a) in tobacco. Tobacco leaves were infiltrated with agrobacteria transformed with SYTL5.2 (272aa)-GFP fusion plasmid (Fig: 17 a). Protoplasts were isolated from leaves expressing Sytl5.2 (272aa)-GFP fusion protein and a confocal laser scanning microscope was used to detect the fluorescence signal. The SYTL5.2 (272aa)-GFP signal overlapped with the chlorophyll auto fluorescence detected in chloroplasts (Fig: 17 b upper panel). Likewise, SYTL5.2 (272aa)-GFP signal in tobacco leaves was detected exclusively in the chloroplast (Fig: 17 b lower panel). Although the GFP fluorescence signal more prominently observed at the chloroplast envelope (Fig: 17 b lower panel), more detailed experiments are required to prove the localization of SYTL5.2 in a specific chloroplast membrane or compartment.

Additionally, *in-vitro* import of radio-labeled protein into pea chloroplasts was also performed to test the localization of full length protein. Indeed, ³⁵S-labeled SYTL5.2 was imported into chloroplasts and processed confirming the observation with the GFP fusion protein (Fig: 17 c). FNR was used as a positive control (Fig: 17 d). Considering that the SYTL5.2 preprotein is 77 kD and the predicted TP is 25 amino acid long, after cleavage of the TP the mature SYTL5.2 would be expected at the size of 74.5 kD. However, the mature SYTL5.2 unexpectedly ran at the size of 66 kD. This 11 kD shift suggest that the TP is larger than predicted and that the preprotein is cleaved after approx. 100 amino acids. Hence the SYTL5.2 (272aa)-GFP fusion protein expressed in tobacco was used to confirm the size of the processed TP. Anti GFP antisera were used to detect the SYTL5.2 (272aa)-GFP fusion protein. After the cleavage of TP of 11kD, 59.4 kD SYTL5.2-272aa fused GFP tagged preprotein is expected to run at around 48 kD. In agreement with the results obtained from the *in vitro* import, anti GFP antisera recognized a band at around 48 kD (Fig: 17 e).

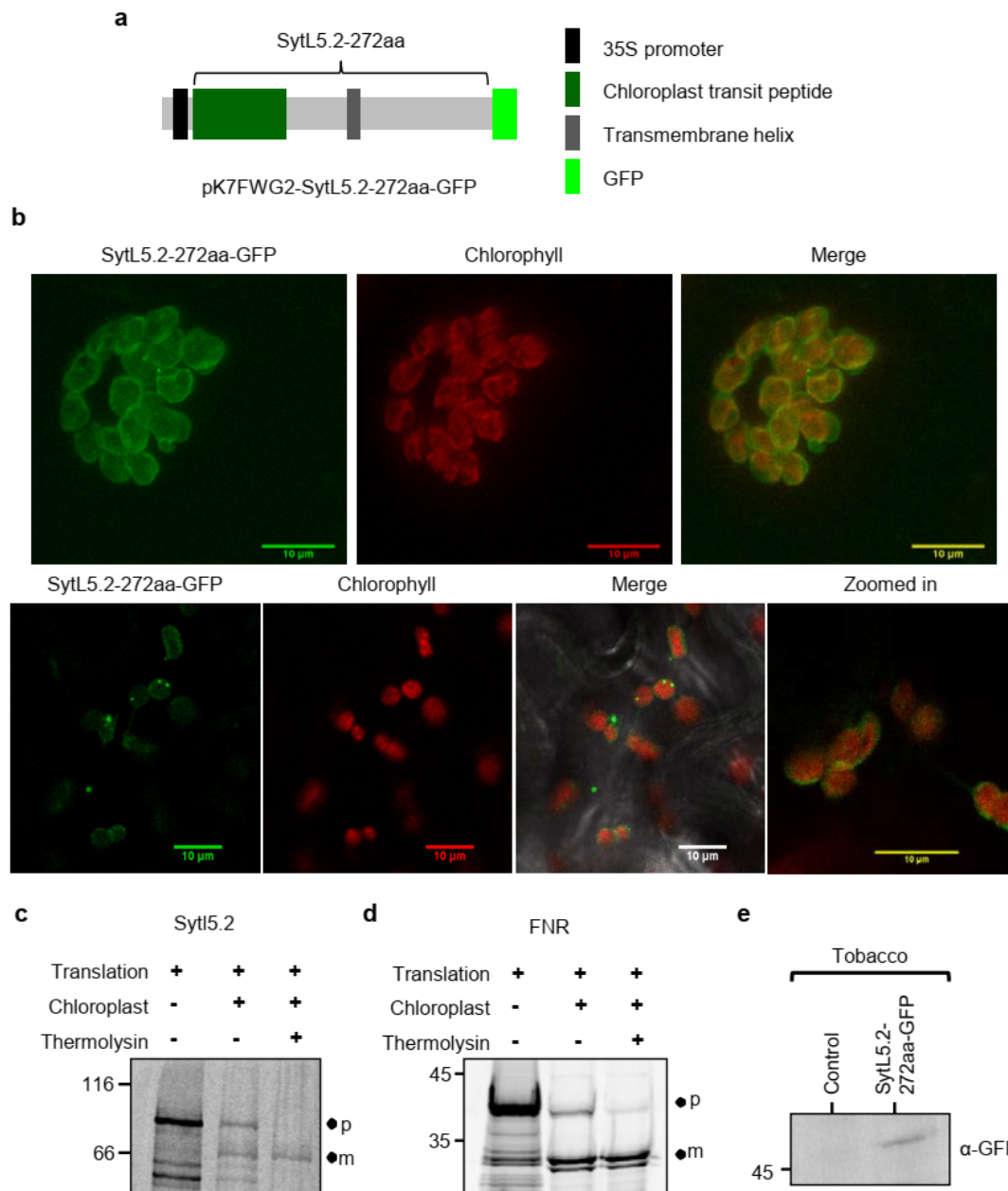


Fig 17: Localization of SYTL5.2

(a) SYTL5.2-272aa-GFP-pK7FWG2 plasmid. Schematic diagram depicting the relative positions of chloroplast transit peptide, transmembrane domain and GFP tag. (b) SYTL5.2-272aa GFP fusion protein was expressed transiently in Tobacco. GFP signal detected in chloroplast as seen in protoplast (upper panel) and whole leaves (bottom panel). Left: SYTL5.2-272aa-GFP fluorescence, middle: chlorophyll auto-fluorescence, right: merged image. (c) In vitro import of SYTL5.2 into chloroplast. Full length SYTL5.2 imported into pea chloroplast and treated with thermolysin. FNR was used as control. p, preprotein; m, mature protein (d) Chloroplast TP of SYTL5.2 is approximately 100 amino acid. SYTL5.2-272aa GFP fusion protein immune-decorated with GFP antisera is detected at ~ 48kD after cleavage of ~11kD TP.

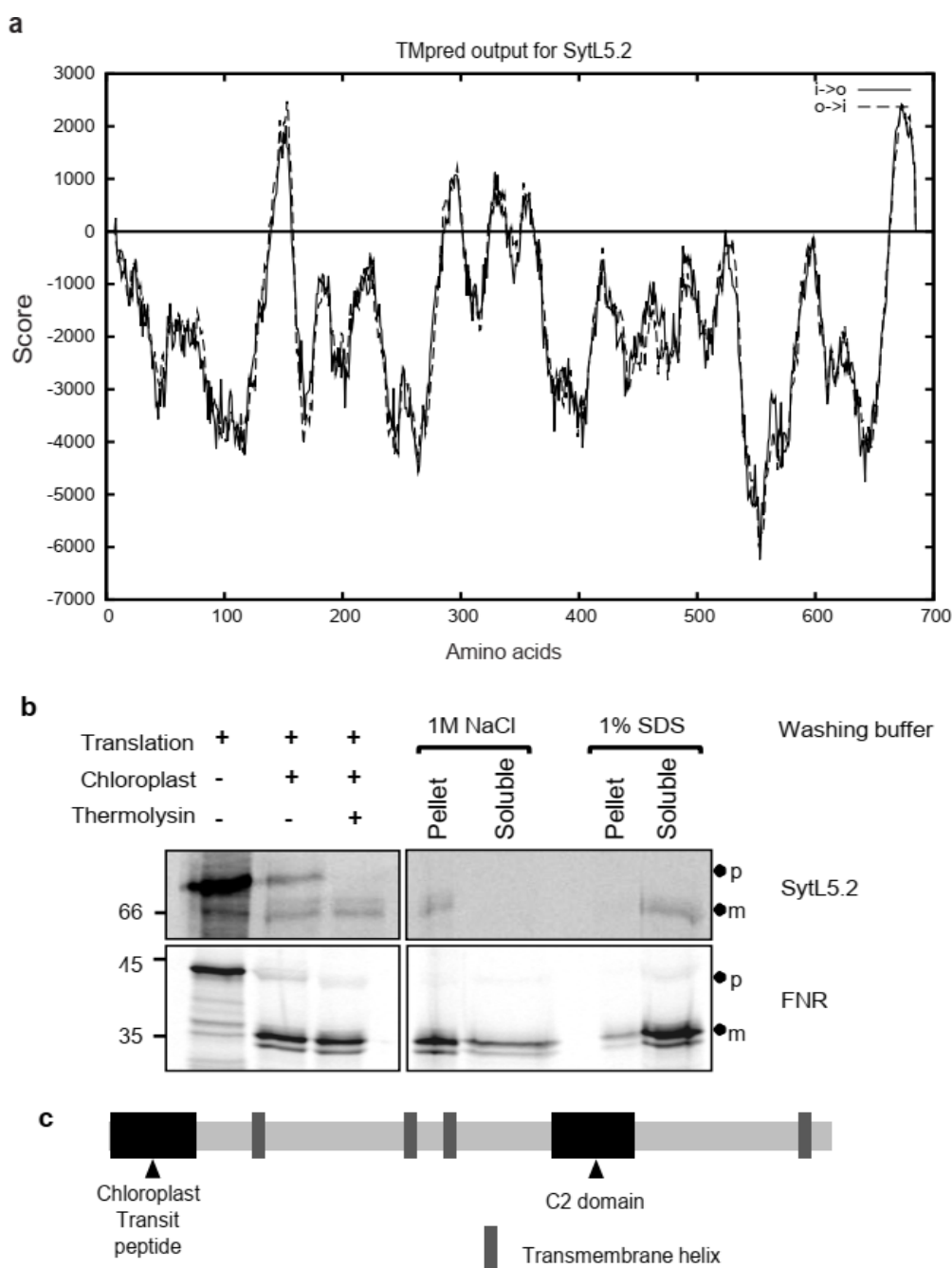


Fig 18: Structure of SYTL5.2

(a) Prediction of transmembrane domain in SYTL5.2 using TM-PRED. Only the regions with scores above 500 were considered as transmembrane domains. (b) SYTL5.2 is an integral membrane protein. Full length SYTL5.2 imported into pea chloroplast and washed with 1M NaCl or 1% SDS. FNR was used as control. p, preprotein; m, mature protein (c) The schematic structure of SYTL5.2 showing relative positions of transit peptide, C2 domain and the predicted transmembrane helices (black, Chloroplast transit peptide or C2 domain as indicated; grey, transmembrane helices).

Classically, most synaptotagmin family proteins are anchored to the membrane through a N-terminal transmembrane helix with the residual protein including the C2 domain/s being largely soluble (Craxton, 2007). Protein sequence analysis of SYTL5.2 using TMpred revealed that unlike most known synaptotagmins, SYTL5.2 is predicted to contain 4 transmembrane helices (Fig: 18 a). Thus SYTL5.2 is most likely an integral membrane protein with the third loop containing the C2 domain. Consequently, ³⁵S-labeled full length SYTL5.2 was imported into pea chloroplasts and further treated with either 1 M NaCl or 1 % SDS to test if the *in vitro* imported protein is inserted integrally into the chloroplast membrane. SYTL5.2 was found in the membrane pellet fraction upon treatment with 1M NaCl but was readily solubilized when treated with 1 % SDS indicating that it is an integral membrane protein (Fig: 18 b). Fig: 18 c depicts the structure of SYTL5.2 with the relative positions of chloroplast targeting peptide, the C2 domain and the transmembrane domains along with revised length of transit peptide. Taken together, these results show that SYTL5.2 is an integral membrane protein localized to chloroplast with approximately 100 amino acid long transit peptide.

3.2.3 Analysis of chloroplast ultra-structure in *sytl5.2* plants

In light of the severity of the phenotype observed in *sytl5.2* mutants, TEM studies were done to study the effects of loss of function mutation of *SYTL5.2* gene on chloroplast morphology. The fourth leaf was harvested before onset of light from 14-day-old plants and the tip as well as the base region of leaf was analyzed. The overview of cells from the tip area (Fig: 19 a and c) display fully differentiated cells with large central vacuoles. However, in *sytl5.2* leaves the spongy parenchyma contained more aerial spaces when compared to WT (Fig: 19 b, d-h). The chloroplasts in both WT and mutant leaves were well developed with comparable thylakoid architecture (Fig: 19 k-p).

The base of leaves contained more densely packed cells as compared to the tip region. Nevertheless, similar to the tip region, there were more aerial spaces within mutant leaves than the WT. Cells were still differentiating and contained many small vacuoles (Fig: 20 b, d-h). Significant differences were seen in the plastid morphology between WT and mutant. Chloroplasts in *sytl5.2* were significantly smaller and spherical as compared to those in WT which were larger and more ellipsoidal. The thylakoid network was less well-organized with lower density unlike in WT where it ran parallel. Vesicle and tubule like structures were also observed in mutant plastids Fig: 20 k-o and r-v). The transmission electron microscopy

experiments have been performed by Dr. Irene Gügel.

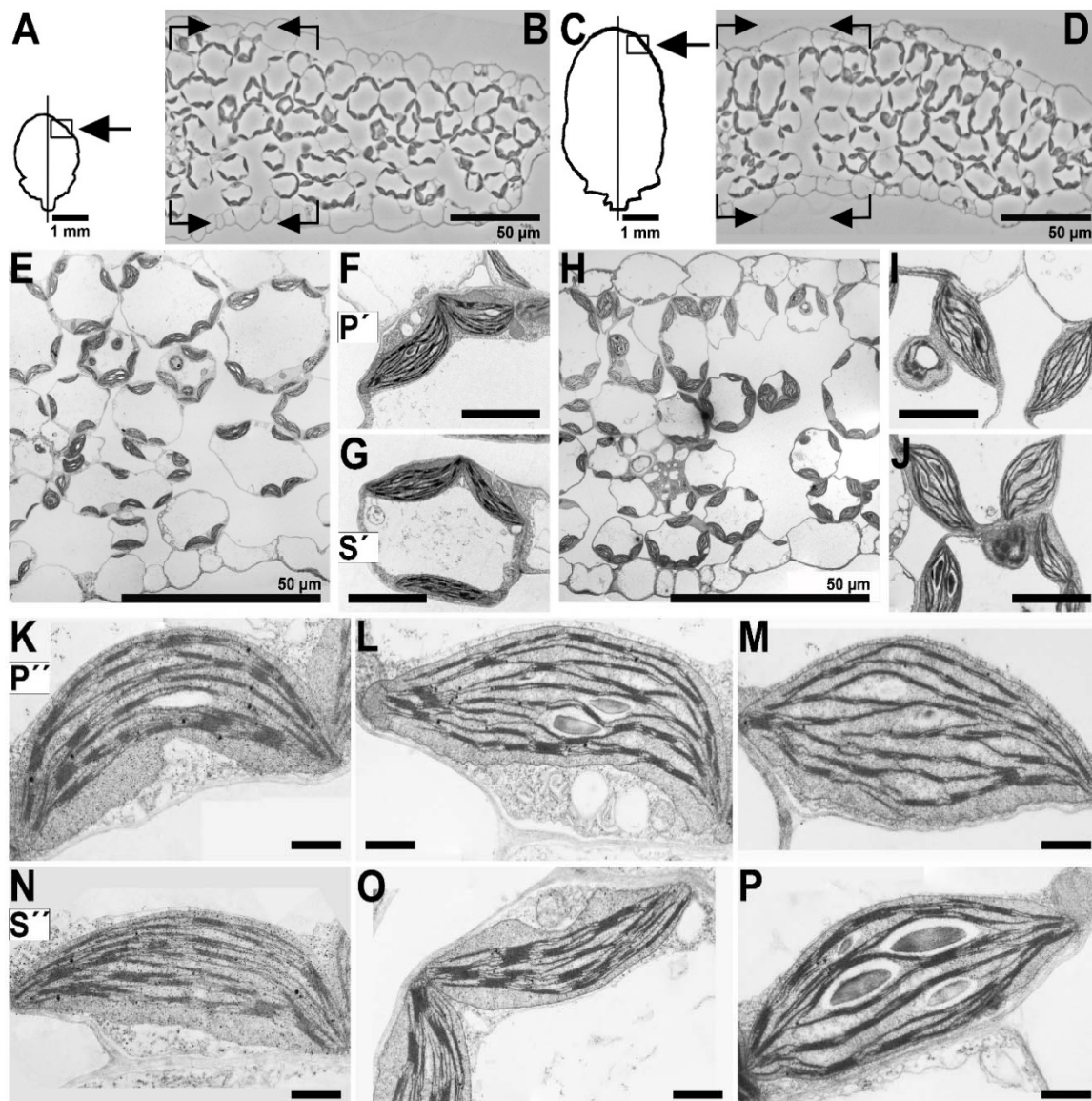


Fig 19: TEM of 14-day-old WT and *syt15.2* mutant leaf tips. *syt15.2* left (A, B, E-G, K, L, N, O) and WT right (C, D, H-J, M, P) vegetative leaf 4 tip. A/C □ indicates leaf segment analyzed; B/D cross-section of the leaf tip by phase-contrast light-microscopy, angulated arrows mark the region of the plant leaf tissue in E and H respectively; E/H TEM overview 1800x magnification; cells and chloroplasts analyzed further in the palisade parenchyma P' and P'' in F, I, K-M; cells and chloroplasts analyzed further in the sponge parenchyma S' and S'' in G, J, N-P. chloroplast in P' resp. S' TEM magnification 7100x, bar 5 μm, in P'' resp. S'' TEM magnification 22000x, bar 1 μm.

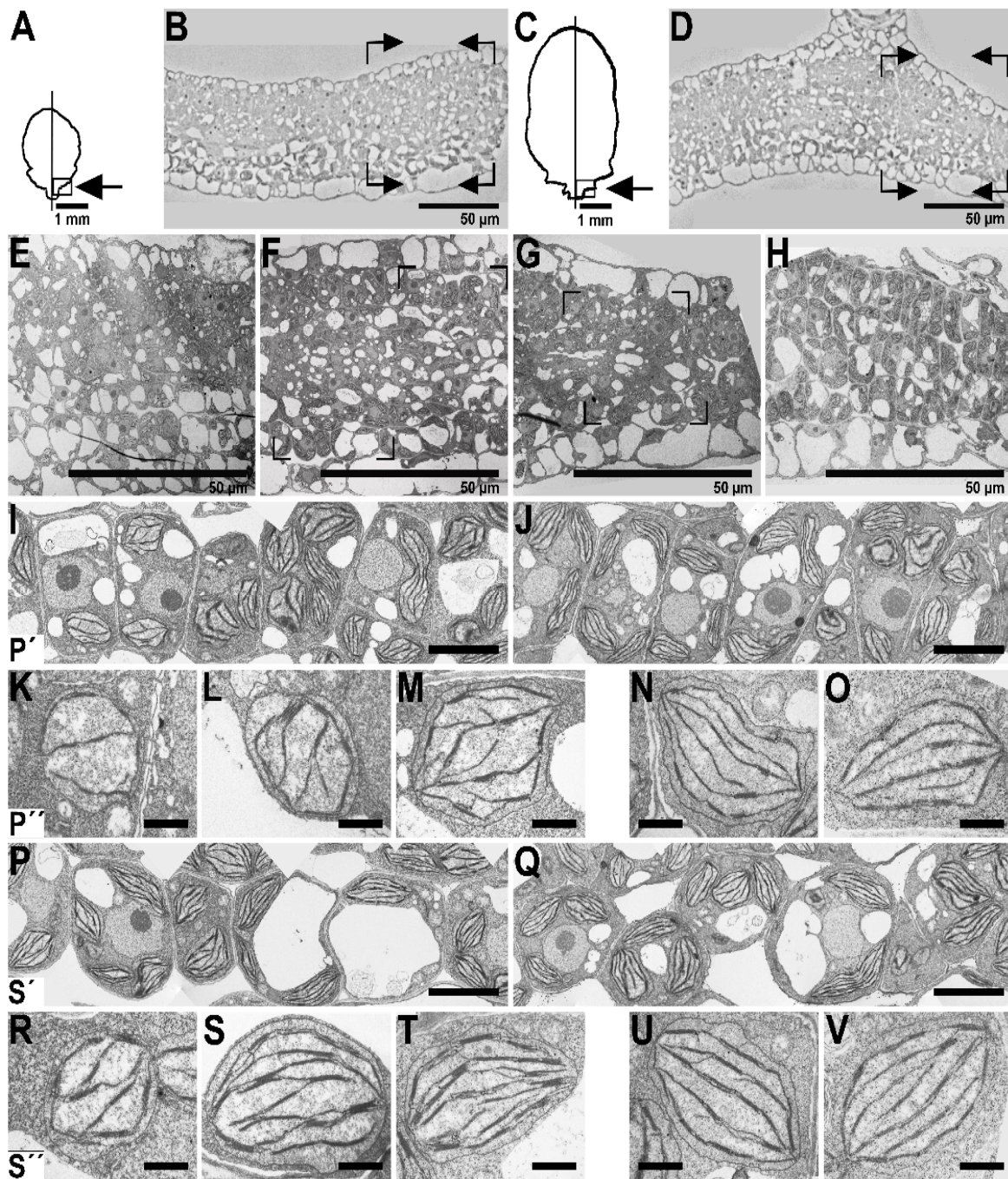


Fig 20: TEM of 14-day-old WT and *sytl5.2* mutant leaf base. *sytl5.2* (A, B, E, F, I, K-M, P, R-T) and WT (C, D, G, H, J, N, O, Q, U, V) vegetative leaf 4 base. A/C □ indicates leaf segment analyzed; B/D cross-section of the leaf base by phase-contrast light-microscopy. E/F and G/H TEM overview 1800x magnification, two different plants each; cells analyzed further in the palisade parenchyma P' and P'' in I, K-M and J, N, O and in the sponge parenchyma S' and S'' in P, R-T and Q, U, V. I/J and P/Q chloroplast in P' resp. S' TEM magnification 7100x, bar 5 μm, K-M and N/O in P'' and R-T and U/V resp. in S'' TEM magnification 22000x, bar 1 μm.

3.2.4 Accumulation of thylakoid membrane proteins in *syt15.2* mutants

Due to the strong phenotype, retarded growth and the altered chloroplast ultrastructure that manifested owing to lack of SYTL5.2, the accumulation of thylakoid membrane proteins was investigated further. Antisera against the subunits of PSII (D1), the cytochrome *b₆f* complex (Cyt*f*), PSI (PsaF, PsaA), the ATP synthase (Atp- β , CF₁- α/β), LHC1a and Curt1 proteins were used for immunoblot analysis. While the levels of CF₁- α/β and Atp- β were reduced to almost 75-50 %, levels of D1 and LHC1a were increased, as compared to WT. The protein levels of the cytochrome *b₆f* complex proteins; Cyt*f* and PSI subunits proteins; PsaF and PsaA were only marginally different (Fig: 21 a). Moreover, the levels of Curt1 were reduced to approximately 50 % in *syt15.2* plants as compared to WT (Fig: 21 a).

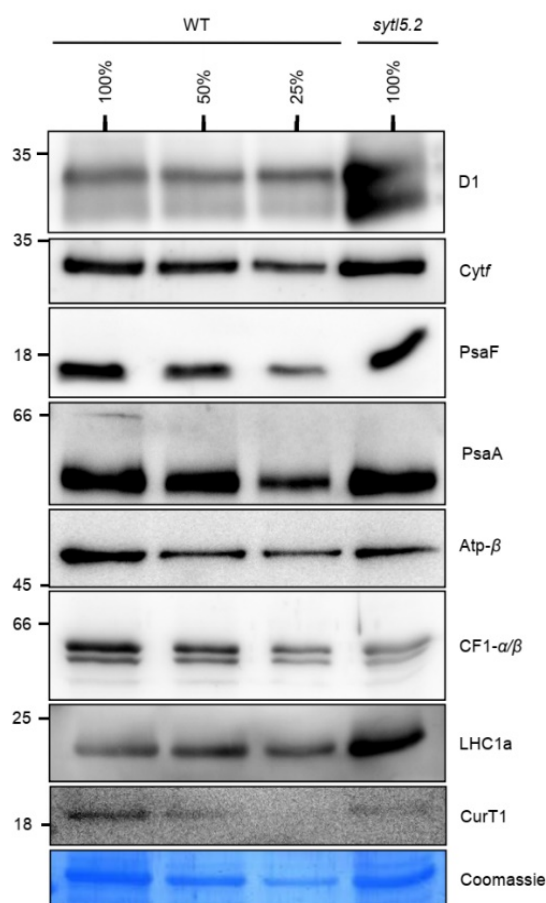


Fig 21: Accumulation of thylakoid membrane proteins in *syt15.2* mutants

(a) Total membrane protein samples isolated from the leaves of 21-day-old WT and *syt15.2* leaves were loaded on a 12 % SDS gel, blotted and probed with antibodies against proteins of the PSI and PSII, cytochrome *b₆f* complex, ATP synthase complex, LHC1a and Curt1 protein. 100 % protein equals 10 μ g of protein.

To further investigate the effect of altered thylakoid protein levels and defects in chloroplast morphology, the photosynthetic performance of WT and *syt15.2* plants was analyzed. No significant difference was observed in the photosynthetic performance (PSII quantum yield) of WT and *syt15.2* plants. More detailed analysis is required to understand effects of lack of SYTL5.2 on chloroplast function.

3.2.5 Generation of SYTL5.2 antibody

Antibodies against N- as well as C-terminal fragments SYTL5.2 were raised in order to detect the endogenously expressed SYTL5.2. For this, N-terminal 242 (31-272) amino acid and C-terminal 149 (516-665) amino acid SYTL5.2 fragments were cloned into pET51b (+) and pET21a (+) vectors respectively (Fig: 22 a and c).

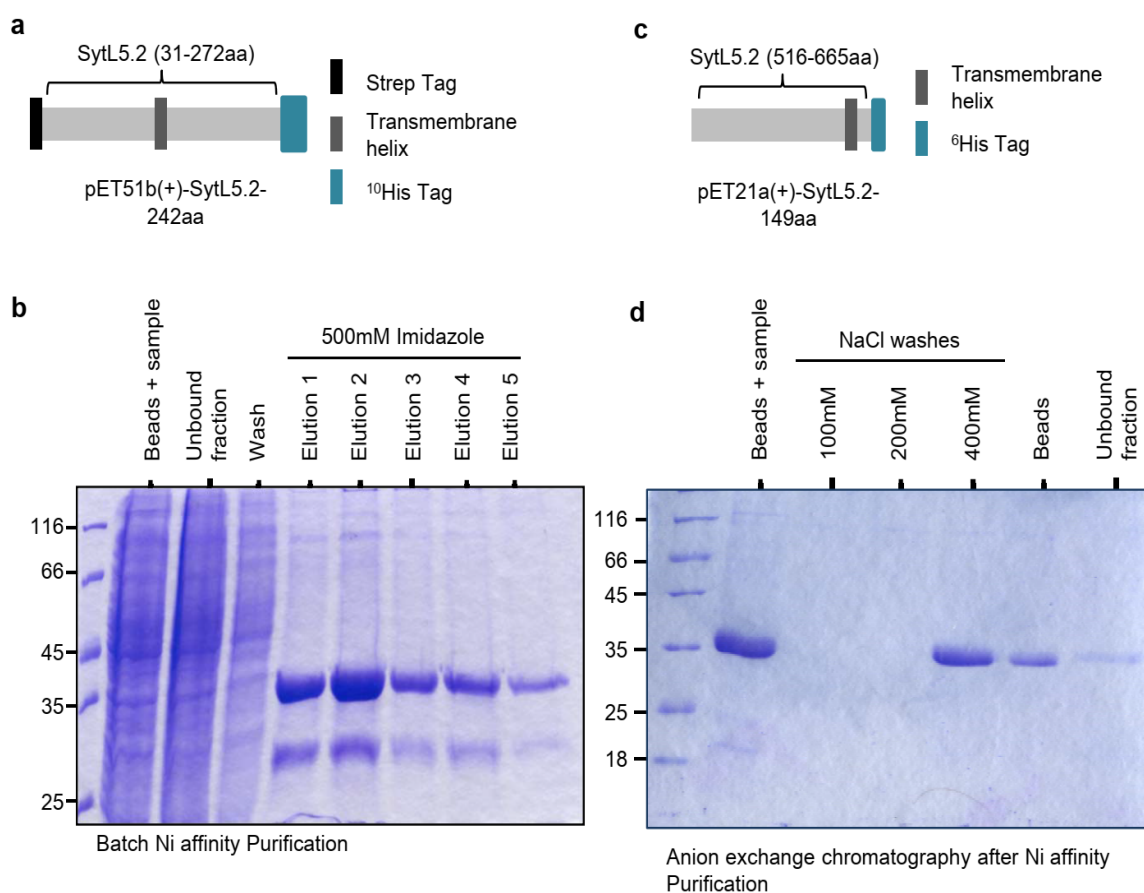


Fig 22: Generation of SYTL5.2 antibodies

(a and b) SYTL5.2 N-terminal antibody generation. **(a)** The schematic diagram of pET51b (+)-SYTL5.2 (242aa) plasmid depicting the relative positions of Strep-tag, transmembrane domain and ¹⁰His-tag. **(b)** The SDS-PAGE gels of SYTL5.2 (242aa) antigen purified by Nickel affinity chromatography used to immunize the rabbits. **(c and d)** SYTL5.2 C-terminal antibody generation. **(c)** The schematic diagram of pET21a (+)-SYTL5.2 (149aa) plasmid

depicting the relative positions of transmembrane domain and ⁶His tag. **(d)** The SDS-PAGE gels of SYTL5.2 (149aa) antigen purified by Nickel affinity chromatography followed by anion exchange chromatography used to immunize the rabbits.

The proteins were overexpressed in *E. coli* and purified to be used as antigens. Both antigen fragments were purified using nickel affinity chromatography and the C-terminal 149 amino acid fragment was further purified by anion exchange chromatography (Fig: 22b and d) before injecting into rabbits. Serum obtained from the immunized rabbits was further used to isolate polyclonal IgGs. Although both antisera could recognize the over-expressed and purified antigens, no band was detected for endogenous SYTL5.2, which could be due to low expression of the protein or selective expression in specific tissues.

Collectively, these results show that SYTL5.2 is a new member of plant synaptotagmin family found in plastids. Further work to understand the function of SYTL5.2 in chloroplasts is being done in collaboration with another research group at University of Bonn.

3.3 SNARE associated protein (SNARE_AP)

SNAREs and SNARE associated proteins are known to mediate vesicle trafficking along with synaptotagmins. Consequently, identification of plastidial SYTL5.2 led us to investigate and characterize SNARE_AP.

3.3.1 Characterization of *snare_ap* mutant line

To investigate the effect of the loss of SNARE_AP, *snare_ap* line (SALK_095443) in Col-0 background with a T-DNA insertion was analyzed (Fig: 23 a). Plants were screened for homozygous mutant lines through genotyping. Sequencing was done to confirm the position of the T-DNA insertion in the 3rd exon (Fig: 23b). Moreover, RT-PCR was done using homozygous plants to confirm that it is a knock-out line (bachelor's thesis by Simon Schrott). The phenotypic analysis of *snare_ap* plants grown in fluorescent light conditions (22°C, 100 µmol / m²s light, 16 / 8 h light / dark) revealed that the cotyledons and leaves of homozygous *snare_ap* plants were significantly paler as compared to WT. Moreover, the cotyledons showed a stronger phenotype as compared to the true leaves (Fig: 23 c-f). To quantify the amount of chlorophyll, leaves were harvested from 21 days old plants and chlorophyll estimations were done as described in Materials and Methods. In agreement with the phenotype observed, the total chlorophyll content was significantly reduced to 73 % as compared to WT (Fig: 23 h - i).

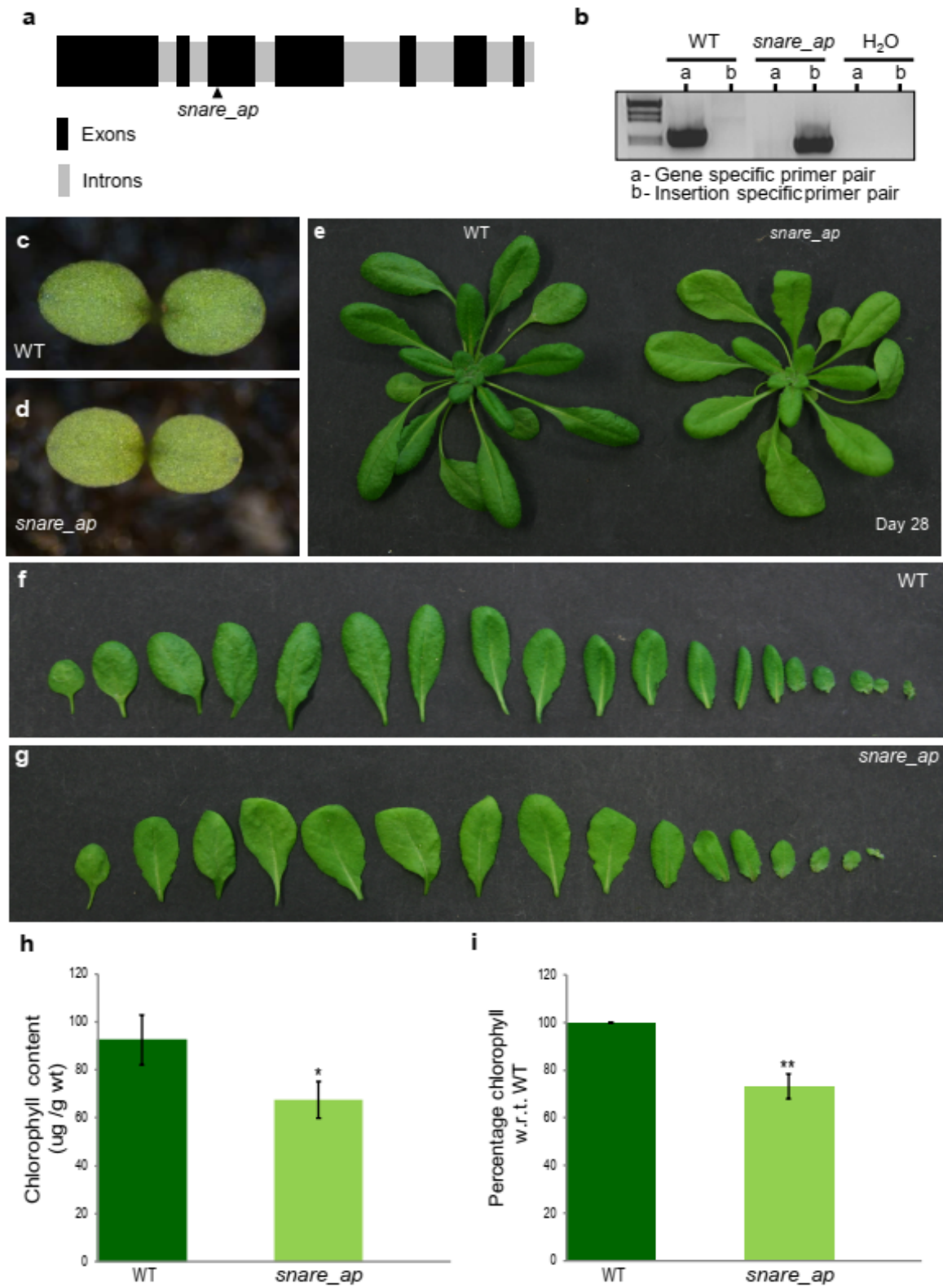


Fig 23: Phenotype of *snare_ap* mutant plants

a) The T-DNA insertion site mapped to the *SNARE_AP* gene in SALK_095443 line as indicated by the black arrowheads (black, exons; grey, introns). **(b)** Genotyping of *snare_ap* mutant and WT lines. **(c-g)** Phenotype of *snare_ap* mutants grown under standard long day, normal light conditions at 100 $\mu\text{M}/\text{s}/\text{m}^2$ intensity. **(c and d)** Cotyledons of WT **(c)** and *snare_ap* mutant **(d)**. **(e)** Rosettes of WT and *snare_ap* mutant. **(f and g)** Leaves of WT **(f)** and *snare_ap* mutant **(g)** separated from the rosette. **(h and i)** Chlorophyll content is reduced in *snare_ap* plants. Total chlorophyll content was measured using 21-day-old leaves. *P*-value: 0.028, *n*=3 **(h)**. Percentage chlorophyll content is reduced *snare_ap* leaves to 73.14% that of WT. *P*-value: 0.0009, *n*=3 **(i)**.

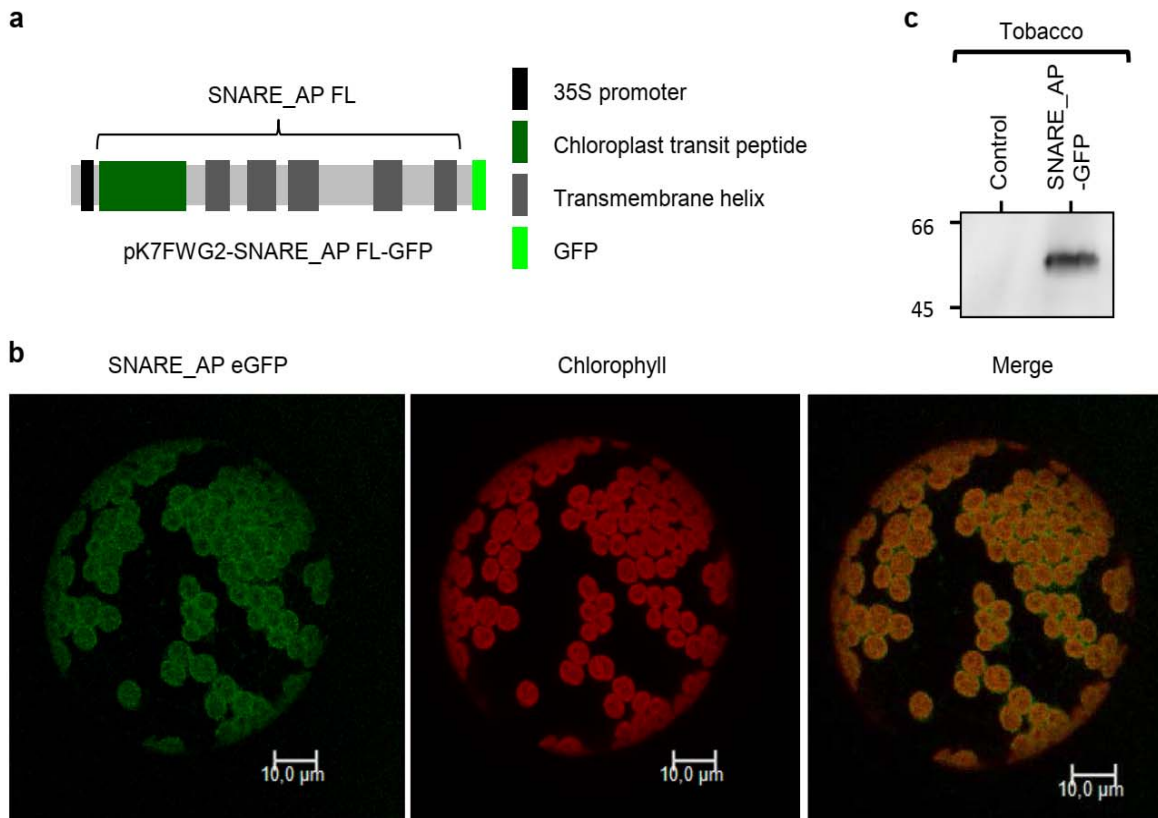


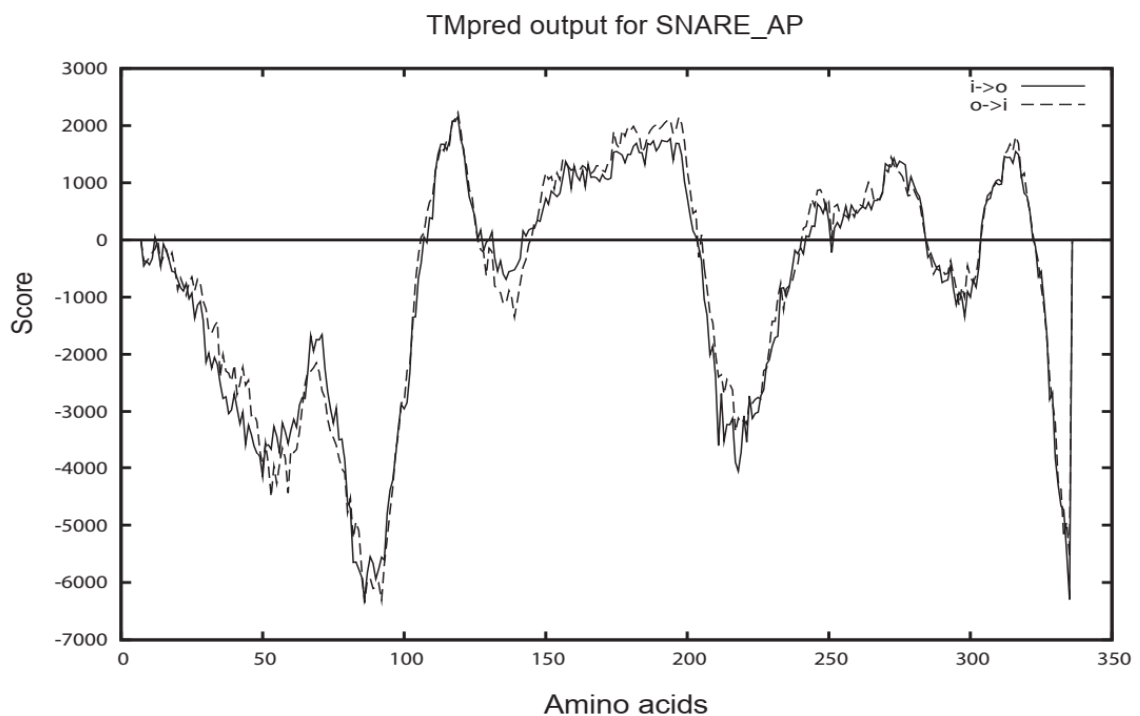
Fig 24: Localization of SNARE_AP

(a) SNARE_AP-GFP-pK7FWG2 plasmid. Schematic diagram depicting the relative positions of chloroplast transit peptide, transmembrane domain and GFP tag. **(b)** SNARE_AP-GFP detected in chloroplast. SNARE_AP FL GFP fusion protein was expressed transiently under the control of 35S promoter in Tobacco. SNARE_AP FL GFP signal in protoplast. Left: SNARE_AP FL GFP fluorescence, middle: chlorophyll auto-fluorescence, right: merged image. **(c)** Chloroplast transit peptide of SNARE_AP-GFP is approximately 91 amino acid. SNARE_AP FL GFP fusion protein immune-decorated with GFP antisera is detected at ~55kD after cleavage of ~10kD transit peptide.

3.3.2 GFP localization of SNARE_AP

SNARE_AP was predicted to have a chloroplast TP of 91 amino acids (TargetP). Consequently, the subcellular localization of SNARE_AP was analyzed by *in vivo* expression of SNARE_AP FL-GFP in tobacco. Protoplasts were isolated from tobacco leaves infiltrated with agrobacteria transformed with SNARE_AP FL-GFP fusion plasmid (Fig: 24 a). The GFP fusion protein expression was detected using a confocal laser scanning microscope. SNARE_AP FL-GFP signal was found in chloroplasts as indicated by overlay with the chlorophyll auto fluorescence (Fig: 24 b).

a



b

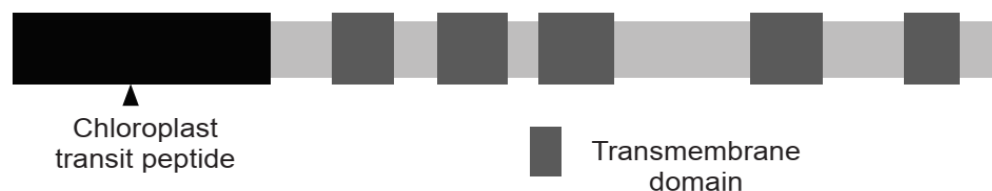


Fig 25: Structure of SNARE_AP

(a) Prediction of transmembrane domains in SNARE_AP using TM-PRED. Only the regions with scores above 500 were considered as transmembrane domains. (b) The schematic structure of SNARE_AP showing relative positions of transit peptide and the predicted transmembrane helices (black, Chloroplast transit peptide; grey, transmembrane helices).

To test the length of the chloroplast TP, immunoblot analysis was performed using anti GFP antiserum. The 65.3 kD SNARE_AP FL-GFP tagged preprotein is expected to run at around 55.3 kD after the cleavage of 91 amino acid long TP (10.3 kD). As expected, the GFP antiserum recognizes a band at about 55 kD (Fig: 24 c) confirming the prediction by TargetP. Moreover, TM Pred predicted that SNARE_AP contains 5 transmembrane helices. Fig: 25 b depicts the predicted domain structure of SNARE_AP with the relative position of the chloroplast targeting peptide and the transmembrane domains. Further experiments are needed to determine whether SNARE_AP is localized to the envelope or to the thylakoid membranes or both.

3.3.3 Analysis of the chloroplast ultrastructure in *snare_ap* mutant lines

To test if the pale green phenotype was accompanied by chloroplast ultrastructural changes, transmission electron microscopy was performed to analyze WT and mutant plants. Chloroplasts from mutant 7-day-old cotyledons and 14-day-old primary leaves analyzed showed that mutant plants developed abnormal as well as normal chloroplasts. In comparison to WT, grana-stacks of thylakoids were loosely appressed, and the lumen was

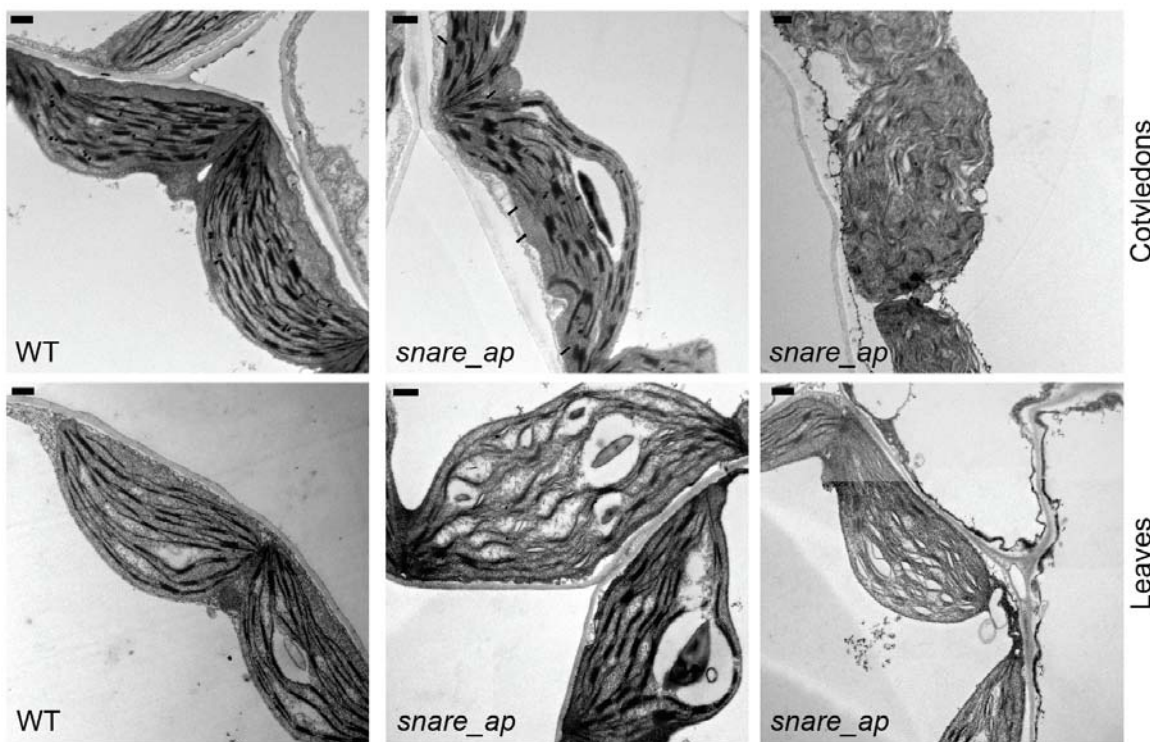


Fig 26: Chloroplast ultrastructure in WT and *snare_ap* plants. TEM images of chloroplasts in 7-day-old cotyledons and 14-day-old leaves from WT and *snare_ap* plants. TEM magnification 22200x, bar 250 nm.

blown up in *snare_ap* plastids. The grana stacks displayed a curved structure with disorganized non-parallel arrangement. In addition, a higher number of vesicles were observed near the envelope in *snare_ap* plastids as compared to WT. The phenotype also appeared to be stronger in cotyledons than in primary leaves (Figure 26). The transmission electron microscopy experiments have been performed by Prof. Dr. Andreas Klingl, LMU Munich.

3.3.4 Lack of SNARE_AP affects the accumulation of photosynthetic complexes and thylakoid membrane proteins but not their assembly

The ultrastructural changes that manifest in the *snare_ap* plastids led us to investigate if the assembly of the photosynthetic complexes and the levels of thylakoid membrane proteins were also affected. BN-PAGE analysis was performed to inspect the assembly of the photosynthetic complexes (Fig. 27 a). Thylakoid membranes were isolated from leaves of 21-day-old WT and *snare_ap* plants. The photosynthetic protein complexes were separated by loading equal amount of protein on a 5-15 % BN gel post solubilization in 1 % dodecyl- β -D-maltoside. Significant reduction was observed in accumulation of PSII-LHCII super-complexes in mutant as compared to WT (Fig. 27 a). In order to test whether this reduction is due to defects in assembly of these super-complexes, ^{35}S -labelling experiments were performed. For this 21-day-old WT and *snare_ap* plants grown on MS plates were used for *in vivo* labelling followed by fractionation of photosynthetic complexes by BN-PAGE. Intriguingly, despite the reduced accumulation of steady-state super-complexes observed, the assembly of these complexes was not affected, indicating that the stability of the complexes is affected (Fig. 27 b).

As a next step, to analyze the accumulation of photosynthetic complex proteins in chloroplasts, immunoblotting was performed. The antisera against subunits of PSII (CP47, D2), PSI (PsaA), the cytochrome *b₆f* complex (Cyt*f*), the ATP synthase (atp β) and Curt1 protein were used (Fig. 27 c). The levels of PSI (PsaA) and PSII (D2 and CP47) components were found to be only marginally different from the WT levels, whereas the amount of Cyt*f* and atp β were reduced to approximately 70% in *snare_ap* plants in comparison to WT. Moreover, levels of Curt1 were found to be comparable to that of WT albeit the disorganized and curved thylakoid membrane system observed in *snare_ap* plastids. (Fig. 27 c). Taken together, these results hint to lack of SNARE_AP affecting the stability rather than the assembly of these complexes.

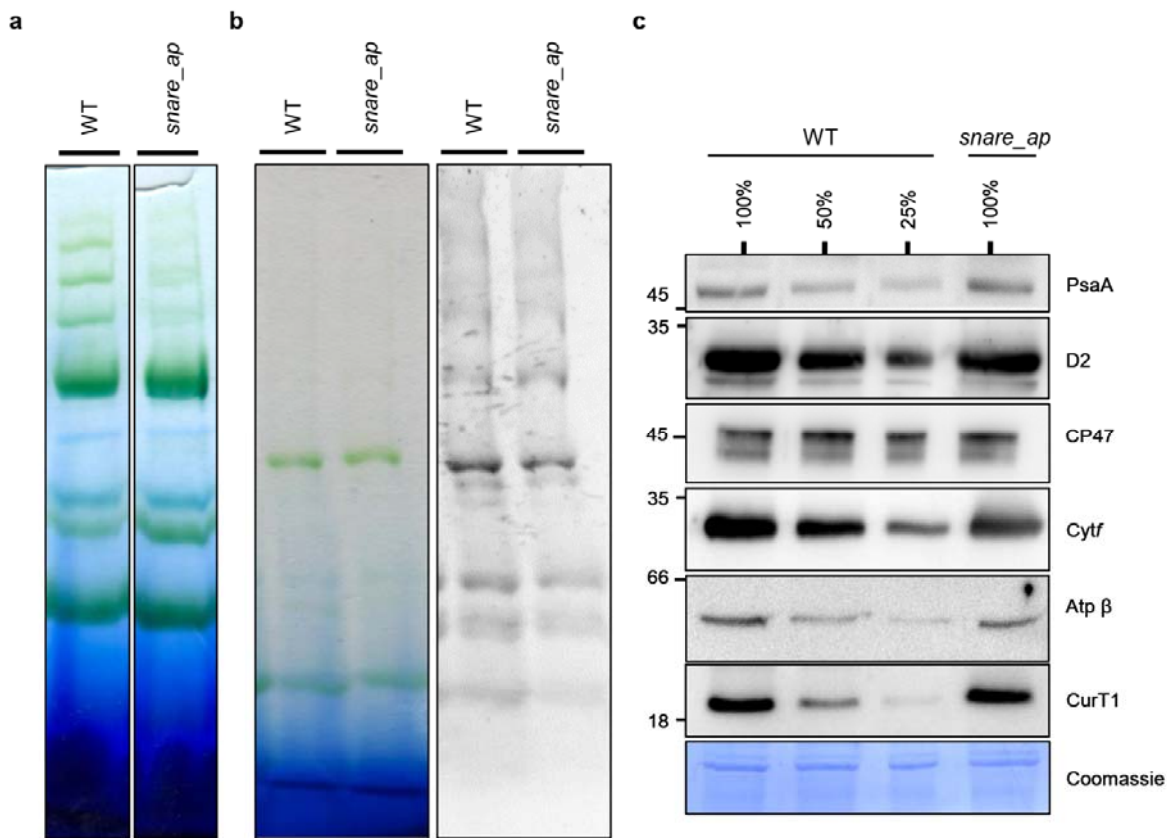


Fig 27: Lack of SNARE_AP affects the accumulation of thylakoid membrane proteins and photosynthetic complexes but not their assembly

(a) Thylakoids were isolated from the leaves of 21-day-old WT and *snare_ap* plants, solubilized in 1 % β -dodecylmaltoside and photosynthetic complexes were separated by BN-PAGE. (b) Thylakoids were isolated after ³⁵S-labelling of 21-day-old WT and *snare_ap* plants grown on MS plates, solubilized in 1 % β -dodecylmaltoside and photosynthetic complexes were separated by BN-PAGE (left panel). The dried gel was used to expose a phosphor-screen and scanned (right panel). (c) Total membrane protein isolated from the leaves of 21-day-old WT and *snare_ap* leaves was loaded on a 12 % SDS gel, blotted and probed with antibodies against proteins of the PSI and PSII, Cytochrome *b₆f* complex, ATP synthase complex and Curt1 protein. 100% protein equals 10 μ g of protein.

3.3.5 Generation of SNARE_AP-FL-GFP lines

Since there is only one *snare_ap* knock-out line available, the mutant line was complemented with full length SNARE_AP fused with GFP at the C-terminal. The pK7FWG2-SNARE_AP-FL-GFP construct (Fig: 24a) was used for transformation of *snare_ap* and WT plants using agrobacteria. The seeds obtained were further selected against kanamycin resistance to obtain the F2 generation of the complemented and overexpression lines. Three independent complemented lines; *snare_ap*:35S: SNARE_AP-GFP comp#1, *snare_ap*:35S: SNARE_AP-

GFP comp#2 and *snare_ap*:35S: SNARE_AP-GFP comp#3 (hereafter referred as *snare_ap* GFP comp#1, #2 ad #3) and two independent overexpression lines; Col-0:35S: SNARE_AP-GFP OE#3 and Col-0:35S: SNARE_AP-GFP OE#7 (hence forth referred as *snare_ap* GFP OE#3 and #7).

The expression of the SNARE_AP-GFP was confirmed using confocal laser scanning microscope in both, complemented (Fig: 28 a) and overexpression lines (Fig: 28 b). Moreover, SNARE_AP FL-GFP signal was detected in chloroplasts as indicated by the chlorophyll auto fluorescence confirming the earlier observation using transient transformation in tobacco (section 3.3.2).

3.3.6 Phenotypic analysis of etiolated *snare_ap* and GFP complementation lines

The effects of the loss of SNARE_AP on de-etiolation of cotyledons was investigated since severe defects were observed in thylakoid structure in cotyledons. The greening defects in seedlings of WT, *snare_ap* and *snare_ap* GFP comp#3 lines were tested. After imbibition of seeds at 4 °C, the plates were illuminated for 2 h in light and then grown in darkness. After six days in darkness, the plates were transferred to light and differences in greening were observed at 2, 6, 8 and 24 h. Chlorophyll isolation and PAM analysis was performed for quantification of differences during chloroplast differentiation. The greening of cotyledons was significantly delayed in *snare_ap* unlike WT and *snare_ap* GFP comp#3 seedlings (Fig: 29 a). This was also evident from the chlorophyll content measured in these samples during the time course of 2, 6 and 24 hours post illumination. The chlorophyll accumulation in the mutant reached to about 62 % of WT level after 4 h and 63 % by 6 h while that of *snare_ap* GFP comp#3 reached to 78 % and 141 % of WT during the same time interval. Nonetheless, chlorophyll accumulation was stabilized to levels comparable to WT after 24 h in both mutant and complemented line suggesting only partial impairment of the greening process (Fig: 29 b). Additionally, the photosynthetic performance of PSII was quantified by measuring the chlorophyll *a* fluorescence for WT and *snare_ap* seedlings. The maximum quantum yield of PSII (Fv/Fm) measured 8 h post illumination as was reduced to 0.45 ± 0.02 in *snare_ap* compared to WT with 0.55 ± 0.07 . Nevertheless, in agreement with the chlorophyll measurements, *snare_ap* seedlings (0.55 ± 0.02) attain similar photosynthetic activity to that of WT (0.6 ± 0.03) 24 h after illumination (Fig: 29 c).

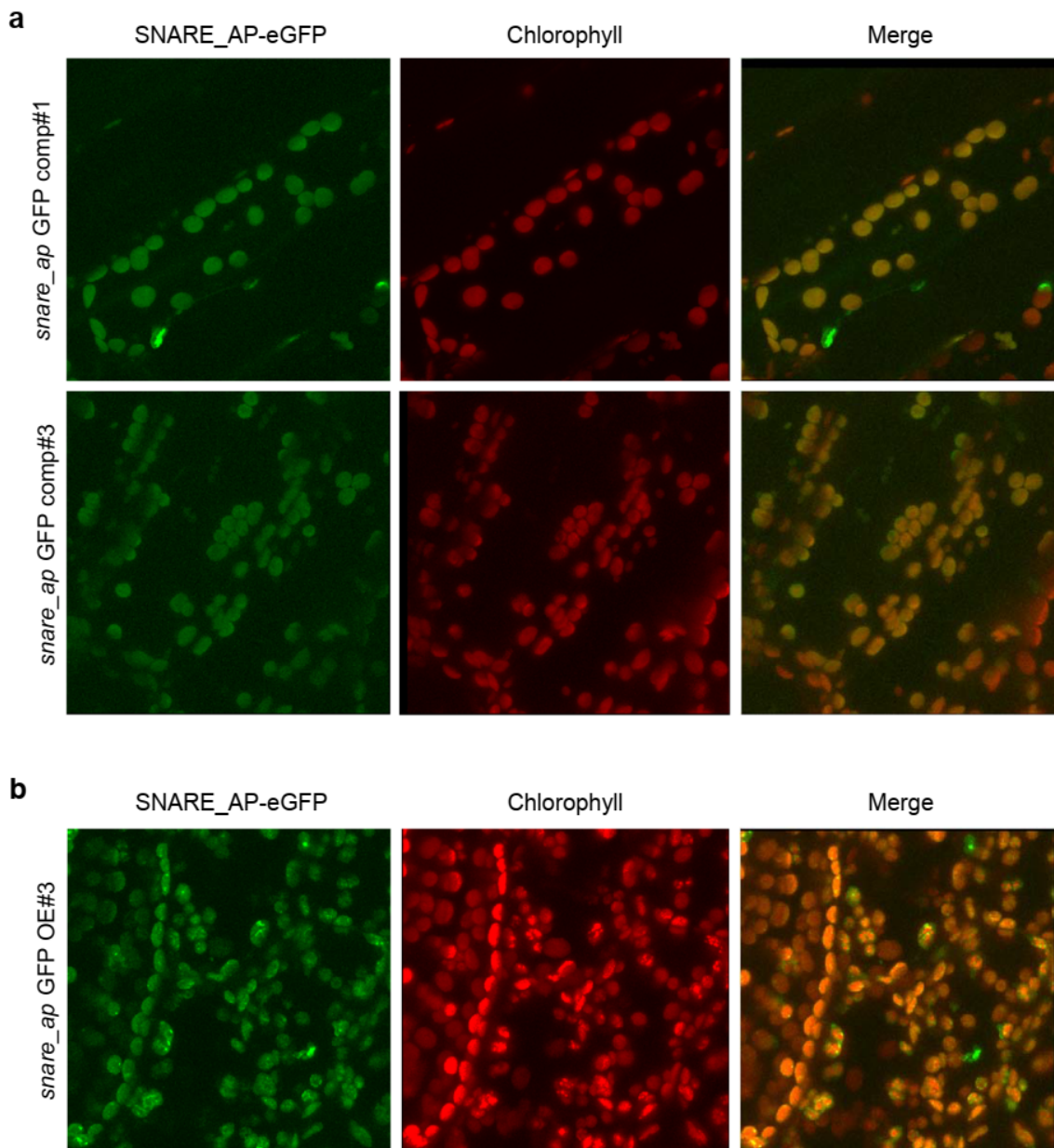


Fig 28: Stable expression of SARE_AP FL-GFP in WT and *snare_ap* mutant lines

SNARE_AP FL GFP fusion protein was expressed stably under the control of 35S promoter *snare_ap* and Col-0 plants. **(a)** SNARE_AP-GFP signal detected in chloroplasts in *snare_ap* plants complemented with SNARE_AP FL-GFP (Upper panel: *snare_ap*:35S: SNARE_AP-GFP comp#1 and lower panel: *snare_ap*:35S: SNARE_AP-GFP comp#3). **(b)** SNARE_AP-GFP signal detected in chloroplasts in Col-0 plants transformed with SNARE_AP FL-GFP (Col-0:35S: SNARE_AP-GFP OE#3). Left: SNARE_AP FL GFP fluorescence, middle: chlorophyll auto-fluorescence, right: merged image.

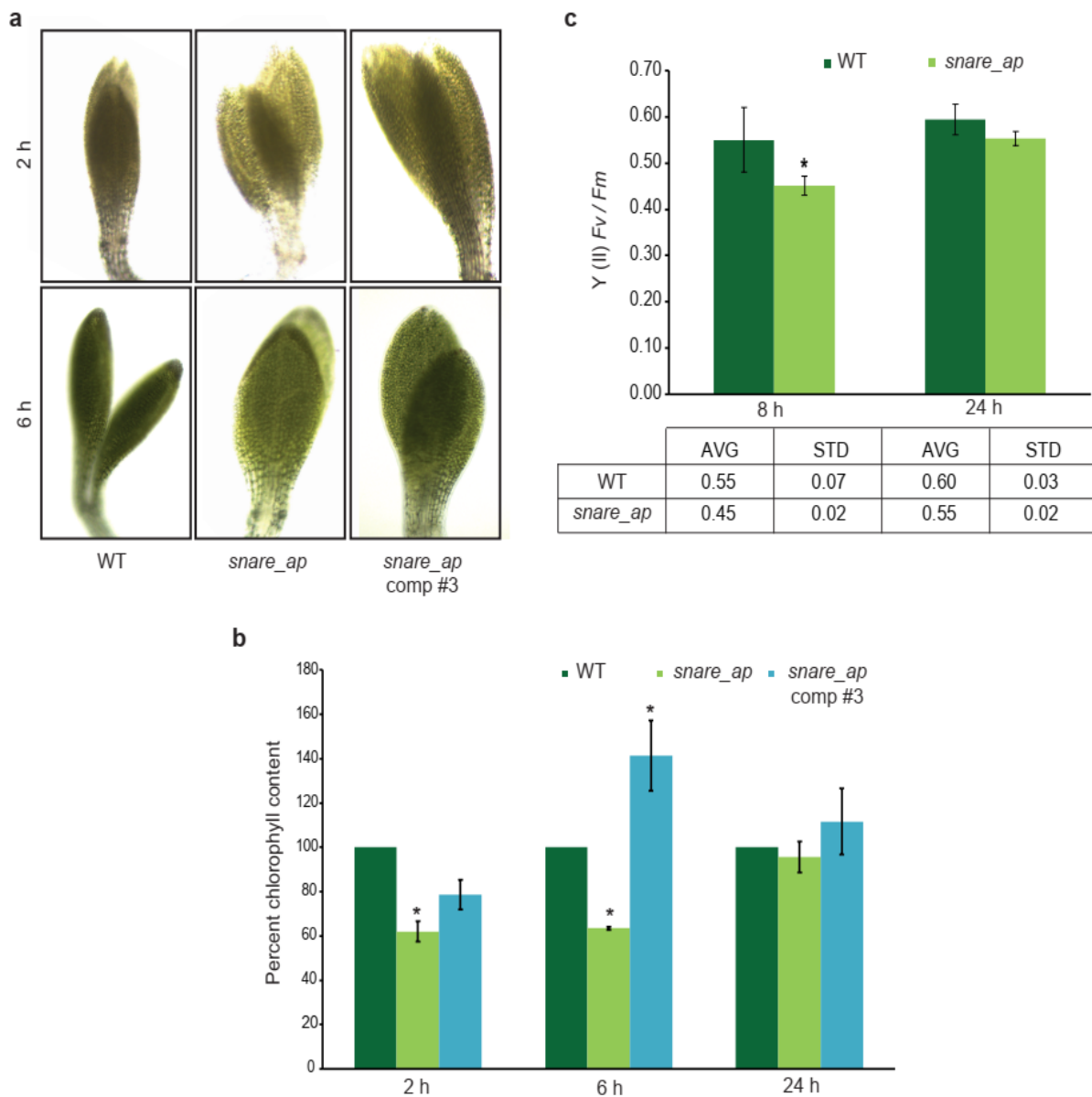


Figure 29: Greening of *snare_ap* mutant plants.

a) Representative seedlings of the WT, *snare_ap* and *snare_ap* GFP comp# 3 lines shown 2hr and 6 h after exposure of etiolated seedlings to light ($100 \mu\text{Em}^{-2}\text{s}^{-1}$) **b)** Percentage chlorophyll concentration with respect to WT measured 2, 6 and 24 h after illumination. ($n = 3$, p value < 0.05) **c)** PSII yield (F_v/F_m) measured at 8 and 24 h post illumination in wild-type and mutant plants ($n = 5$, p value < 0.05).

3.3.7 Generation of SNARE_AP antibody

With an aim to detect the endogenously expressed SNARE_AP, an antibody was raised against the recombinant SNARE_AP protein. SNARE_AP-TP (250aa) was cloned into pMal-c5x vector (Fig: 30 a), overexpressed in bacteria (partially soluble) and further purified using batch nickel

affinity chromatography (Fig: 30 b and c). Mass spectroscopy was used to confirm that the purified antigen is indeed SNARE_AP protein fragment and further used to immunize two rabbits. The serum obtained from these was further used to isolate polyclonal IgG. Though both antisera could recognize the over-expressed and purified antigens, no band was detected for the endogenous SNARE_AP. Further purification of the antisera and optimization of the immunoblotting protocol is necessary to use the antibodies for future experiments.

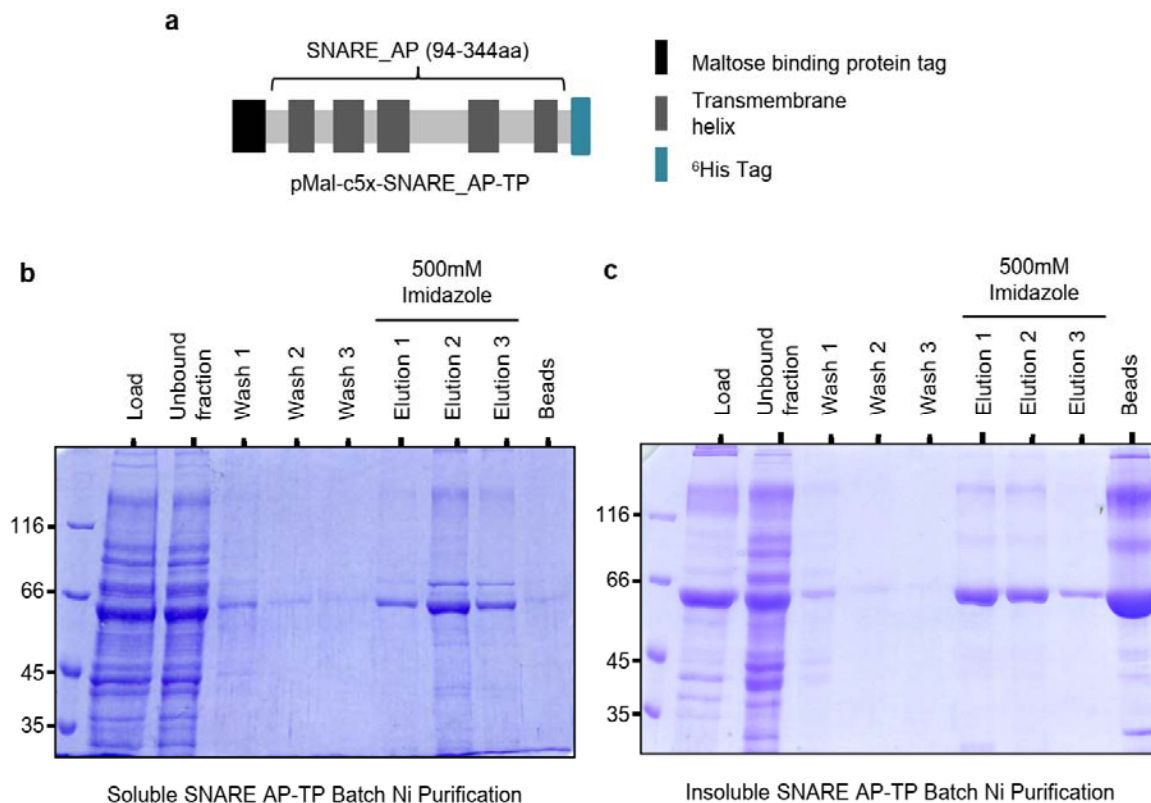


Fig 30: Generation of SNARE_AP antibody

(a) The schematic diagram of pMal-c5x-SNARE_AP-TP (250aa) plasmid depicting the relative positions of Maltose binding protein tag, transmembrane domain and ⁶His tag. (b and c) The SDS-PAGE gels of SNARE_AP-TP (250aa) antigen purified by Nickel affinity chromatography (Batch) used to immunize the rabbits.

4 Discussion

Chloroplast development and in particular thylakoid biogenesis is a complex process. The proplastids containing very little internal membrane structure differentiate into fully functional mature chloroplasts with an elaborate internal membrane network. It is well accepted now that vesicles and tubules originating from the envelope membrane form the thylakoid network and that vesicle trafficking is an ongoing process inside chloroplasts (Charuvi et al., 2012; Lindquist et al., 2016; Vothknecht and Westhoff, 2001; Westphal et al., 2001). It is assumed that these vesicles and tubules carry the cargo for thylakoid membrane biogenesis as well as maintenance (Jilly et al. 2018; Karim and Aronsson 2014; Waters and Langdale 2009; Westphal et al. 2001). Although the structural changes in the architecture of thylakoid membranes is becoming more and more clear with the use of transmission electron microscopy and electron tomography studies (Charuvi et al., 2012; Liang et al., 2018), the evidence regarding molecular players involved in proplastid-chloroplast transition is still mostly speculative. Several mutants with defects in chloroplast ultrastructure and thylakoid grana stacking such as Chlorata-42 (CH-42) (Apchelimov et al., 2007), grana-deficient chloroplast 1 (GDC1) (Cui et al., 2011), angulate 10 (ANU10) (Casanova-Sáez et al., 2014), snow-white leaf 1 (SWL1) (Hayashi-Tsugane et al., 2014) etc. have been characterized so far. Naturally most of these mutants showed reduced amount of thylakoid membrane proteins such as LHCs. It is assumed that the process of photosynthetic complex assembly and thylakoid network formation occurs in parallel. Thus, it is difficult to segregate and dissect these extremely entangled processes clearly (Junglas and Schneider, 2018).

Proteomic and transcriptomics studies, genetic screening as well as bioinformatic approaches have been utilized in search of candidate proteins and have made important contributions to elucidating various biochemical pathways. Few potential chloroplast vesicle trafficking proteins like Vipp1 (Kroll et al., 2001), THF1 (Wang, 2004), Sar1 (Garcia et al., 2010), CURT1 (Armbruster et al., 2013b) and CPRabA5e (Karim et al., 2014) were identified using these approaches. Nonetheless, detailed molecular mechanisms still remain unknown. In the present work, three potential chloroplast vesicle trafficking candidate proteins; FZL, SYTL5.2 and SNARE_AP were characterized.

4.1 FZL: The Fuzzy Onion-Like protein

4.1.1 *fzl* mutant characterization

The *fzl* mutants in Col-0 background were previously reported to have pale green leaves and fewer, but larger, chloroplasts with changes in the grana stacks and stroma lamellae

organization in thylakoids (Gao et al., 2006). Since no differences in total lipid and/or fatty acid composition were observed in *fzl* relative to WT, the changes in chloroplast size were considered to be a secondary effect and the function of *fzl* remained unclear.

In the present study, all three independent T-DNA insertion lines analyzed for *fzl* showed a pale green phenotype from 11 days onwards when grown under LED light. Interestingly, there was no visible phenotype observed in younger plants. The phenotype was more prominent in plants grown in LED light compared to those grown under fluorescent light. Also, the chlorophyll content in *fzl* plants was about 70% that of WT. (Fig: 6 and 7). Additionally, the higher average diameter of chloroplasts observed in all mutant leaves along with reduced chlorophyll corroborated the phenotype and is in agreement with the earlier reports (Fig: 7) (Gao et al. 2006; Michela Landoni et al. 2013)

4.1.2 FZL is primarily localized at the inner envelope membrane of the chloroplast

Gao et al. have generated an *Arabidopsis* line overexpressing an FZL-GFP fusion protein and found it to be localized to chloroplasts. Besides, with increasing expression levels, FZL-GFP puncta could be seen at the envelope as well as inside the chloroplast. Subsequently, they sub-fractionated chloroplasts from these lines and showed that FZL-GFP is localized to both the chloroplast inner envelope and the thylakoid membrane using a GFP-specific antibody (Gao et al., 2006). Moreover, the same FZL-GFP fusion proteins expression line was used to localize FZL to grana margins using immunogold labeling against GFP (Liang et al., 2018). Nevertheless, the localization was analyzed only for the overexpressed FZL-GFP protein and not that of the endogenous one. Therefore, FZL specific antibody was raised and immunoblotting analysis using WT and *fzl* leaf samples was performed to confirm the specificity (Fig: 6 e). The endogenously expressed FZL was primarily present in the inner envelope of the chloroplast based on the tests with pea chloroplast sub-fractions. (Fig. 8 a). The discrepancy with the results of Gao et al. could be due to miss-localization of GFP tagged FZL owing to its overexpression.

FZL is the only protein homologous to the mitochondrial fusion factor, FZO, found in plants. Although *in silico* analysis predicted FZL to be localized to chloroplasts and/or mitochondria, immunoblotting with FZL antisera failed to detect endogenous FZL in mitochondria (Fig: 8 b), thus confirming earlier observations using fluorescence tagged FZL (Gao et al., 2006; Tremblay et al., 2016).

4.1.3 Photosynthetic performance of *fzl* mutants is affected

As the phenotype of *fzl* became apparent in mature leaves after approx. 11-13 days post germination, the accumulation of thylakoid membrane proteins was tested. The results show that the levels of cytochrome *b₆f* (Cyt*f* and Cyt*b₆*) complex proteins as well as D1

were significantly reduced in 20-day-old plants, although the steady-state concentrations of PSI (PsaF) and PSII (D1 and CP47) components were only slightly reduced. On the other hand, the Levels of the ATP synthase (CF₁- α/β) were marginally higher. Similar effects have been noted previously in mutants of low molecular weight subunits of the cytochrome *b₆f* complex (PetL, PetG, and PetN) (Schwenkert et al. 2007). Interestingly, no significant changes were observed in younger, 10-day-old plants, showing that the phenotype is age dependent (Fig. 10).

The cytochrome *b₆f* complex is involved the transfer of electrons from PSII to PSI and thus functions as a rate limiting step in photosynthesis (Schottler et al. 2007). It plays a predominant role in photosynthetic flux control and is consequently involved in the redox regulation in close coordination with ATP synthase (Schottler et al. 2015). The low Cyt_f and Cyt_{b₆} levels indicated towards impaired electron flow from PSII to PSI as corroborated by the photosynthetic measurements of the ETR (Fig: 9). The biogenesis of the cytochrome *b₆f* complex is known to occur mainly in younger leaves and the turn-over rate decreases over time in mature leaves. This is in contrast to the turn-over rates of components of PSI and PSII, which remain higher in mature leaves (Schottler et al. 2007). These considerations point towards the hypothesis that loss of FZL impairs thylakoid maintenance or remodeling in mature leaves, rather than thylakoid biogenesis itself. It can be assumed that when the other components of the photosynthetic electron transport chain are still largely intact, the selective decrease in levels of the cytochrome *b₆f* complex in 20-day-old *fzI* mutants is due to differences in its turn-over rates in mature leaves.

4.1.4 Global transcriptome analysis of WT vs *fzI*

To shed more light on the processes that are affected by the loss of FZL, a global transcriptomic study to identify genes that are differentially regulated in the *fzI* mutant relative to WT before and after the onset of a visible phenotype was performed (For data refer sup. table 1, (Patil et al. 2018). Tetrapyrrole synthesis genes were found to be significantly deregulated, which is displayed by the decrease in chlorophyll content in *fzI* mutants (Fig. 7 c). Interestingly, though the genes for the light harvesting complex (LHCs) proteins were unexpectedly up-regulated to a little extent, no significant changes were observed when analyzed at the protein level (Fig: 13 a). Transcriptomic analysis also revealed down-regulation in the levels of genes encoding enzymes of carbohydrate metabolism. However, despite this downregulation at the transcriptional level, GAPC1 and G6PDH protein levels were higher, TIP levels were unchanged and amounts of SDH4 were found to be reduced in the *fzI* mutant as compared to WT (Fig: 13 b). This inconsistency can be accounted for by difference between the regulation of mRNA transcription and protein translation processes.

FZL was reported to be responsible for regulating cell death and defense responses in *fzI* (Ler) mutants displaying LMM phenotype. The LMM phenotype persisted in heterozygotes obtained by crossing *fzI* (Col-0) with *fzI* (Ler) and several senescence-, autophagy- and defense-related genes were up-regulated (Landoni et al. 2013; Tremblay et al. 2016). Although *fzI* (Col-0) does not show a specific senescence related phenotype; the transcriptome data was searched for changes in senescence-related genes to indicate a general role for FZL in this process owing to the LMM phenotype in the Ler background. No significant changes in the expression patterns of senescence- and autophagy- related genes were found before or after the appearance of the pale green phenotype. This is corroborated by the results by Landoni *et al.* wherein the LMM phenotype in *fzI* (Ler) mutants could be rescued by the growth at high temperature and under low light conditions, indicating that the defense and cell death responses are probably a secondary effect due to the loss of FZL (Landoni et al. 2013).

4.1.5 *In silico* structural modelling of FZL and its role in vesicle trafficking

Due to the observed increase in number of vesicles in chloroplasts of mutants leaves; a dynamin-like GTPase, FZL has long been hypothesized to be involved in vesicle mediated thylakoid membrane biogenesis processes (Gao et al. 2006; Jilly et al. 2018; Karim and Aronsson 2014; Waters and Langdale 2009). Further support for a role of FZL in membrane fission or fusion came from the studies on bacterial dynamin-like protein (BDLP), the closest cyanobacterial homolog of FZL. The bacterial BDLP and FZL share 29% overall identity that is mainly contributed by the GTPase domain although FZL has a longer N-terminal extension as compared to BDLP, which includes the transit peptide. The crystal structure of BDLP was resolved and the mechanism of BDLP induced membrane curvature was analyzed by the group of Jan Löwe using cryo-electron microscopy reconstruction studies (Low and Löwe, 2006; Low et al., 2009). This GDP bound BDLP protein structure was used as template in one to one threading for *in silico* structural prediction of FZL (288-912 aa). The results show that the structures are highly similar with 100 % confidence (Fig: 14), indicating that FZL could act in analogous way to mediate membrane fission or fusion. Moreover, experiments using anti FZL antisera showing that FZL is primarily localized to the inner envelope (Fig: 8 a) together with trypsin protease treatment experiments by Gao *et al.* suggest that the GTPase domain and the coiled-coiled domain are exposed on the stromal side. Therefore, FZL could mediate vesicle fission at the inner envelope membrane. However, the postulated role of FZL in membrane fission does not agree with the increased number of vesicles seen in *fzI* chloroplast by Gao *et al* (Gao et al., 2006). Additionally, no vesicle accumulation could be seen in the electron micrographs shown by Tremblay *et al* (Tremblay et al., 2016). This discrepancy

in regard to presence or absence as well as number of vesicles could arise from various factors including the developmental stage of leaf, age of plants, or growth conditions (Gügel and Soll, 2017). Moreover, none of the known or predicted chloroplast vesicle trafficking proteins were found to be dysregulated at least in the transcriptomic study, thus FZL could be a novel factor. In a recent study by Liang et al, 3D architecture of thylakoid network during proplastid to chloroplast transition in cotyledons was studied in *fz/* plants. They observed that the thylakoid formation in chloroplasts of *fz/* cotyledons was in general retarded as compared to WT. More importantly, they observed that after 120 hours post imbibition (hpi) of seeds, in WT plastids contain well organized and tightly appressed grana stacks that are well connected by stroma lamellae. However, in *fz/* mutant plastids exhibited multiple elongated, spiral pre-grana thylakoids with small diameter that were not interconnected with stroma lamellae suggesting lack of fusion events (Liang et al., 2018). Intriguingly, they also observed that most of the vesicles that were present in 36 hpi in *fz/* plastids underwent fusion event by 60 hpi forming pre-grana and small grana stacked thylakoids similar to WT. It is possible to imagine that there are multiple proteins mediating fusion events at distinct stages of thylakoid formation.

Collectively, these results show that FZL is primarily localized to the chloroplast inner envelope and not to the thylakoids, but nevertheless seems to affect the maintenance of thylakoid membranes and photosynthetic protein complexes. (Passages of the text were taken from of a previous publication of the author (Patil et al. 2018).

4.2 Synaptotagmin 5.2

4.2.1 *sytl5.2* mutant characterization

In the present work, an atypical synaptotagmin family protein, SYTL5.2 was analyzed using a T-DNA insertion line. The genotype of *sytl5.2* plants was confirmed to be homozygous using genotyping RT-PCRs. However, all the attempts to confirm the same using RT-PCRs to detect the transcript as well as at the protein expression failed. The expression profile of *SYTL5.2* gene is not available for *Arabidopsis* since AtH chip gene set does not include *SYTL5.2*. Moreover, attempts to detect the expression of endogenous SYTL5.2 using self-raised anti-SYTL5.2 antibodies against both N and C terminal end of the protein or by promoter GUS assays were unsuccessful as well. The expression of SYTL5.2 protein in *Arabidopsis* was nevertheless confirmed by two independent proteomic studies. The peptides of SYTL5.2 have been detected in our mass spectrometry analysis of chloroplast membranes (unpublished data) and by Davidi *et al.* (Davidi et al., 2015). Recently, RNA-Seq and TRAP RNA-Seq data was analyzed in rice that showed *OsSYTL5* gene was constitutively expressed in various tissues. However, the relative transcript

values based on qRT-PCR are very low (Huang et al., 2017). The expression pattern of *SYTL5.2* in different organs and at various developmental stages is yet unknown and could be the reason for the unsuccessful RT-PCRs, GUS assays and immune-blot analysis. Additionally, another possibility is that *SYTL5.2* is expressed and / or active only under certain conditions, and / or only in very small amounts, therefore making it difficult to detect when tested under normal growth conditions. Although *SYT1* is ubiquitously expressed, similar differential activity was indeed observed in regulation of sensitivity to osmotic stress. *SYT1* was found to be differentially active in meristematic cells of root tips as compared to the cells in elongation zone (Schapire et al., 2008). Further experiments using other methods like *in situ* hybridization to detect *SYTL5.2* RNA using complementary digoxigenin-labelled riboprobes could possibly elucidate the expression pattern.

Phenotypic analysis of the homozygous knock out *syt15.2* plants showed a crumpled leaf phenotype in true leaves, cauline leaves, sepals and petals along with broad, vascular petioles (Fig: 15). There was overall retardation of growth with delay in elongation of inflorescence. Additionally, the synchronous maturation of anthers and stigma observed in flowers was reflected by the reduced seed set in *syt15.2* as compared to WT (Fig: 15). Besides, complementation of *syt15.2* lines was done with endogenous *SYTL5.2* which resulted in complete rescue of the phenotype (Fig:16) confirming that the observed crumpled leaf effect was indeed caused due to lack of *SYTL5.2*. Intriguingly, a similar phenotype was earlier observed in asymmetric leaves 1 (AS1) mutants (Byrne et al., 2000). AS1 is an adaxial gene, a transcription factor responsible for maintenance of leaf morphology along adaxial-abaxial, medial-lateral and distal-proximal symmetry axes in coordination with AS2 (Machida et al., 2015). It is primarily expressed in globular and heart stage embryos in subepidermal cells later forming cotyledons, leaf founder cells in the primordia and later in the floral primordia in the inflorescence (Byrne et al., 2000; Machida et al., 2015). Although the expression pattern of *SYTL5.2* remains to be found out, it is possible that the nuclear transcription factor, AS1 in some yet unknown mechanism regulates expression of *SYTL5.2*. A similar role of nuclear transcription factors in chloroplast development is well known, especially for GOLDEN2-LIKE (GLK) transcription factors (Pogson and Albrecht-Borth, 2014; Pogson et al., 2015; Waters and Langdale, 2009). GLK1 and GLK2 regulate plastidial protein expression of light harvesting chlorophyll *a/b* binding proteins (LHCs) and of proteins involved in chlorophyll biosynthesis thus responsible in maintenance of thylakoid morphology (Chen et al., 2016; Waters et al., 2008, 2009).

4.2.2 SYTL5.2 is chloroplast localized member of plant synaptotagmin family

SYTL5.2 is a NTMC2-type-5 protein belonging to plant synaptotagmin family. It has a unique structure consisting of predicted 25 aa long transit peptide (Target P prediction) and a single C2 domain between the last two of the four transmembrane helices (Fig: 5, Craxton, 2007). It is intriguing that SYTL5.2 was predicted to be localized to chloroplast even though so far SYTs have not been associated directly or indirectly with a role in chloroplasts. Although synaptotagmin was also one of the proteins identified in analysis of the plastoglobuli proteome of the halotolerant green algae, it has not been further characterized so far (Davidi et al., 2015).

Subcellular localization can provide hints regarding the function of a protein. The roles of SYT1 and SYT7 in neurotransmission at the synapses and plasma membrane repair were originally proposed based on their localization in synaptic vesicles and lysosomes, respectively (Matthew et al., 1981; Reddy et al., 2001). Consequently, the localization of SYTL5.2 was analyzed using two methods: via *in-vivo* expression of GFP- SYTL5.2 fusion protein in tobacco and *in-vitro* import of ³⁵S-labeled SYTL5.2 protein. SYTL5.2-GFP signal was found to overlap with the chlorophyll autofluorescence, indicating the chloroplast localization. *In-vitro* import of ³⁵S-labeled full length SYTL5.2 protein into chloroplast was also performed to test the chloroplast localization since only first 272 of the 693 amino acids long SYTL5.2 were fused to GFP in *in-vivo* expression experiment (Fig: 17). Likewise, this also remedies the issue of miss localization of overexpressed proteins to due to bulky GFP tag or miss-folding. Further experiments need to be done to analyze the membrane or compartment of chloroplasts in which SYTL5.2 resides.

Moreover, the results presented here demonstrate that SYTL5.2 is an integral membrane protein with an N-terminal transit peptide of about 100 amino acids rather than the predicted 25 amino acids (Target P) (Fig: 18). Animal synaptotagmins seldom contain more than one transmembrane domains and frequently undergo post translational modification such as phosphorylation, palmitoylation, acylation etc. Human SYT1 is known to undergo phosphorylation and palmitoylation that is essential for its function in neurotransmission (Craxton, 2007; Südhof, 2002). Also, animal synaptotagmins have a putative fatty-acylation site just after the N-terminal transmembrane domain which assists in their oligomerization which is absent in plants (Fukuda, 2007; Südhof, 2002, 2013). As of now, none of the characterized plant synaptotagmins have been found to harbor more than one transmembrane domain and undergo post translational modification. Peptides belonging to SYTL5.2 were detected in a phospho-proteomic mass spectroscopic analysis done after irreversible phosphatase inhibition using pervanadate treatment. Although further analysis is required to find the relevance of phosphorylation in chloroplasts, SYTL5.2 does undergo phosphorylation in most likelihood. Taken together,

SYTL5.2 is a new member of synaptotagmin family localized to chloroplasts and contains single C2 domain with multiple transmembrane domains.

4.2.3 SYTL5.2 affects initial stages of chloroplast differentiation in leaves

TEM imaging of both the base and the tip region of the leaves was performed to analyze the effects of lack of SYTL5.2 on chloroplast morphology. Not much difference was observed at the tip of the leaf in regard to cellular differentiation and thylakoid architecture (Fig: 19). In contrast to this, a delay in differentiation of chloroplast with disorganized thylakoid membrane network was observed at the base in *syt15.2* leaves as compared to WT (Fig: 20). This gradual cellular differentiation along the lateral-distal axis is typical in dicotyledonous plants like *Arabidopsis* (Pyke, 1999). In a normal leaf, the cells at base and along the margins, especially at the serrations are younger with immature chloroplasts while the ones at tip and in vicinity of the mid vein have reached full differentiation. A spatial gradient in cellular differentiation is also observed, with cells at the distal end being first to reach full differentiation (Gügel and Soll, 2017; Pyke, 1999). Additionally, a higher number of vesicles and tubule like structures were also observed in *syt15.2* mutant plastids. Chloroplast differentiation and thylakoid biogenesis not only requires proteins but also membrane forming lipids especially at the early stage. The presence of vesicles and tubules is typical for undifferentiated chloroplasts and thought to transport lipids synthesized at the inner envelope membrane of the chloroplast (Gügel and Soll, 2017; Benning, 2009). Synaptotagmins are known to interact with lipids via their C2 domains (Bai and Chapman, 2004; Chapman, 2002; Fukuda, 2007; Sutton et al., 1995). Moreover, C2 domains of the plant SYT1 was also reported to bind phospholipids, a fundamental feature of synaptotagmins (Schapire et al., 2008). It is possible to speculate that SYTL5.2 binds to the lipids although further experiments are required to prove the same. Surprisingly, no delay in the greening was observed in *syt15.2* plants compared to WT when etiolated seeding were illuminated with light to allow etioplasts to chloroplast transition. These observations imply the possible involvement of SYTL5.2 during initial stages of chloroplast differentiation in leaves either directly or indirectly.

4.2.4 Lack of SYTL5.2 affects accumulation of thylakoid membrane proteins but not the overall photosynthetic activity

As an obvious next step to characterize a novel plastidial protein, accumulation of photosynthetic proteins was tested. The western analysis revealed that the levels of ATP synthase (CF₁- α/β and Atp- β) were significantly reduced and those of PSII (D1) had slightly increased. Although steady-state concentrations of PSI (PsaF and PsaA) and cytochrome *b₆f* (Cyt*f* and Cyt*b₆*) complex proteins remained more or less unchanged,

LHC1a levels were surprisingly higher (Fig: 21 a). The ATP synthase produces ATP from ADP and inorganic phosphate by utilizing the proton motive force generated by splitting of water molecule at the PSII and electron transport from PSII to PSI via cytochrome *b₆f* complex. It is likely that the effect on the PSI proteins is to regulate / balance the excessive electron flow from PSII and cytochrome *b₆f* complex and avoid damage due to reactive oxygen species in case of reduced ATP synthase activity. Similar effects were previously reported for the deficiency of plastid ATP synthase 1 (*dpa1*) mutant (Dal Bosco et al., 2004). In accordance with the protein levels, PSII quantum yield and ETR were comparable in *sytl5.2* and WT plants. However surprisingly very little differences were observed in non-photochemical quenching (NPQ) of the fluorescence which is very typical for ATP synthase deficient mutants (Dal Bosco et al., 2004; Schottler et al., 2015). It is possible that the changes in the photosynthetic performance and NPQ are not very apparent for the whole leaf / plant since the delay in chloroplast maturation at the base is recovered as the cells differentiate further near the tips. Detailed analysis of the PSI activity and especially the activity of ATP synthase in various physiological conditions for example during extended light-dark is required for further understanding the implication of reduced ATP synthase complex proteins.

Collectively the data presented confirms SYTL5.2 as a new member of plant synaptotagmin family that is localized to chloroplasts. *Arabidopsis* SYTL5.2 T-DNA insertion lines exhibit crumpled vegetative and cauline leaves, deformed floral appendages and decreased seed yield as phenotype which is completely rescued by complementation with SYTL5.2 under endogenous promoter. The reduction in components of ATP synthase probably causes the growth retardation observed nevertheless the net photosynthetic activity of *sytl5.2* plants is not significantly affected. TEM analysis revealed differences in chloroplast ultrastructure at the younger tissue of the leaf. More importantly, a delay observed in chloroplast maturation at the leaf base when compared to WT but not at the tips which have progressed further in cellular differentiation suggesting a role in early chloroplast development.

4.3 SNARE_AP

4.3.1 Chloroplast localized SNARE_AP disrupts thylakoid network organization

The SNARE_AP protein is homologous to Tvp38 / Ded proteins in bacteria and yeast that are thought to play a role in maintenance of cell membrane and vesicle trafficking respectively. It was first identified in cyanobacteria (Inadome et al., 2007, Sikdar et al., 2013, Keller and Schneider 2013). As a part of this work, knockout mutant of SNARE_AP in *Arabidopsis* was isolated and characterized (Fig: 23 a and b). The cotyledons and

leaves of mutant *snare_ap* plants exhibited a pale green phenotype which was corroborated by the reduced chlorophyll content in the leaves (Fig: 23 c-i). As a next step the subcellular localization of SNARE_AP was investigated by expression of GFP fusion protein. Transient expression GFP tagged SNARE_AP in tobacco leaves showed that SNARE_AP is localized to chloroplast. Similar results were obtained for stable expression of SNARE_AP-GFP in *Arabidopsis* (Fig: 24 and 28). Besides, immunoblot analysis using GFP antibody could detect overexpressed SNARE_AP-GFP at approximately 25.6 kDa after cleavage of its 91 aa long transit peptide (Fig: 24). Attempts were made to test the expression and localization of endogenously expressed SNARE_AP protein using anti-SNARE_AP antibody. However, no SNARE_AP specific band could be detected in WT samples that was missing in *snare-ap* mutant. This is probably due to strong cross reactivity with other proteins like LHCS that run at a size comparable to SNARE_AP. Furthermore, this could also be due to inherent low antigenicity of SNARE_AP proteins. Never-the-less, SNARE_AP-GFP lines generated as a part of this study could be utilized to analyze the membrane / membranes to which SNARE_AP is localized.

As a next step, TEM was performed to investigate the changes in chloroplast morphology if any in cotyledons and primary leaves. Indeed, in agreement with the pale green phenotype and reduced chlorophyll content, both normal chloroplast and chloroplast with ultrastructural changes were observed. Chloroplast in *snare_ap* displayed loosely appressed grana-stacks with blown up luminal spaces. The grana and stroma thylakoids were more disorganized and curved in *snare_ap* plastids having lost the parallel arrangement typically seen in WT chloroplasts. Additionally, vesicle accumulation was also observed in *snare_ap* plastids. Previously, mutants with reduced photosynthetic complex protein import due to lack of STY kinases (Lamberti et al., 2011), reduced ATP synthase complex proteins (Bosco et al., 2004) or its assembly (Benz et al., 2009) have been reported to show similar ultrastructural changes. Moreover, in agreement with the expression profile of SNARE_AP on the *Arabidopsis* BAR eFP browser (Winter et al., 2007), the effect on thylakoid architecture was more severe in cotyledons than in leaves (Fig 26). Further detailed imaging will clarify if the observed effects due to lack of SNARE_AP are limited to younger tissue with active chloroplast biogenesis or also present in more differentiated cells requiring structural maintenance of chloroplast. Also, quantitative analysis needs to be performed to analyze the ratio of normal verses abnormal chloroplast in both cotyledons and true leaves.

4.3.2 Deletion of SNARE_AP influences the accumulation of photosynthetic complexes but not their assembly

Frequently, the pale phenotype and associated ultrastructural changes manifest with

defects in accumulation, assembly and stability of the photosynthetic complexes. Thus BN-PAGE and immunoblot analysis was performed to test the photosynthetic protein complexes. Significant reduction in the accumulation of PSII-LHCII super-complexes was evident from the BN-PAGE analysis. Although, changes below the detection range (i.e. to 70 or 80% protein of WT) might not be clearly seen in immune blots, the levels of ATP β protein of ATP synthase complex were reduced in mutant as compared to WT (Fig. 27). Interestingly, Zagari et al reported similar result in *Arabidopsis* and Lotus snowy cotyledon 2 (*sco2*) mutants (Zagari et al., 2017). Expression pattern of SCO2 and SNARE_AP is similar with highest levels found in cotyledons (Shimada et al., 2007; Albrecht et al., 2010). Chloroplast in *sco2* leaves also show drastically reduced accumulation of PSII-LHC super complexes with corresponding increase in PSII assembly complexes. Although snowy cotyledon (*sco*) family proteins were initially described to regulate chloroplast biogenesis in cotyledons but not primary leaves, further analysis of mutants grown under different light conditions revealed a more elaborate role of these proteins (Albrecht et al., 2006, 2008, 2010, Zagari et al., 2017). Immunoblot analysis done using antibody against PSII protein D2 suggested role of SCO2 in assembly of PSII_LHC super complexes (Zagari et al., 2017). However, ³⁵S-labelling experiment performed using *snare_ap* plants show that SNARE_AP does not affect the assembly of the super complexes (Fig. 27 b). Surprisingly, *snare_ap* mutants showed no significant photoinhibition (data not shown) as compared to WT indicating that the photosynthetic efficiency is somehow not affected by the observed decline in PSII_LHC super-complexes. This can be attributed to presence of normal chloroplast along with the ones with thylakoid malformations (Fig: 26). Further analysis is required to elucidate whether *snare_ap* regulates the stability of the super-complexes. Additionally, the analysis of the levels of individual photosystem component proteins and if SNARE_AP interacts with any of them remains to be investigated.

4.3.3 SNARE_AP is potentially involved in preliminary stages of chloroplast differentiation

The etioplasts to chloroplast transition during “greening” has been long used as a model to study chloroplast biogenesis and identify potential candidate proteins. Although some argue the physiological relevance and validity of the model, etioplasts are indeed found under natural conditions. They are present in the seedlings that germinate under the soil and need a few days to reach the surface or in leaves plants growing under limited light conditions. Another instance is development in light intensity gradient providing a shading effect on growing leaves like covered leaved of the cabbage head or in leaf primordia or buds (Solymosi and Schoefs 2010). Consequently, greening experiments to study etioplast-chloroplast transition can still give valuable insights leading to better

understanding of the biogenesis process.

The greening process involves formation of photosynthetic complexes along with elaborate thylakoid membrane system in chloroplast in cotyledons. Seedlings of WT, *snare_ap* and *snare_ap* GFP comp#3 lines screened for de-etiolation related phenotype. Not surprisingly, *snare_ap* seedlings showed considerable delay in greening of cotyledons with chlorophyll accumulation down to about 60% that of WT. Additionally, the photosynthetic activity (maximum quantum yield of PSII Fv/Fm) of *snare_ap* seedlings was also significantly reduced in agreement with the greening delay (Fig: 29). Nevertheless, after 24 h the PSII yield and chlorophyll amounts in *snare_ap* cotyledons reach to the WT levels. Similar trend was observed for the SNARE_AP-GFP complemented line albeit less significant differences. However, no homozygous lines were obtained prior to the experiment. Thus, the observed trend could be attributed to the mixed population of SNARE_AP-GFP complementation seeds which were either homozygous, heterozygous and WT for insertion of the SNARE_AP-GFP construct. Moreover, this could also due to partial complementation of *snare_ap* lines. It is interesting that STY kinase mutants with analogous chloroplast ultrastructure defects as that of *snare_ap* mutants have been previously reported to have similar greening defects (Lamberti et al., 2011). Additionally, mutants of various phytohormones and GUN mutants have been known to display similar greening defects (Ruckle et al., 2007; Pogson and Albrecht, 2011). Nevertheless, delayed greening of etiolated *snare_ap* seedlings suggest towards a function early during development although further analysis of *snare_ap* mutants during de-etiolation will help in pin pointing its role during chloroplast biogenesis.

In summary SNARE associated protein (SNARE_AP), identified via bioinformatics screen for plastidial COPI related vesicle trafficking proteins (Khan et al., 2013) is indeed localized in chloroplast. Knock out mutants of SNARE_AP have pale green cotyledons and leaves. Moreover, they contain normal as well as deformed chloroplasts with higher number of vesicles and have reduced PSII-LHC super complexes. Moreover, this along with de-etiolation experiments point towards a role early during development of chloroplasts.

5. Conclusion

Biosynthesis and maintenance of chloroplast thylakoid membranes is a complex, multifarious process thought to involve vesicle trafficking. Although the molecular mechanistic have essentially remained unresolved so far owing to varied reasons (Vothknecht and Westhoff, 2001; Nickelsen et al., 2011), structural changes transpiring during proplastid to chloroplast differentiation are now becoming clear (Charuvi et al., 2012; Liang et al., 2018). This study concerns three putative chloroplast vesicle trafficking candidate proteins; FZL, SytL5.2 and SNARE_AP that were investigated in regard to their role in chloroplast biogenesis.

I. FZL:

The fuzzy onion-like protein, FZL is dynamin like GTPase primarily located at the inner envelope of the chloroplast. Loss of FZL affects the stability of the cytochrome *b₆f* complex and in turn decreases the photosynthetic efficiency of plants especially in the midvein region of the leaves. Collectively, the inner envelope protein FZL affects the maintenance of thylakoid membranes and therefore the function of photosynthetic complexes.

II. Synaptotagmin 5.2:

A plant synaptotagmin family protein, SytL5.2 localized to chloroplast was found and characterized as a part of this work. *SytL5.2* mutants displayed an overall crumpled leaf phenotype with delay in chloroplast maturation at the leaf base as compared to WT. This retardation in chloroplast recovers along the proximal-distal axis as the cells differentiate further near the tips. Taken together, these results imply that SytL5.2 plays a role in early chloroplast biogenesis in leaves.

III. SNARE_AP:

A predicted vesicle trafficking SNARE associated protein, SNARE_AP is a plastidial protein. The *snare_ap* mutants are pale green harbouring chloroplast with disorganized thylakoid architecture with higher number of vesicles. The mutants exhibit reduced accumulation of photosynthetic complexes but not their assembly. Moreover, delayed greening of etiolated *snare_ap* seedlings along with more severe chloroplast morphology in cotyledons than in leaves indicate towards a role early during development of chloroplasts.

References:

1. Adam, Z., Charuvi, D., Tsabari, O., Knopf, R.R., and Reich, Z. (2011). Biogenesis of thylakoid networks in angiosperms: Knowns and unknowns. *Plant Mol. Biol.* **76**, 221–234.
2. Albinak, A.M., Baglieri, J., and Robinson, C. (2012). Targeting of luminal proteins across the thylakoid membrane. *J. Exp. Bot.* **63**, 1689–1698.
3. Andersson, M.X. (2001). Chloroplast Biogenesis. Regulation of Lipid Transport to the Thylakoid in Chloroplasts Isolated from Expanding and Fully Expanded Leaves of Pea. *Plant Physiol.* **127**, 184–193.
4. Andersson, M.X., and Sandelius, A.S. (2004). A chloroplast-localized vesicular transport system: A bio-informatics approach. *BMC Genomics* **5**, 40.
5. Andrews, N.W. (2005). Membrane Resealing: Synaptotagmin VII Keeps Running the Show. *Sci. Signal.* **2005**, pe19-pe19.
6. Andrews, N.W., and Chakrabarti, S. (2005). There's more to life than neurotransmission: The regulation of exocytosis by synaptotagmin VII. *Trends Cell Biol.* **15**, 626–631.
7. Ansoorge, W. (1985). Fast and sensitive detection of protein and DNA bands by treatment with potassium permanganate. *J. Biochem. Biophys. Methods* **11**, 13–20.
8. Apchelimonov, A.A., Soldatova, O.P., Ezhova, T.A., Grimm, B., and Shestakov, S. V. (2007). The analysis of the Chll 1 and Chll 2 genes using acifluorfen-resistant mutant of *Arabidopsis thaliana*. *Planta* **225**, 935–943.
9. Armbruster, U., Ruhle, T., Kreller, R., Strotbek, C., Zuhlke, J., Tadini, L., Blunder, T., Hertle, A.P., Qi, Y., Rengstl, B., et al. (2013a). The PHOTOSYNTHESIS AFFECTED MUTANT68-LIKE Protein Evolved from a PSII Assembly Factor to Mediate Assembly of the Chloroplast NAD(P)H Dehydrogenase Complex in *Arabidopsis*. *Plant Cell* **25**, 3926–3943.
10. Armbruster, U., Labs, M., Pribil, M., Viola, S., Xu, W., Scharfenberg, M., Hertle, A.P., Rojahn, U., Jensen, P.E., Rappaport, F., et al. (2013b). *Arabidopsis* CURVATURE THYLAKOID1 Proteins Modify Thylakoid Architecture by Inducing Membrane Curvature. *Plant Cell* **25**, 2661–2678.
11. Aseeva, E., Ossenbühl, F., Eichacker, L., Wanner, G., Soll, J., and Vothknecht, U. (2004). The J. Bio. Chem. **279**, 35535-35541.
12. Aseeva, E., Ossenbühl, F., Sippel C., Cho W., Stein B., Eichacker L., Meurer J., Wanner G., Westhoff P., Soll J. and Vothknecht U. (2007). Vipp1 is required for basic thylakoid membrane formation but not for the assembly of thylakoid protein complexes. *Plant physio. and biochem.* **45**, 119-28.
13. Bai, J., and Chapman, E.R. (2004). The C2 domains of synaptotagmin - Partners in exocytosis. *Trends Biochem. Sci.* **29**, 143–151.
14. Balsera, M., Soll, J., and Bölter, B. (2009). Protein import machineries in endosymbiotic organelles. *Cell. Mol. Life Sci.* **66**, 1903–1923.
15. Bang, W., Hata, A., Jeong, I., Umeda, T., Masuda, T., Chen, J., Yoko, I., Suwastika, I., Kim, D., Im, C., et al. (2009). AtObgC, a plant ortholog of bacterial Obg, is a chloroplast-targeting GTPase essential for early embryogenesis. *Plant Mol. Bio.* **71**, 379-390.
16. Bang, W., Chen, J., Jeong, I., Kim, S., Kim, C., Jung, H., Lee, K., Kweon, H., Yoko, I., Shiina, T., et al. (2012). Functional characterization of ObgC in ribosome biogenesis during chloroplast development. *The Plant J.* **71**, 122-134.
17. Barton, M.K. (2010). Twenty years on: The inner workings of the shoot apical meristem, a developmental dynamo. *Dev. Biol.* **341**, 95–113.
18. Bassham, D.C., Brandizzi, F., Otegui, M.S., and Sanderfoot, A.A. (2008). The Secretory System of *Arabidopsis*. *Arab. B.* **6**, e0116.
19. Benjamini, Y., and Hochberg, Y. (1995). Controlling the false discovery rate: a practical and powerful approach to multiple testing. *J. R. Stat. Soc.* **57**, 289–300.
20. Benning, C. (2009). Mechanisms of Lipid Transport Involved in Organelle Biogenesis in Plant Cells. *Annu. Rev. Cell Dev. Biol.* **25**, 71–91.
21. Benz, M., Bals, T., Gügel, I.L., Piotrowski, M., Kuhn, A., Schünemann, D., Soll, J., and Ankele, E. (2009). Alb4 of *Arabidopsis* promotes assembly and stabilization of a non chlorophyll-binding photosynthetic complex, the CF1CF0-ATP synthase. *Mol. Plant* **2**, 1410–1424.
22. Bischof, S., Baerenfaller, K., Wildhaber, T., Troesch, R., Vidi, P.-A., Roschitzki, B., Hirsch-Hoffmann, M., Hennig, L., Kessler, F., Gruissem, W., et al. (2011). Plastid Proteome Assembly without Toc159: Photosynthetic Protein Import and Accumulation of N -Acetylated Plastid Precursor Proteins. *Plant Cell* **23**, 3911–3928.
23. van der Bliek, A.M., Shen, Q., and Kawajiri, S. (2013). Mechanisms of mitochondrial fission and fusion. *Cold Spring Harb. Perspect. Biol.* **5**.
24. Bölter, B., and Soll, J. (2017). Ycf1/Tic214 Is Not Essential for the Accumulation of Plastid Proteins. *Mol. Plant* **10**, 219–221.
25. Bonifacino, J. and Glick, B. (2004). The mechanisms of vesicle budding and fusion. *Cell* **116**, 153-66
26. Buick, R. (2008). When did oxygenic photosynthesis evolve? *Philos. Trans. R. Soc. B Biol. Sci.* **363**, 2731–2743.
27. Byrne, M.E., Barley, R., Curtis, M., Arroyo, J.M., Dunham, M., Hudson, A., and Martienssen, R.A. (2000). Asymmetric leaves1 mediates leaf patterning and stem cell function in *Arabidopsis*. *Nature*

- 408, 967–971.
28. Casanova-Sáez, R., Mateo-Bonmatí, E., Kangasjärvi, S., Candela, H., and Micol, J.L. (2014). Arabidopsis ANGULATA10 is required for thylakoid biogenesis and mesophyll development. *J. Exp. Bot.* **65**, 2391–2404.
 29. Chang, W.L., Soll, J., and Bolter, B. (2012). The gateway to chloroplast: Re-defining the function of chloroplast receptor proteins. *Biol. Chem.* **393**, 1263–1277.
 30. Chapman, E.R. (2002). Synaptotagmin: A Ca²⁺ sensor that triggers exocytosis? *Nat. Rev. Mol. Cell Biol.* **3**, 498–508.
 31. Chapman, E.R. (2008). How Does Synaptotagmin Trigger Neurotransmitter Release? *Annu. Rev. Biochem.* **77**, 615–641.
 32. Charuvi, D., Kiss, V., Nevo, R., Shimoni, E., Adam, Z., and Reich, Z. (2012). Gain and Loss of Photosynthetic Membranes during Plastid Differentiation in the Shoot Apex of Arabidopsis. *Plant Cell* **24**, 1143–1157.
 33. Chen, M., Ji, M., Wen, B., Liu, L., Li, S., Chen, X., Gao, D., and Li, L. (2016). GOLDEN 2-LIKE Transcription Factors of Plants. *Front. Plant Sci.* **7**, 1509.
 34. Chicka, M.C., Hui, E., Liu, H., and Chapman, E.R. (2008). Synaptotagmin arrests the SNARE complex before triggering fast, efficient membrane fusion in response to Ca²⁺. *Nat. Struct. Mol. Biol.* **15**, 827–835.
 35. Chigri F., Sippel C., Kolb M., and Vothknecht U. (2009). Arabidopsis OBG-Like GTPase (AtOBGL) Is Localized in Chloroplasts and Has an Essential Function in Embryo Development. *Mol. Plant.* **2**, 1373–1383
 36. Craxton, M. (2001). Genomic analysis of synaptotagmin genes. *Genomics* **77**, 43–49.
 37. Craxton, M. (2004). Synaptotagmin gene content of the sequenced genomes. *BMC Genomics* **5**, 43.
 38. Craxton, M. (2007). Evolutionary genomics of plant genes encoding N-terminal-TM-C2 domain proteins and the similar FAM62 genes and synaptotagmin genes of metazoans. *BMC Genomics* **8**, 259.
 39. Craxton, M. (2010). A manual collection of Syt, Esyt, Rph3a, Rph3al, Doc2, and Dblc2 genes from 46 metazoan genomes - an open access resource for neuroscience and evolutionary biology. *BMC Genomics* **11**, 37.
 40. Cui, Y.-L., Jia, Q.-S., Yin, Q.-Q., Lin, G.-N., Kong, M.-M., and Yang, Z.-N. (2011). The GDC1 Gene Encodes a Novel Ankyrin Domain-Containing Protein That Is Essential for Grana Formation in Arabidopsis. *Plant Physiol.* **155**, 130–141.
 41. Dal Bosco, C., Lezhneva, L., Bieh, A., Leister, D., Strotmann, H., Wanner, G., and Meurer, J. (2004). Inactivation of the Chloroplast ATP Synthase γ Subunit Results in High Non-photochemical Fluorescence Quenching and Altered Nuclear Gene Expression in Arabidopsis thaliana. *J. Biol. Chem.* **279**, 1060–1069.
 42. Davidi, L., Levin, Y., Ben-Dor, S., and Pick, U. (2015). Proteome Analysis of Cytoplasmic and Plastidic β -Carotene Lipid Droplets in *Dunaliella bardawil*. *Plant Physiol.* **167**, 60–79.
 43. Dorne, A.J., Joyard, J., and Douce, R. (1990). Do thylakoids really contain phosphatidylcholine? *Proc. Natl. Acad. Sci.* **87**, 71–74.
 44. Duy, D., Wanner, G., Meda, A.R., von Wiren, N., Soll, J., and Philippar, K. (2007). PIC1, an Ancient Permease in Arabidopsis Chloroplasts, Mediates Iron Transport. *Plant Cell Online* **19**, 986–1006.
 45. Dyall, S.D., Brown, M.T., and Johnson, P.J. (2004). Ancient Invasions: From Endosymbionts to Organelles. *Science (80-.)*. **304**, 253–257.
 46. Emanuelsson, O., Nielsen, H., Brunak, S., and Von Heijne, G. (2000). Predicting subcellular localization of proteins based on their N-terminal amino acid sequence. *J. Mol. Biol.*, **300**, 1005–1016.
 47. Fernández-Chacón, R., Shin, O.-H., Königstorfer, A., Matos, M.F., Meyer, A.C., Garcia, J., Gerber, S.H., Rizo, J., Südhof, T.C., and Rosenmund, C. (2002). Structure/function analysis of Ca²⁺ binding to the C2A domain of synaptotagmin 1. *J Neurosci.* **22**, 8438–8446.
 48. Fernandez, I., Araç, D., Ubach, J., Gerber, S.H., Shin, O.H., Gao, Y., Anderson, R.G.W., Südhof, T.C., and Rizo, J. (2001). Three-dimensional structure of the synaptotagmin 1 C2B-domain: Synaptotagmin 1 as a phospholipid binding machine. *Neuron* **32**, 1057–1069.
 49. Fukuda, M. (2007). The Role of Synaptotagmin and Synaptotagmin-Like Protein (Slp) in Regulated Exocytosis. In *Molecular Mechanisms of Exocytosis*, (New York, NY: Springer New York), pp. 42–61.
 50. Fuson, K.L., Montes, M., Robert, J.J., and Sutton, R.B. (2007). Structure of human synaptotagmin 1 C2AB in the absence of Ca²⁺ reveals a novel domain association. *Biochemistry* **46**, 13041–13048.
 51. Gao, H., Sage, T.L., and Osteryoung, K.W. (2006). FZL, an FZO-like protein in plants, is a determinant of thylakoid and chloroplast morphology. *Proc. Natl. Acad. Sci.* **103**, 6759–6764.
 52. Garcia, C., Khan, N.Z., Nannmark, U., and Aronsson, H. (2010). The chloroplast protein CPSAR1, dually localized in the stroma and the inner envelope membrane, is involved in thylakoid biogenesis. *Plant J.* **63**, 73–85.
 53. Gray, M.W. (2017). Lynn Margulis and the endosymbiont hypothesis: 50 years later. *Mol. Biol. Cell* **28**, 1285–1287.
 54. Grise, F., Taib, N., Monterrat, C., Lagrée, V., and Lang, J. (2007). Distinct roles of the C₂A and the C₂B domain of the vesicular Ca²⁺ sensor synaptotagmin 9 in endocrine β -cells. *Biochem. J.* **403**, 483–492.
 55. Grzyb, J.M., Solymosi, K., Strzalka, K., and Mysliwa-Kurczel, B. (2013). Visualization and

- characterization of prolamellar bodies with atomic force microscopy. *J. Plant Physiol.* **170**, 1217–1227.
56. Gügel, I.L., and Soll, J. (2017). Chloroplast differentiation in the growing leaves of *Arabidopsis thaliana*. *Protoplasma* **254**, 1857–1866.
 57. Gustavsson, N., Wei, S.H., Hoang, D.N., Lao, Y., Zhang, Q., Radda, G.K., Rorsman, P., Südhof, T.C., and Han, W. (2009). Synaptotagmin-7 is a principal Ca²⁺-sensor for Ca²⁺-induced glucagon exocytosis in pancreas. *J. Physiol.* **587**, 1169–1178.
 58. Hayashi-Tsugane, M., Takahara, H., Ahmed, N., Himi, E., Takagi, K., Iida, S., Tsugane, K., and Maekawa, M. (2014). A mutable albino allele in rice reveals that formation of thylakoid membranes requires the SNOW-WHITE LEAF1 gene. *Plant Cell Physiol.* **55**, 3–15.
 59. Heidrich, J., Thurotte, A., and Schneider, D. (2017). Specific interaction of IM30/Vipp1 with cyanobacterial and chloroplast membranes results in membrane remodeling and eventually in membrane fusion. *Biochim. Biophys. Acta - Biomembr.* **1859**, 537–549.
 60. Hennig, R., Heidrich, J., Saur, M., Schmäser, L., Roeters, S.J., Hellmann, N., Woutersen, S., Bonn, M., Weidner, T., Markl, J., et al. (2015). IM30 triggers membrane fusion in cyanobacteria and chloroplasts. *Nat. Commun.* **6**, 7018.
 61. Hörmann, F., Küchler, M., Sveshnikov, D., Oppermann, U., Li, Y., and Soll, J. (2004). Tic32, an essential component in chloroplast biogenesis. *J. Biol. Chem.* **279**, 34756–34762.
 62. Huang, R., Zhao, J., Liu, J., Wang, Y., Han, S., and Zhao, H. (2017). Genome-wide analysis and expression profiles of NTMC2 family genes in *Oryza sativa*. *Gene* **637**, 130–137.
 63. Huang, W., Chen, Q., Zhu, Y., Hu, F., Zhang, L., Ma, Z., He, Z., and Huang, J. (2013). *Arabidopsis thaliana* thylakoid formation 1 is a critical regulator for dynamics of PSII-LHCII complexes in leaf senescence and excess light. *Mol. Plant* **6**, 1673–1691.
 64. Hwang, I., and Robinson, D.G. (2009). Transport vesicle formation in plant cells. *Curr. Opin. Plant Biol.* **12**, 660–669.
 65. Inadome, H., Noda, Y., Kamimura, Y., Adachi, H., and Yoda, K. (2007). Tvp38, Tvp23, Tvp18 and Tvp15: Novel membrane proteins in the Tlg2-containing Golgi/endosome compartments of *Saccharomyces cerevisiae*. *Exp. Cell Res.* **313**, 688–697.
 66. Irizarry, R.A., Hobbs, B., Collin, F., Beazer-Barclay, Y.D., Antonellis, K.J., and Speed, T.P. (2018). Exploration, Normalization, and Summaries of High Density Oligonucleotide Array Probe Level Data. *Biostatistics* **4**, 249–264.
 67. Jahn, R., and Scheller, R.H. (2006). SNAREs - Engines for membrane fusion. *Nat. Rev. Mol. Cell Biol.* **7**, 631–643.
 68. Jarvis, P., and López-Juez, E. (2013). Biogenesis and homeostasis of chloroplasts and other plastids. *Nat. Rev. Mol. Cell Biol.* **14**, 787–802.
 69. Jiménez, J.L., and Davletov, B. (2007). ??-strand recombination in tricalbin evolution and the origin of synaptotagmin-like C2 domains. *Proteins Struct. Funct. Genet.* **68**, 770–778.
 70. Junglas, B., and Schneider, D. (2018). What is Vipp1 good for? *Mol. Microbiol.* **108**, 1–5.
 71. Karim, S., Alezzawi, M., Garcia-Petit, C., Solymosi, K., Khan, N.Z., Lindquist, E., Dahl, P., Hohmann, S., and Aronsson, H. (2014). A novel chloroplast localized Rab GTPase protein CPRabA5e is involved in stress, development, thylakoid biogenesis and vesicle transport in *Arabidopsis*. *Plant Mol. Biol.* **84**, 675–692.
 72. Kasmati, A.R., Töpel, M., Khan, N.Z., Patel, R., Ling, Q., Karim, S., Aronsson, H., and Jarvis, P. (2013). Evolutionary, Molecular and Genetic Analyses of Tic22 Homologues in *Arabidopsis thaliana* Chloroplasts. *PLoS One* **8**, e63863.
 73. Kawamura, Y., and Uemura, M. (2003). Mass spectrometric approach for identifying putative plasma membrane proteins of *Arabidopsis* leaves associated with cold acclimation. *Plant J.* **36**, 141–154.
 74. Keeling, P.J. (2010). The endosymbiotic origin, diversification and fate of plastids. *Philos. Trans. R. Soc. B Biol. Sci.* **365**, 729–748.
 75. Keller, R., and Schneider, D. (2013). Homologs of the yeast Tvp38 vesicle-associated protein are conserved in chloroplasts and cyanobacteria. *Front. Plant Sci.* **4**, 467.
 76. Khan, N.Z., Lindquist, E., and Aronsson, H. (2013). New Putative Chloroplast Vesicle Transport Components and Cargo Proteins Revealed Using a Bioinformatics Approach: An *Arabidopsis* Model. *PLoS One* **8**, e59898.
 77. Kikuchi, S., Bédard, J., Hirano, M., Hirabayashi, Y., Oishi, M., Imai, M., Takase, M., Ide, T., and Nakai, M. (2013). Uncovering the protein translocon at the chloroplast inner envelope membrane. *Science* (80-.). **339**, 571–574.
 78. Kim, H., Kwon, H., Kim, S., Kim, M.K., Botella, M.A., Yun, H.S., and Kwon, C. (2016). Synaptotagmin 1 Negatively Controls the Two Distinct Immune Secretory Pathways to Powdery Mildew Fungi in *Arabidopsis*. *Plant Cell Physiol.* **57**, 1133–1141.
 79. Kleine, T., Maier, U.G., and Leister, D. (2009). DNA Transfer from Organelles to the Nucleus: The Idiosyncratic Genetics of Endosymbiosis. *Annu. Rev. Plant Biol.* **60**, 115–138.
 80. Kobayashi, K., Kondo, M., Fukuda, H., Nishimura, M., and Ohta, H. (2007). Galactolipid synthesis in chloroplast inner envelope is essential for proper thylakoid biogenesis, photosynthesis, and embryogenesis. *Proc. Natl. Acad. Sci.* **104**, 17216–17221.
 81. Kovács-Bogdán, E., Soll, J., and Bölter, B. (2010). Protein import into chloroplasts: The Tic complex and its regulation. *Biochim. Biophys. Acta - Mol. Cell Res.* **1803**, 740–747.
 82. Kowalewska, Ł.M., Mazur, R., Suski, S., Garstka, M., and Mostowska, A. (2016). Three-dimensional

- visualization of the internal plastid membrane network during runner bean chloroplast biogenesis. Dynamic model of the tubular-lamellar transformation. *Plant Cell* 28, tpc.01053.2015.
83. Kroll, D., Meierhoff, K., Bechtold, N., Kinoshita, M., Westphal, S., Vothknecht, U.C., Soll, J., and Westhoff, P. (2001). VIPP1, a nuclear gene of *Arabidopsis thaliana* essential for thylakoid membrane formation. *Proc. Natl. Acad. Sci.* 98, 4238–4242.
 84. Ku, C., Nelson-Sathi, S., Roettger, M., Sousa, F.L., Lockhart, P.J., Bryant, D., Hazkani-Covo, E., McInerney, J.O., Landan, G., and Martin, W.F. (2015). Endosymbiotic origin and differential loss of eukaryotic genes. *Nature* 524, 427–432.
 85. Laemmli, U.K. (1970). Cleavage of structural proteins during the assembly of the head of bacteriophage T4. *Nature* 227, 680–685.
 86. Landoni, M., De Francesco, A., Bellatti, S., Delledonne, M., Ferrarini, A., Venturini, L., Pilu, R., Bononi, M., and Tonelli, C. (2013). A mutation in the FZL gene of *Arabidopsis* causing alteration in chloroplast morphology results in a lesion mimic phenotype. *J. Exp. Bot.* 64, 4313–4328.
 87. Lewis, J.D., and Lazarowitz, S.G. (2010). *Arabidopsis* synaptotagmin SYTA regulates endocytosis and virus movement protein cell-to-cell transport. *Proc. Natl. Acad. Sci.* 107, 2491–2496.
 88. Li, H. min, Kaneko, Y., and Keegstra, K. (1994). Molecular cloning of a chloroplastic protein associated with both the envelope and thylakoid membranes. *Plant Mol. Biol.* 25, 619–632.
 89. Li, N., Gügel, I.L., Giavalisco, P., Zeisler, V., Schreiber, L., Soll, J., and Philippar, K. (2015). FAX1, a Novel Membrane Protein Mediating Plastid Fatty Acid Export. *PLoS Biol.* 13, e1002053.
 90. Liang, Z., Zhu, N., Mai, K.K., Liu, Z., Tzeng, D.T.W., Osteryoung, K.W., Zhong, S., Staehelin, A., and Kang, B.-H. (2018). Thylakoid-Bound Polysomes and a Dynamin-Related Protein, FZL, Mediate Critical Stages of the Linear Chloroplast Biogenesis Program in Greening *Arabidopsis* Cotyledons. *Plant Cell* tpc.00972.2017.
 91. LICHTENTHALER, H.K., and WELLBURN, A.R. (1983). Determinations of total carotenoids and chlorophylls *a* and *b* of leaf extracts in different solvents. *Biochem. Soc. Trans.* 11, 591–592.
 92. Lindquist, E., Solymosi, K., and Aronsson, H. (2016). Vesicles Are Persistent Features of Different Plastids. *Traffic* 17, 1125–1138.
 93. Lohse, M., Nunes-Nesi, A., Kruger, P., Nagel, A., Hannemann, J., Giorgi, F.M., Childs, L., Osorio, S., Walther, D., Selbig, J., et al. (2010). Robin: An Intuitive Wizard Application for R-Based Expression Microarray Quality Assessment and Analysis. *Plant Physiol.* 153, 642–651.
 94. Low, H.H., and Löwe, J. (2006). A bacterial dynamin-like protein. *Nature* 444, 766–769.
 95. Low, H.H., Sachse, C., Amos, L.A., and Löwe, J. (2009). Structure of a Bacterial Dynamin-like Protein Lipid Tube Provides a Mechanism For Assembly and Membrane Curving. *Cell* 139, 1342–1352.
 96. Lübeck, J., Soll, J., Akita, M., Nielsen, E., and Keegstra, K. (1996). Topology of IEP110, a component of the chloroplastic protein import machinery present in the inner envelope membrane. *EMBO J.* 15, 4230–4238.
 97. Machida, C., Nakagawa, A., Kojima, S., Takahashi, H., and Machida, Y. (2015). The complex of ASYMMETRIC LEAVES (AS) proteins plays a central role in antagonistic interactions of genes for leaf polarity specification in *Arabidopsis*. *Wiley Interdiscip. Rev. Dev. Biol.* 4, 655–671.
 98. Martens, S., and McMahon, H.T. (2008). Mechanisms of membrane fusion: Disparate players and common principles. *Nat. Rev. Mol. Cell Biol.* 9, 543–556.
 99. Martens, S., Kozlov, M.M., and McMahon, H.T. (2007). How synaptotagmin promotes membrane fusion. *Science* (80-.). 316, 1205–1208.
 100. Martin, W., and Herrmann, R.G. (1998). Gene Transfer from Organelles to the Nucleus: How Much, What Happens, and Why? *Plant Physiol.* 118, 9–17.
 101. Martin, W., Stoebe, B., Goremykin, V., Hansmann, S., Hasegawa, M., and Kowallik, K. V. (1998). Gene transfer to the nucleus and the evolution of chloroplasts. *Nature* 393, 162–165.
 102. Martin, W.F., Garg, S., and Zimorski, V. (2015). Endosymbiotic theories for eukaryote origin. *Philos. Trans. R. Soc. B Biol. Sci.* 370, 20140330.
 103. Matthew, W.D., Tsavaler, L., and Reichardt, L.F. (1981). Identification of a synaptic vesicle-specific membrane protein with a wide distribution in neuronal and neurosecretory tissue. *J. Cell Biol.* 91, 257–269.
 104. Morré, D.J., Selldén, G., Sundqvist, C., and Sandelius, A.S. (1991a). Stromal low temperature compartment derived from the inner membrane of the chloroplast envelope. *Plant Physiol.* 97, 1558–1564.
 105. Morré, D.J., Selldén, G., Sundqvist, C., and Sandelius, A.S. (1991b). Stromal low temperature compartment derived from the inner membrane of the chloroplast envelope. *Plant Physiol.* 97, 1558–1564.
 106. Mozdy, A.D., and Shaw, J.M. (2003). A fuzzy mitochondrial fusion apparatus comes into focus. *Nat. Rev. Mol. Cell Biol.* 4, 468–478.
 107. Nickel, C., Brylok, T., and Schwenkert, S. (2016). In vivo radiolabeling of *Arabidopsis* chloroplast proteins and separation of thylakoid membrane complexes by blue native PAGE. *Methods Mol. Biol.* 1450, 233–245.
 108. Nielsen, E., Cheung, A., and Ueda, T. (2008). The Regulatory RAB and ARF GTPases for Vesicular Trafficking. *Plant Physiol.* 147, 1516–1526.
 109. Nielsen, H., Engelbrecht, J., Brunak, S., and von Heijne, G. (1997). Identification of prokaryotic and eukaryotic signal peptides and prediction of their cleavage sites. *Protein engineering.* 10, 1–6.

110. Ohnishi, N., Zhang, L., and Sakamoto, W. (2018). VIPP1 involved in chloroplast membrane integrity has GTPase activity in vitro. *Plant Physiol.* *177*, pp.00145.2018.
111. Paddock, B.E., Striegel, A.R., Hui, E., Chapman, E.R., and Reist, N.E. (2008). Ca²⁺-Dependent, Phospholipid-Binding Residues of Synaptotagmin Are Critical for Excitation-Secretion Coupling In Vivo. *J. Neurosci.* *28*, 7458–7466.
112. Paul, M.J., and Frigerio, L. (2007). Coated vesicles in plant cells. *Semin. Cell Dev. Biol.* *18*, 471–478.
113. Pérez-Sancho, J., Vanneste, S., Lee, E., McFarlane, H.E., Esteban del Valle, A., Valpuesta, V., Friml, J., Botella, M.A., and Rosado, A. (2015). The Arabidopsis Synaptotagmin1 Is Enriched in Endoplasmic Reticulum-Plasma Membrane Contact Sites and Confers Cellular Resistance to Mechanical Stresses. *Plant Physiol.* *168*, 132–143.
114. Pogson, B.J., and Albrecht-Borth, V. (2014). An overview of chloroplast biogenesis and development. *Plast. Biol.* *155*, 115–128.
115. Pogson, B.J., Ganguly, D., and Albrecht-Borth, V. (2015). Insights into chloroplast biogenesis and development. *Biochim. Biophys. Acta - Bioenerg.* *1847*, 1017–1024.
116. Porra, R.J., Thompson, W.A., and Kriedemann, P.E. (1989). Determination of accurate extinction coefficients and simultaneous equations for assaying chlorophylls a and b extracted with four different solvents: verification of the concentration of chlorophyll standards by atomic absorption spectroscopy. *BBA - Bioenerg.* *975*, 384–394.
117. Pyke, K. (1999). Plastid division and development. *Plant Cell* *11*, 549–556.
118. Pyke, K. (2007). Plastid biogenesis and differentiation. In *Topics in Current Genetics*, R. Bock, ed. (Berlin-Heidelberg: Springer), pp. 1–28.
119. Rast, A., Heinz, S., and Nickelsen, J. (2015). Biogenesis of thylakoid membranes. *Biochim. Biophys. Acta* *1847*, 821–830.
120. Reddy, A., Caler, E. V., and Andrews, N.W. (2001). Plasma membrane repair is mediated by Ca²⁺-regulated exocytosis of lysosomes. *Cell* *106*, 157–169.
121. Reumann, S., Inoue, K., and Keegstra, K. (2005). Evolution of the general protein import pathway of plastids. *Mol. Membr. Biol.* *22*, 73–86.
122. Reyes, F.C., Buono, R., and Otegui, M.S. (2011). Plant endosomal trafficking pathways. *Curr. Opin. Plant Biol.* *14*, 666–673.
123. Rudolf, M., MacHettira, A.B., Groß, L.E., Weber, K.L., Bolte, K., Bionda, T., Sommer, M.S., Maier, U.G., Weber, A.P.M., Schleiff, E., et al. (2013). In vivo function of Tic22, a protein import component of the intermembrane space of chloroplasts. *Mol. Plant* *6*, 817–829.
124. Rutherford, S. and Moore, I. (2002) The Arabidopsis Rab GTPase family: another enigma variation. *Curr Opin Plant Biol.* *5*, 518–528
125. Saito, C., and Ueda, T. (2009). Chapter 4 Functions of RAB and SNARE Proteins in Plant Life. In *International Review of Cell and Molecular Biology*, pp. 183–233.
126. Schapiro, A.L., Voigt, B., Jasik, J., Rosado, A., Lopez-Cobollo, R., Menzel, D., Salinas, J., Mancuso, S., Valpuesta, V., Baluska, F., et al. (2008). Arabidopsis Synaptotagmin 1 Is Required for the Maintenance of Plasma Membrane Integrity and Cell Viability. *Plant Cell Online* *20*, 3374–3388.
127. Schulz, T.A., and Creutz, C.E. (2004). The Tricalbin C2 Domains: Lipid-Binding Properties of a Novel, Synaptotagmin-Like Yeast Protein Family. *Biochemistry* *43*, 3987–3995.
128. Schünemann, D. (2007). Mechanisms of protein import into thylakoids of chloroplasts. *Biol. Chem.* *388*, 907–915.
129. Schwacke, R., Schneider, A., Van Der Graaff, E., Fischer, K., Catoni, E., Desimone, M., Frommer, W., Flügge, U., Kunze, R. (2003). ARAMEMNON, a Novel Database for Arabidopsis Integral Membrane Proteins. *Plant Physiol.* *131*, 16–26.
130. Schweiger, R., and Schwenkert, S. (2014). Protein-protein Interactions Visualized by Bimolecular Fluorescence Complementation in Tobacco Protoplasts and Leaves. *J. Vis. Exp.*
131. Schweiger, R., Muller, N.C., Schmitt, M.J., Soll, J., and Schwenkert, S. (2012). AtTPR7 is a chaperone-docking protein of the Sec translocon in Arabidopsis. *J. Cell Sci.* *125*, 5196–5207.
132. Schwenkert, S., Soll, J., and Bölter, B. (2011). Protein import into chloroplasts-How chaperones feature into the game. *Biochim. Biophys. Acta - Biomembr.* *1808*, 901–911.
133. Sharma, V.K. (2002). Maintenance of Shoot and Floral Meristem Cell Proliferation and Fate. *Plant Physiol.* *129*, 31–39.
134. Shimoni, E. (2005). Three-Dimensional Organization of Higher-Plant Chloroplast Thylakoid Membranes Revealed by Electron Tomography. *Plant Cell Online* *17*, 2580–2586.
135. Sjuts, I., Soll, J., and Bölter, B. (2017). Import of Soluble Proteins into Chloroplasts and Potential Regulatory Mechanisms. *Front. Plant Sci.* *8*.
136. Smyth, G.K. (2004). Linear Models and Empirical Bayes Methods for Assessing Differential Expression in Microarray Experiments. *Stat. Appl. Genet. Mol. Biol.* *3*, 1–25.
137. Soll, J., and Schleiff, E. (2004). Plant cell biology: Protein import into chloroplasts. *Nat. Rev. Mol. Cell Biol.* *5*, 198–208.
138. Solymosi, K., and Schoefs, B. (2010). Etioplast and etio-chloroplast formation under natural conditions: The dark side of chlorophyll biosynthesis in angiosperms. *Photosynth. Res.* *105*, 143–166.
139. Stengel, A., Benz, J.P., Buchanan, B.B., Soll, J., and Bölter, B. (2009). Preprotein import into chloroplasts via the toc and tic complexes is regulated by redox signals in *pisum sativum*. *Mol. Plant* *2*, 1181–1197.

140. Südhof, T.C. (2002). Synaptotagmins: Why so many? *J. Biol. Chem.* **277**, 7629–7632.
141. Südhof, T.C. (2013). Neurotransmitter release: The last millisecond in the life of a synaptic vesicle. *Neuron* **80**, 675–690.
142. Sutton, R.B., Davletov, B.A., Berghuis, A.M., Südhof, T.C., and Sprang, S.R. (1995). Structure of the first C2domain of synaptotagmin I: A novel Ca²⁺/phospholipid-binding fold. *Cell* **80**, 929–938.
143. Sutton, R.B., Ernst, J.A., and Brunger, A.T. (1999). Crystal structure of the cytosolic C2A-C2B domains of synaptotagmin III: Implications for Ca²⁺-independent SNARE complex interaction. *J. Cell Biol.* **147**, 589–598.
144. Tremblay, A., Seabolt, S., Zeng, H., Zhang, C., Böckler, S., Tate, D.N., Duong, V.T., Yao, N., and Lu, H. (2016). A Role of the FUZZY ONIONS LIKE Gene in Regulating Cell Death and Defense in Arabidopsis. *Sci. Rep.* **6**, 37797.
145. Uchiyama, A., Shimada-Beltran, H., Levy, A., Zheng, J.Y., Javia, P.A., and Lazarowitz, S.G. (2014). The Arabidopsis synaptotagmin SYTA regulates the cell-to-cell movement of diverse plant viruses. *Front. Plant Sci.* **5**, 584.
146. Uemura, T. and Ueda, T. (2014). Plant vacuolar trafficking driven by RAB and SNARE proteins. *Current Opinion in Plant Bio.* **22**, 116-121.
147. Usadel, B., Poree, F., Nagel, A., Lohse, M., Czedik-Eysenberg, A., and Stitt, M. (2009). Usadel, B., Poree, F., Nagel, A., Lohse, M., Czedik-Eysenberg, A., Stitt, M. 2009. A guide to using MapMan to visualize and compare Omics data in plants: A case study in the crop species, Maize. *Plant Cell Environ.* **32**, 2009.
148. Vothknecht, U.C., and Soll, J. (2005). Chloroplast membrane transport: Interplay of prokaryotic and eukaryotic traits. *Gene* **354**, 99–109.
149. Vothknecht, U.C., and Westhoff, P. (2001). Biogenesis and origin of thylakoid membranes. *Biochim. Biophys. Acta - Mol. Cell Res.* **1541**, 91–101.
150. Vothknecht, U.C., Otters, S., Hennig, R., and Schneider, D. (2012). Vipp1: A very important protein in plastids?! *J. Exp. Bot.* **63**, 1699–1712.
151. Wang, Q. (2004). Deletion of the Chloroplast-Localized Thylakoid Formation1 Gene Product in Arabidopsis Leads to Deficient Thylakoid Formation and Variegated Leaves. *Plant Physiol.* **136**, 3594–3604.
152. Wang, H., Han, S., Siao, W., Song, C., Xiang, Y., Wu, X., Cheng, P., Li, H., Jásik, J., Mičičeta, K., et al. (2015). Arabidopsis Synaptotagmin 2 Participates in Pollen Germination and Tube Growth and Is Delivered to Plasma Membrane via Conventional Secretion. *Mol. Plant* **8**, 1737–1750.
153. Waters, M.T., and Langdale, J.A. (2009). The making of a chloroplast. *EMBO J.* **28**, 2861–2873.
154. Waters, M.T., Moylan, E.C., and Langdale, J.A. (2008). GLK transcription factors regulate chloroplast development in a cell-autonomous manner. *Plant J.* **56**, 432–444.
155. Waters, M.T., Wang, P., Korkaric, M., Capper, R.G., Saunders, N.J., and Langdale, J.A. (2009). GLK Transcription Factors Coordinate Expression of the Photosynthetic Apparatus in Arabidopsis. *Plant Cell Online* **21**, 1109–1128.
156. Westphal, S., Soll, J., and Vothknecht, U.C. (2001). A vesicle transport system inside chloroplasts. *FEBS Lett.* **506**, 257–261.
157. Westphal, S., Soll, J., and Vothknecht, U.C. (2003). Evolution of chloroplast vesicle transport. *Plant Cell Physiol.* **44**, 217–222.
158. von Wettstein, D. (1995). Chlorophyll Biosynthesis. *Plant Cell Online* **7**, 1039–1057.
159. Yadav, R.K., Girke, T., Pasala, S., Xie, M., and Reddy, G. V. (2009). Gene expression map of the Arabidopsis shoot apical meristem stem cell niche. *Proc. Natl. Acad. Sci.* **106**, 4941–4946.
160. Valencia, J. P., Goodman, K. and Otegui, M. (2016). Endocytosis and Endosomal Trafficking in Plants. *Annual Review of Plant Biology.* **67**, 309-335.
161. Yamazaki, T., Kawamura, Y., Minami, A., and Uemura, M. (2008). Calcium-Dependent Freezing Tolerance in Arabidopsis Involves Membrane Resealing via Synaptotagmin SYT1. *Plant Cell Online* **20**, 3389–3404.
162. Younis, M.E., Hasaneen, M.N.A., and Abdel-Aziz, H.M.M. (2012). Certain growth and metabolic indices of stress induced by visible light and UV radiation in broad bean seedlings. *Phyt. - Ann. Rei Bot.* **52**, 203–218.
163. Yun, H.S., Kang, B.G., and Kwon, C. (2016). Arabidopsis immune secretory pathways to powdery mildew fungi. *Plant Signal. Behav.* **11**, e1226456.
164. Zhang, H., Zhang, L., Gao, B., Fan, H., Jin, J., Botella, M.A., Jiang, L., and Lin, J. (2011). Golgi apparatus-localized synaptotagmin 2 is required for unconventional secretion in Arabidopsis. *PLoS One* **6**, e26477.
165. Zhou, Q., Lai, Y., Bacaj, T., Zhao, M., Lyubimov, A.Y., Uervirojnangkoorn, M., Zeldin, O.B., Brewster, A.S., Sauter, N.K., Cohen, A.E., et al. (2015). Architecture of the synaptotagmin-SNARE machinery for neuronal exocytosis. *Nature* **525**, 62–67.
166. Zhou, Q., Zhou, P., Wang, A.L., Wu, D., Zhao, M., Südhof, T.C., and Brunger, A.T. (2017). The primed SNARE-complexin-synaptotagmin complex for neuronal exocytosis. *Nature* **548**, 420–425.

Curriculum Vitae

MANALI PATIL

PERSONAL INFORMATION

Date of birth : December 5th, 1988
 Nationality : Indian

EDUCATION

Since July 2013 : Ph.D. Student
 Plant Biochemistry and Physiology
 Ludwig-Maximilian-Universität München (LMU), Munich, Germany
 PhD thesis: Role of putative vesicle trafficking proteins FZL, Synaptotagmin 5.2 and SNARE_AP in chloroplast development

June 2011- May 2013 : Research Student / Assistant
 Department of Biology, Indian Institute of Science Education and Research (IISER), Pune, India

June 2006- May 2011 : Integrated B.Sc. & M.Sc.
 Biotechnology and Bioinformatics
 Institute of Bioinformatics and Biotechnology (IBB),
 University of Pune, Pune, India.
 Master's thesis: Role of phosphor-Caveolin 1 as a novel tumor suppressor.

PUBLICATIONS

1. Ras-dependent GEF, RGL1, is a novel regulator of differential RaIA activation downstream of integrins and oncogenic Ras. Neha Deshpande, Archana Pawar, Ki-Bum Kim, Siddhi Inchanalkar, Manali Patil, Kaushik Inamdar, Martin Schwartz, Nagaraj Balasubramanian. (Manuscript in preparation).
2. FZL is primarily localized to the inner chloroplast membrane however influences thylakoid maintenance. Manali Patil, Stephanie Seifert, Franka Seiler, Jürgen Soll and Serena Schwenkert. *Plant Mol Biol* (2018) 97: 421
3. OEP23 forms an ion channel in the chloroplast outer envelope. Götze TA, Patil M, Jeshen I, Bölter B, Grahl S, Soll J. *BMC Plant Biology* 15(1):445 · December 2015.

CONFERENCES

1. 68th Mosbach Colloquium on Cell Organelles: Origin, Dynamics, Communication. GMB. Presented a Poster. (March 2017)

Veröffentlichungen

Teile dieser Arbeit wurden veröffentlicht in:

Patil M, Seifert S, Seiler F, Soll J, Schwenkert S (2018) FZL is primarily localized to the inner chloroplast membrane however influences thylakoid maintenance. *Plant Molecular Biology* 97: 421–433

Eidesstattliche Versicherung

Ich versichere hiermit an Eides statt, dass die vorgelegte Dissertation von mir selbstständig und ohne unerlaubte Hilfe angefertigt wurde. Ich habe weder anderweitig versucht, eine Dissertation einzureichen oder eine Doktorprüfung durchzuführen, noch habe ich diese Dissertation oder Teile derselben einer anderen Prüfungskommission vorgelegt.

München, 28th August 2018

Manali Kishor Patil

Acknowledgements

Firstly, I would like to express my deepest sense of gratitude to my doktorvater Prof. Dr. Jürgen Soll for his patient guidance and excellent advice throughout this study. His constructive criticism encouraged me to improve myself at my short comings and to put in my best efforts. He was always available to answer all my questions even after he had finished all his day's work and having a beer with Prof. Dr. Jörg Nickelsen. I would like to thank PD. Dr. Bettina Bölter, PD. Dr. Serena Schwenkert, Dr. Chris Carrie and Dr. Irene Gügel for all the support they provided regarding day-to-day lab affairs. I thank Serena for guiding me patiently and being there to solve even the silliest of my doubts. She kept me motivated during the low times when the experiments were working. Most importantly, I would like to thank her for understanding me and helping me explain myself point better whenever I was in doubt. This was especially helpful during our discussion with Chef and while writing the paper. I thank Chris for helping me with cloning of synaptotagmin gene when most of us were unable to do it. Without it the I would not be able to do much with the project.

I wish to express my sincere gratitude and heartfelt thanks to my lab mates Tamy, Roberto, Li, Sophie, Thomas, Cathi, Melanie M., Stephi, Annabel, Ahmed, Petra, Renuka, Kerstin, Karl, Korbi, Inga, Betty, Melanie B., Sebnem and Pit for their constant help throughout my project. Thank you Tamy and Stephi for everything, just your mere presence in lab was enough to cheer me up during the low times. Thank you, guys, for listening me talk so fast and so long, being patient with me during all those times when I was too happy or too sad. Also, I would like to thank all, especially Tamy, Stephi, Petra, Kerstin, Ahmed and Roberto for hearing all the rambling when I had difficulty in explaining what I wanted to say.

I would like to sincerely thank my friends, Martina, Dhawal, Ekatharina, Christoph, Stephan, Tom, Karan, Nimisha, Kathrin, Varun, Ayush, Nitin, Vinay and Smita for making the time I spent in Munich eventful and memorable. A special thanks to Gaby, Stephi and Chintan, the pottery sessions helped me take my mind away from lab work.

I would like to thank my family for being there for me during thick and thin. I would like to thank Priyanka, Rachana and Ajinkya for their constant support, encouragement and understanding during these difficult times. Arnab, I cannot express in enough words but just your presence at times has turned my terrible day into happy one. Your constant support, criticism, encouragement allowed me to keep going despite all odds. It contributed in making the PhD experience extremely pleasant and enjoyable. Finally, to my parents, Mugdha and Ameya, thank you for having faith in me and giving me freedom to do what I was interested in.

August 2018

Manali Kishor Patil.